The Scientific World Journal

Innovative Targeting Strategies in Drug Therapy for Inflammatory Diseases: Mechanistic Approaches

Guest Editors: Duen-Suey Chou, Joen-Rong Sheu, Philip A. Thomas, and Muniyan Sakthivel

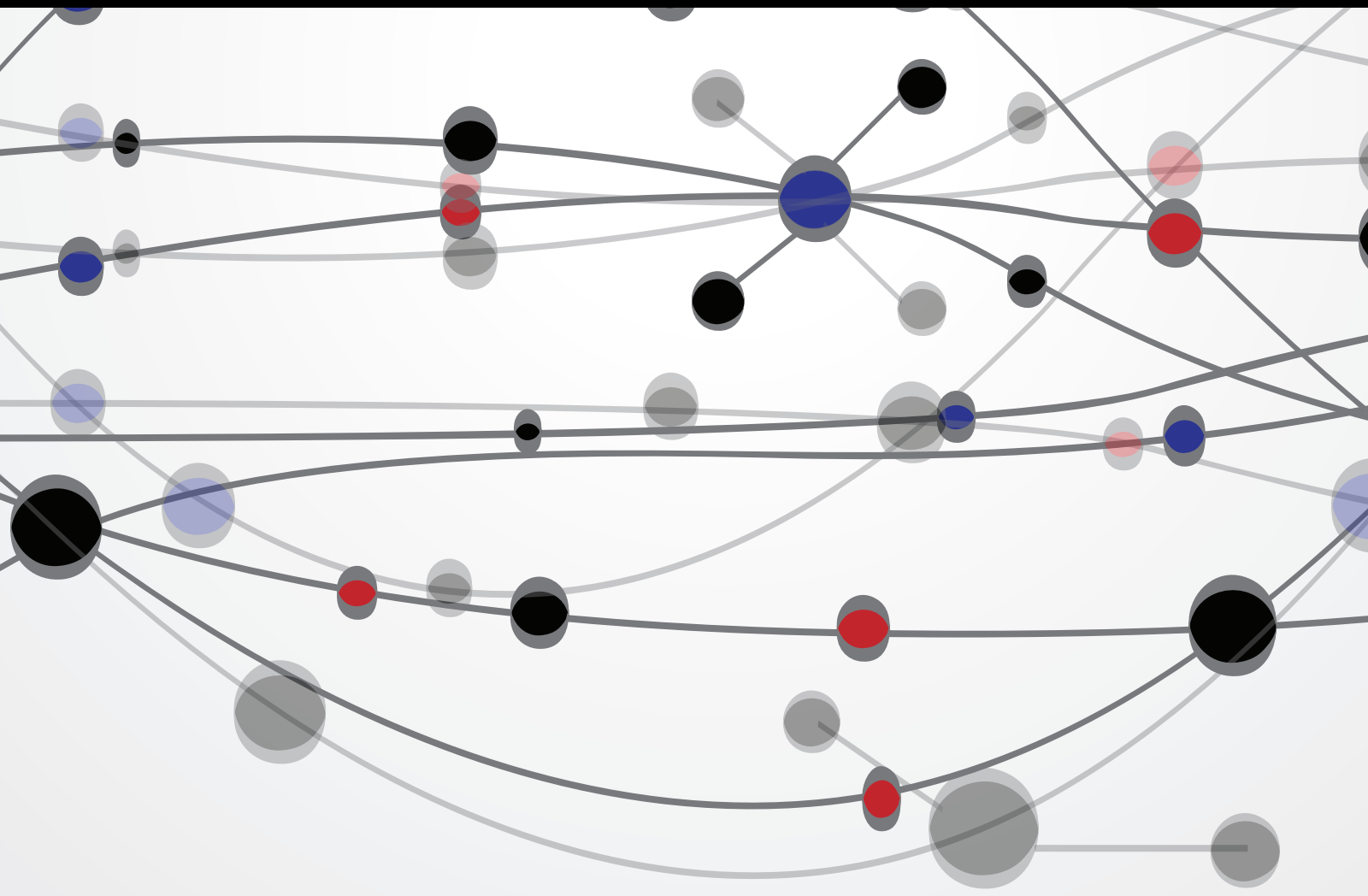

Innovative Targeting Strategies in Drug Therapy for Inflammatory Diseases: Mechanistic Approaches

The Scientific World Journal

Innovative Targeting Strategies in Drug Therapy for Inflammatory Diseases: Mechanistic Approaches

Guest Editors: Duen-Suey Chou, Joen-Rong Sheu, Philip A. Thomas, and Muniyan Sakthivel

Contents

Hindawi Publishing Corporation
The Scientific World Journal
Volume 2015, Article ID 891676, 2 pages
http://dx.doi.org/10.1155/2015/891676

Editorial

Innovative Targeting Strategies in Drug Therapy for Inflammatory Diseases: Mechanistic Approaches

Duen-Suey Chou,[1] Joen-Rong Sheu,[1] Philip A. Thomas,[2] and Muniyan Sakthivel[3]

[1]*Graduate Institute of Medical Sciences, College of Medicine, Taipei Medical University, Taipei 110, Taiwan*
[2]*Department of Microbiology, Institute of Ophthalmology, Joseph Eye Hospital, Tiruchirappalli, Tamil Nadu 620 001, India*
[3]*Department of Biochemistry and Molecular Biology, University of Nebraska Medical Center, Omaha, NE 68198, USA*

Correspondence should be addressed to Duen-Suey Chou; fird@tmu.edu.tw

Received 12 March 2015; Accepted 12 March 2015

The treatment of inflammatory disease is conquered by the administration of anti-inflammatory and immunosuppressive drugs, which defeat the inflammatory burden and recover the disease-related symptoms. Conventional treatment strategies are characterized by limited therapeutic efficacy and the occurrence of adverse drug reactions. Therefore, the progress of novel disease-targeted drug delivery stratagems is proposed for a more effective therapy. Though numerous harmonizing and conventional treatment strategies have been assimilated into experimental and clinical practices, the pertinent molecular mechanisms are still under investigation. Hence, we invited researchers to contribute original research articles as well as review articles to offer solid suggestion to sustain the application of innovative drugs in prevention and treatment of inflammatory diseases.

A paper in this special issue investigates the effect of *Antrodia camphorata,* a rare Taiwanese medicinal mushroom that is popularly known as "niu cheng zhi" in Taiwan, on inflammatory arterial thrombosis-mediated platelet activation and also the pivotal role of protein kinase C in this situation was investigated. This paper demonstrated clearly that *Antrodia camphorata* holds antiplatelet activity via inhibiting Ca^{2+}, PKC cascades, and Akt signaling pathway. These alterations may reduce platelet activity and ultimately inhibit platelet aggregation. Another interesting paper in this special issue addresses the same aspect that combinative therapy of *Antrodia camphorata* with aspirin offers enhanced neuroprotective efficacy without increasing side effects. This paper thoroughly planned and demonstrated that *Antrodia camphorata* alone or combined with aspirin enhanced neuroprotective efficacy by reducing brain infarct volume, neurobehavioral score, cerebral blood perfusion, and subarachnoid and intracerebral hemorrhage incidence. This paper also showed that *Antrodia camphorata* alone or with aspirin did not alter the level of hemoglobin, as this treatment is safe and does not cause hemorrhagic incident. The findings of these papers suggested that *Antrodia camphorata* may be a potential therapeutic agent for preventing or treating thromboembolic disorders without causing any major side effects.

This special issue also published an inspiring paper that has investigated the mechanisms of the inhibitory effects of andrographolide, a most active and critical constituent isolated from the leaves of *Andrographis paniculata* in vascular smooth muscle cells (VSMCs) exposed to a proinflammatory stimulus, tumor necrosis factor-α (TNF-α). This mechanistic study proposed that andrographolide can benefit the treatment of vascular inflammatory diseases, and andrographolide-mediated inhibition of NF-κB activity in TNF-α-stimulated VSMCs may occur through the JNK-Akt-p65 signaling cascade, an IκBα-independent mechanism. In addition, an interesting piece of work in this special issue examined the effect of an ethanolic extract of *Sanguis draconis*, a kind of dragon's blood resin that was obtained from *Daemonorops draco* (Palmae), on human umbilical vein endothelial cells (HUVEC) under high-glucose stimulation.

This paper showed that *Sanguis draconis* attenuated high-glucose induced cell toxicity, nitrite, lipid peroxidation, and reactive oxygen species (ROS) formation in HUVEC. This treatment method abolished phosphorylation of ERK 1/2, NF-κB, VCAM-1, and E-selectin, and it seems to block the breakdown of PARP-116 kDa protein. Furthermore, this paper found that *Sanguis draconis* increased the expression of Bcl-2 and decreased Bax protein expression. The results of this paper suggest that *Sanguis draconis* may have a therapeutic potential in vascular inflammation due to the decreased levels of oxidative stress, apoptosis, and PARP-1 activation. Overall, we expect that this special issue grants progressive awareness to upsurge the therapeutic significance for drug development to treat or prevent inflammatory diseases.

Duen-Suey Chou
Joen-Rong Sheu
Philip A. Thomas
Muniyan Sakthivel

Hindawi Publishing Corporation
The Scientific World Journal
Volume 2015, Article ID 417124, 8 pages
http://dx.doi.org/10.1155/2015/417124

Research Article

VEGF Correlates with Inflammation and Fibrosis in Tuberculous Pleural Effusion

Mauo-Ying Bien,[1,2] Ming-Ping Wu,[3,4] Wei-Lin Chen,[5] and Chi-Li Chung[1,2]

[1] *School of Respiratory Therapy, College of Medicine, Taipei Medical University, Taipei 110, Taiwan*
[2] *Division of Pulmonary Medicine, Department of Internal Medicine, Taipei Medical University Hospital, Taipei 110, Taiwan*
[3] *Department of Obstetrics and Gynecology, Chi-Mei Medical Center, Tainan 710, Taiwan*
[4] *Department of Obstetrics and Gynecology, College of Medicine, Taipei Medical University, Taipei 110, Taiwan*
[5] *Graduate Institute of Medical Sciences and Department of Pharmacology, College of Medicine, Taipei Medical University, Taipei 110, Taiwan*

Correspondence should be addressed to Chi-Li Chung; clchung@tmu.edu.tw

Received 25 September 2014; Accepted 3 December 2014

Academic Editor: Muniyan Sakthivel

Objective. To investigate the relationship among angiogenic cytokines, inflammatory markers, and fibrinolytic activity in tuberculous pleural effusion (TBPE) and their clinical importance. *Methods*. Forty-two patients diagnosed with TBPE were studied. Based on chest ultrasonography, there were 26 loculated and 16 nonloculated TBPE patients. The effusion size radiological scores and effusion vascular endothelial growth factor (VEGF), interleukin- (IL-) 8, plasminogen activator inhibitor type-1 (PAI-1), and tissue type plasminogen activator (tPA) were measured. Treatment outcome and pleural fibrosis, defined as radiological residual pleural thickening (RPT), were assessed at 6-month follow-up. *Results*. The effusion size and effusion lactate dehydrogenase (LDH), VEGF, IL-8, PAI-1, and PAI-1/tPA ratio were significantly higher, while effusion glucose, pH value, and tPA were significantly lower, in loculated than in nonloculated TBPE. VEGF and IL-8 correlated positively with LDH and PAI-1/tPA ratio and negatively with tPA in both loculated and nonloculated TBPE. Patients with higher VEGF or greater effusion size were prone to develop RPT ($n = 14$; VEGF, odds ratio 1.28, $P = 0.01$; effusion size, odds ratio 1.01, $P = 0.02$), and VEGF was an independent predictor of RPT in TBPE (receiver operating characteristic curve AUC = 0.985, $P < 0.001$). *Conclusions*. Effusion VEGF correlates with pleural inflammation and fibrosis and may be targeted for adjunct therapy for TBPE.

1. Introduction

Tuberculosis (TB) remains a major global public health issue and continues to cause significant morbidity and mortality worldwide [1]. Tuberculous pleural effusion (TBPE) is the most common form of extrapulmonary TB and often complicated with pleural fibrosis [2]. This pleural fluid is enriched in proteins, inflammatory cells, and various angiogenic cytokines [3], including vascular endothelial growth factor (VEGF) and interleukin- (IL-) 8, which stimulate migration of leukocytes, induce vascular hyperpermeability and pleural fluid production, activate coagulation cascade, and repress fibrinolytic activity within the pleural cavity [4, 5].

Fluid loculation with fibrin septation, a hallmark of pleural inflammation, is commonly found to be the initial presentation of TBPE [6]. Loculated effusion, defined as effusion that does not move freely in the pleural space due to fibrinous adhesion between parietal and visceral pleura, makes reabsorption or drainage of such fluid collection very difficult and leads to persistent dyspnea [6]. Fibrin turnover in the pleural cavity is affected by fibrinolytic activity mediated by plasmin, which is regulated by the equilibrium between plasminogen activators (PAs) and plasminogen activator inhibitors (PAIs) [7]. An imbalance between PAI-1 and tissue type plasminogen activator (tPA) may elicit fibrin gel formation in the pleural space and lead to pleural fluid loculation, fibrin neomatrix remodeling, and fibrosis [6, 8].

VEGF may facilitate the genesis of fibrin gel in infectious pleural effusions [9]. Previous studies reported that VEGF

might play a role in the modulation of tPA and PAI-1 [10] and that anti-VEGF antibody could reduce fluid volume of inflammatory pleural effusion and attenuate pleural inflammation and fibrosis [11–13]. These findings suggest that VEGF may be involved in the regulation of inflammation, fibrin turnover and fluid loculation in the pleural cavity, and subsequent residual pleural thickening (RPT) or fibrosis [9], which was observed in our previous study on parapneumonic effusions [14]. However, the clinical relevance of angiogenic cytokines and fibrinolytic activity in TBPE remains unclear. The aim of the present study was to evaluate the relationship among angiogenic cytokines (VEGF, IL-8), inflammatory markers (lactate dehydrogenase (LDH), glucose, pH value), and fibrinolytic parameters (tPA and PAI-1) in TBPE and their clinical implication.

2. Methods

2.1. Study Design. This single-center prospective study intended to assess the clinical importance of angiogenic cytokines and fibrinolytic activity in TBPE. Ethics approval (CRC-05-11-01) was obtained from the Institutional Review Board of Taipei Medical University (Taipei, Taiwan), and all patients gave written informed consent before entering the study.

2.2. Patient Selection. Consecutive patients with pleural effusion (PE) of unknown cause admitted to Taipei Medical University Hospital were eligible for this study and were included when a diagnosis of TBPE was established by the demonstration of granulomatous pleuritis on closed pleura biopsy specimens with or without the presence of acid-fast bacilli. Exclusion criteria were as follows: history of invasive procedures directed into the pleural cavity; recent severe trauma, hemorrhage, or stroke; bleeding disorder or anticoagulant therapy; use of streptokinase in the previous 2 years; and lack of dyspnea caused by effusions.

2.3. Imaging of PE. All patients were subjected to routine chest radiography (CXR, frontal and lateral views), lateral decubitus view with the lesioned side down, real-time chest ultrasonography (US), and/or thoracic computed tomography (CT) to determine the loculated or nonloculated PE as previously described [6]. Loculated effusion was diagnosed if the fluid collection (1) appeared as a fixed lenticular shape on a frontal CXR and was unchanged in appearance on a decubitus CXR or (2) had a lobulated or lentiform configuration with a convex smooth border on chest US or CT imaging.

2.4. CXR Scoring. The posteroanterior CXR films were read and scored by two radiologists who were blind to any clinical information to determine (a) the largest linear width of pleural opacity and (b) effusion size CXR score: the estimated overall percentage of pleural shadowing in the hemithorax [15].

2.5. Thoracentesis and Pleural Fluid Analysis. With the guidance of chest US, 50 mL of pleural fluid was aspirated immediately or within 24 hours after hospitalization. When PE was multiloculated, the fluid was aspirated from the largest loculus. Pleural fluid analyses, adenosine deaminase (ADA), and microbiological studies were performed routinely.

2.6. Measurement of Effusion VEGF, IL-8, PAI-1, and tPA. The commercially available enzyme-linked immunosorbent assay kits were used to measure effusion levels of VEGF, IL-8 (R & D System; Minneapolis, MN, USA), tPA, and PAI-1 (American Diagnostica; Greenwich, CT, USA) as previously described [6].

2.7. Management of TBPE. Standard anti-TB medications in addition to pigtail drainage were administered once TB pleurisy was diagnosed. Intrapleural injection therapy started on the following day and was done once daily for three continuous days. Patients with nonloculated effusion underwent intrapleural injection with 50 mL normal saline. Patients with loculated effusions received intrapleural injection with solutions containing 50 mL normal saline with 250,000 IU of dissolved streptokinase (Aventis, Marburg, Germany). After injection, the pigtail tube was clamped for 2 hours and then opened for free drainage. CXR was performed after the third day of treatment. Complete drainage was defined as no or minimal pleural effusion on CXR. The pigtail tube was removed when the net drainage was less than 50 mL during the previous 24 hours.

2.8. Outcome Measures. CXR and pulmonary function testing with spirometry were performed on discharge and 6 months later, respectively. RPT was measured and defined as a lateral pleural thickening of ≥10 mm shown on CXR and confirmed by chest US or CT at the end of 6-month follow-up [16].

2.9. Statistical Analysis. Data were expressed as mean ± SD, median (interquartile range or range), or frequency (%), where appropriate. Comparisons of continuous data were made using an unpaired t-test or Mann-Whitney U test between two groups where appropriate. The correlations between variables were determined by Spearman rank correlation coefficients. Categorical variables between two groups were examined using χ^2 method and/or Fisher's exact test, when appropriate. A two-tailed P value <0.05 was considered to be statistically significant.

Multivariate logistic regression analyses were performed to determine factors independently associated with development of RPT. Variables found to be significant in the univariate analysis were entered into a binary logistic regression analysis. Results of multivariable analyses are reported as odds ratios (OR) with 95% confidence intervals and P values. The optimal sensitivity, specificity, and cutoff value of pleural fluid variables to predict RPT were evaluated by the receiver operating characteristics (ROC) by analyzing the area under the curve (AUC).

Table 1: Demographic and clinical data of the patients studied.

	All patients ($n = 42$)	Loculated TBPE ($n = 26$)	Nonloculated TBPE ($n = 16$)	P value[†]
Male, n (%)	27 (64)	18 (69)	9 (56)	0.511
Age, yrs, mean ± SD	62 ± 21	61 ± 22	63 ± 21	0.824
Patients with comorbidities, n (%)[*]	28 (67)	18 (70)	10 (63)	0.742
Symptom onset to treatment, days, median (range)	10 (7–19)	10 (8–20)	10 (6–16)	0.547
Side of pleural effusion				
Right/left, n (%)	27/15 (64/36)	17/9 (65/35)	10/6 (63/37)	0.733

TBPE: uncomplicated parapneumonic effusion.
[*]Comorbidities including alcoholism, diabetes mellitus, neurologic, cardiac, respiratory, liver, and kidney diseases.
[†]For comparisons between loculated and nonloculated TBPE groups.

Table 2: Pleural effusion variables between loculated and nonloculated tuberculous pleural effusion.

	All patients ($n = 42$)	Loculated TBPE ($n = 26$)	Nonloculated TBPE ($n = 16$)	P value[†]
Effusion CXR score, %, mean ± SD	53 ± 20	56 ± 21	43 ± 12	0.025
ADA, IU/L	99 (66–185)	108 (82–203)	86 (59–149)	0.100
pH value	7.30 (7.22–7.35)	7.27 (7.22–7.30)	7.36 (7.33–7.41)	<0.001
Glucose, mg/dL	116 (75–138)	98 (75–118)	120 (99–142)	0.038
Protein, g/L	5.0 (4.1–5.3)	4.8 (4.1–5.2)	5.2 (4.2–5.6)	0.089
LDH, IU/dL	307 (229–533)	387 (287–723)	210 (154–388)	0.002
Leukocyte count, cells/μL	1598 (963–3880)	1665 (1330–3880)	1437 (720–2000)	0.449
PAI-1, ng/mL	114.6 (105.5–199.0)	138.5 (114.8–213.0)	105.5 (96.0–113.0)	<0.001
tPA, ng/mL	17.0 (10.0–23.0)	15.9 (8.4–20.5)	24.9 (14.4–28.7)	<0.01
PAI-1/tPA ratio	7.6 (5.0–14.0)	13.4 (7.6–18.4)	4.6 (1.8–6.8)	0.036
IL-8, pg/mL	365 (220–637)	419 (312–1442)	167 (79–395)	<0.001
VEGF, pg/mL	693 (499–1909)	969 (571–2054)	510 (161–713)	<0.001

TBPE: tuberculous pleural effusion; effusion CXR score: portion of hemithorax opacified by pleural effusion on posteroanterior chest radiograph; ADA: adenosine deaminase; LDH: lactate dehydrogenase; PAI-1: plasminogen activator inhibitor-1; tPA: tissue type plasminogen activator; IL-8: interleukin-8; VEGF: vascular endothelial growth factor.
Data are presented as median (IQR) unless specified.
[†]For comparisons between loculated and nonloculated TBP groups.

3. Results

3.1. Patient Characteristics. Consecutive 50 patients with TBPE were eligible for this study. Eight patients were excluded because of recent stroke in three, recent gastrointestinal bleeding in two, and informed consent unavailable in three cases, respectively. Finally, 42 patients were enrolled, including 27 men and 15 women with an age range from 22 to 91 years (mean age, 62 years) (Table 1), and all completed 6 months of follow-up from March 2011 through June 2014.

3.2. Comparisons between Loculated and Nonloculated TBPE. There were 26 patients with loculated TBPE and 16 patients with nonloculated TBPE (Table 1). Clinical data, pleural fluid characteristics, angiogenic cytokines, and parameters related to fibrinolytic activities in pleural fluids are shown in Table 2. Compared to patients with nonloculated TBPE, loculated TBPE patients had significantly higher effusion CXR score on admission. No significant differences between the two groups were found in terms of age, gender, comorbidities, and duration of illness before treatment. Patients with loculated TBPE

Table 3: Correlation among angiogenic cytokines, fibrinolytic parameters, pleural fluid characteristics, and effusion CXR scores.

	pH	Glucose	LDH	Leukocyte count	PAI-1	tPA	PAI-1/tPA ratio	Effusion CXR score
Loculated TBPE ($n = 26$)								
IL-8	−0.42*	−0.40*	0.39*	0.36	0.28	−0.40*	0.42*	0.21
VEGF	−0.57†	−0.58†	0.49*	0.25	0.77‡	−0.53†	0.76‡	0.63‡
Effusion CXR score	−0.14	−0.12	−0.18	0.13	0.39*	−0.22	0.12	—
Nonloculated TBPE ($n = 16$)								
IL-8	−0.46	−0.48	0.55*	0.28	0.24	−0.62†	0.59*	0.32
VEGF	−0.52*	−0.56*	0.67†	0.17	0.59*	−0.44*	0.43*	0.47*
Effusion CXR score	−0.22	−0.29	−0.11	0.29	0.21	−0.11	0.10	—

See Table 2 for definition of the abbreviations.
*Correlation is statistically significant at the level of 0.05.
†Correlation is statistically significant at the level of 0.01.
‡Correlation is statistically significant at the level of 0.001.

Table 4: Pleural fluid variables and pulmonary function in patients with or without development of residual pleural thickening (RPT).

	RPT (+) ($n = 14$)	RPT (−) ($n = 28$)	P value
Effusion status			
Effusion CXR score, %, mean ± SD	71 ± 20	44 ± 12	<0.001
Loculation, n (%)	14 (100)	0 (0)	0.002
Pleural fluid			
pH value	7.27 (7.22–7.30)	7.35 (7.25–7.39)	0.013
Glucose, mg/dL	100 (73–140)	106 (76–129)	0.947
LDH, IU/dL	328 (229–666)	289 (154–532)	0.126
Leukocyte count, cells/μL	2840 (1521–4410)	1437 (720–2000)	0.028
PAI-1, ng/mL	143.1 (111.1–208.0)	113.7 (78.0–122.5)	0.043
tPA, ng/mL	10.4 (8.2–12.7)	15.8 (4.8–21.0)	0.028
PAI-1/tPA ratio	11.7 (5.0–16.7)	5.2 (2.9–8.4)	<0.001
IL-8, pg/mL	419 (312–985)	248 (96–502)	0.025
VEGF, pg/mL	2054 (1909–3387)	516 (274–693)	<0.001
FVC, % predicted			
At 6 months	74 (73–75)	80 (79–81)	<0.001

See Table 2 for definition of the abbreviations. RPT: residual pleural thickening ≥10 mm shown on CXR at the end of 6-month follow-up; FVC: forced vital capacity.
Data are presented as median (IQR) unless specified.

had significantly higher levels of effusion LDH, VEGF, IL-8, PAI-1, and PAI-1/tPA ratio, and lower values of pH, glucose, and tPA than did nonloculated TBPE patients. Moreover, the ADA level, protein concentrations, and leukocyte counts were comparable between two groups.

3.3. Correlations among Effusion Angiogenic Cytokines, Fibrinolytic Parameters, Pleural Fluid Characteristics, and Effusion CXR Score. As shown in Table 3, the effusion levels of IL-8 and VEGF were positively correlated with those of LDH and PAI-1/tPA ratio and negatively correlated with those of tPA in both loculated and nonloculated TBPE. In addition, VEGF correlated positively with PAI-1 and negatively with pH value and glucose in both loculated and nonloculated TBPE, suggesting that VEGF is implicated in pleural inflammation and fibrinogenesis.

The effusion CXR score had significant positive correlation with the effusion levels of VEGF in both loculated and nonloculated TBPE. However, there was no significant correlation between the effusion size and the effusion levels of IL-8.

3.4. Comparisons between TBPE Patients with and without RPT. All patients were successfully treated with anti-TB medications and intrapleural instillation of normal saline or streptokinase and were discharged uneventfully. All patients finished the 6-month anti-TB medications and improved clinically over time, showing no recurrence of the disease. RPT was observed in 14 patients (33%) at the end of 6-month follow-up (Table 4). All of them (100%) had loculation of pleural effusions initially. The effusion CXR score on admission and the effusion levels of leukocyte count, PAI-1, PAI-1/tPA ratio, IL-8, and VEGF were significantly higher, and the effusion pH value and tPA were significantly lower in the patients with RPT than in those without RPT. Moreover,

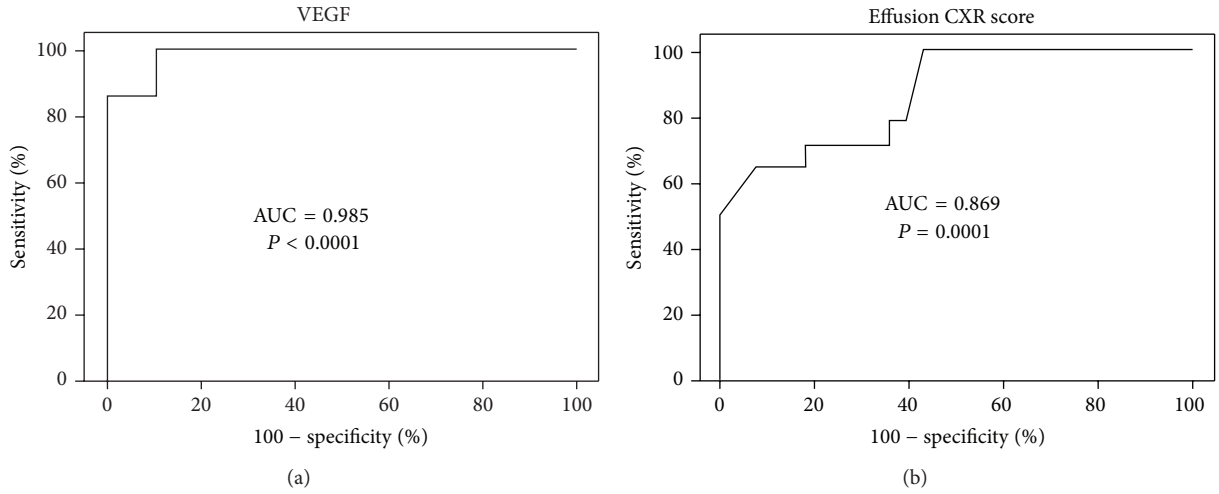

Figure 1: Receiver operating characteristic curves for (a) effusion vascular endothelial growth factor (VEGF) level and (b) effusion chest radiography (CXR) score to predict residual pleural thickening (RPT) in tuberculous pleural effusion (TBPE). AUC = area under the curve.

patients with RPT had significant lower forced vital capacity (FVC) than those without RPT.

3.5. Multivariate Logistic Regression Analysis. Furthermore, multivariate logistic regression analysis was used to identify the independent factors associated with RPTin TBPE after 6-month anti-TB medications (Table 5). Variables of significance in univariate analysis were included for analysis which demonstrated that only higher effusion VEGF level and greater effusion CXR score were independent predictors for RPT in TBPE.

3.6. Optimal Sensitivity, Specificity, and Cutoff Value of Variables to Predict RPT. The ROC curve showed that the effusion VEGF at the cutoff level >842 pg/mL had the highest sensitivity and specificity for predicting RPT in TBPE patients (area under the ROC curve = 0.985, 95% CI = 0.957–1.012; sensitivity 100%, 95% CI = 76.8–100%; specificity 89.3%, 95% CI = 71.8–97.7%) (Figure 1(a)), followed by effusion CXR score >62% (area under the ROC curve = 0.869, 95% CI = 0.757–0.981; sensitivity 64.3%, 95% CI = 35.1–87.2%; specificity 92.9%, 95% CI = 76.5–99.1%) (Figure 1(b)).

Table 5: Multivariate logistic regression analyses of factors associated with residual pleural thickening (RPT).

	Odds ratio	95% CI	*P* value
Effusion status			
Effusion CXR score, %	1.01	1.00–1.02	0.02
Loculation	1.00	0.99-1.00	0.99
Pleural fluid			
pH value	1.01	0.98–1.04	0.52
Leukocyte count, cells/μL	1.00	0.99-1.00	0.87
PAI-1, ng/mL	0.99	0.97–1.03	0.76
tPA, ng/mL	1.00	0.99-1.00	0.99
PAI-1/tPA ratio	1.01	0.98–1.04	0.52
IL-8, pg/mL	1.00	0.99-1.00	0.93
VEGF, pg/mL	1.28	1.06–1.51	0.01

See Table 2 for definition of the abbreviations. CI: confidence interval.

4. Discussion

Our results demonstrated that effusion size, LDH, VEGF, IL-8, PAI-1, and PAI-1/tPA ratio were significantly higher, while effusion glucose, pH value, and tPA were significantly lower, in loculated than in nonloculated TBPE. VEGF and IL-8 correlated positively with LDH and PAI-1/tPA ratio and negatively with tPA in both loculated and nonloculated TBPE. Additionally, VEGF had positive correlation with effusion size in both loculated and nonloculated TBPE. Fourteen patients who developed RPT at the end of 6-month follow-up had larger effusion size and higher levels of VEGF and PAI-1/tPA ratio than those who did not. Moreover, VEGF and effusion size were independent predictors of RPT in TBPE. To our knowledge, this is the first study to demonstrate that VEGF correlated significantly with TB pleural inflammation and fibrinolytic activity and that elevated VEGF level was associated with development of pleural fibrosis in TBPE.

Previous studies showed that the level of VEGF was consistently higher in exudative than in transudative pleural effusions [17, 18] and TBPE contained significantly higher levels of VEGF than did pleural fluid of heart failure patient [19]. Another report demonstrated that compared to patients with inactive pulmonary TB and control subjects, serum VEGF levels were increased in patients with active pulmonary TB and were decreased after successful treatment, indicating that VEGF may serve as a marker of disease activity [20]. Likewise, the present study revealed that VEGF levels were significantly higher in loculated than in nonloculated TBPE and correlated substantially with pleural inflammatory markers such as LDH, pH, and glucose in both groups. As pleural inflammation and increased vascular permeability and leakage are

essential for the development of exudative PE, VEGF may represent a key mediator in pleural fluid formation [21]. In parallel, our data disclosed a substantial correlation between effusion VEGF level and effusion CXR score in both loculated and nonloculated TBPE. All these results suggest that VEGF is implicated in pleural inflammation and may be crucial for the formation of TBPE.

VEGF induces extravascular leakage of plasma proteins and is important in the modulation of extracellular matrix proteolysis by regulating the expression of tPA and PAI-1 in endothelial cells [10]. Furthermore, VEGF has been reported to increase PAI-1 expression in keloid fibroblasts and to contribute to dermal fibrosis [22]. Another angiogenic factor IL-8 has been shown to increase vascular permeability and fluid exudation in endotoxin-induced pleurisy *in vivo* [23] and correlated positively with PAI-1 and negatively with tPA in exudative PE [24]. All these findings indicate that angiogenic cytokines may elicit exudative effusions and modulate fibrinolytic activity in pleural space by altering the balance of PAI-1 and tPA. In line with the previous reports [10, 22–24], our data demonstrated that in both loculated and nonloculated TBPE, the levels of VEGF and IL-8 correlated positively with the values of PAI-1/tPA ratio and negatively with tPA level, though only VEGF levels correlated positively with PAI-1 values. In addition, the levels of VEGF, IL-8, PAI-1, and PAI-1/tPA ratio were significantly higher and the values of tPA were significantly lower in loculated than in nonloculated TBPE. These findings are in keeping with the results of the previous *in vitro* study [10] and raise the possibility that angiogenic cytokines, particularly VEGF, may attenuate pleural fibrinolytic activity by disrupting the balance of PAI-1 and tPA elaborated by endothelial and/or mesothelial cells and that the increase in VEGF is associated with the decrease in fibrinolytic activity and subsequent fibrin deposition and fluid loculation in TBPE.

The sequel of RPT of >10 mm may cause significant functional disturbance [25]. However, the predictors affecting the development of RPT in patients with TBPE remain elusive. Previous studies reported that the concentrations of C-reactive protein, IL-1, IL-8, tumor necrosis factor-α, transforming growth factor-β1, interferon-γ, and PAI-1 were significantly higher and the values of pH, glucose, and tPA were significantly lower in TBPE complicated with RPT than those without [6, 26–30]. Moreover, pleural fluid loculation or fibrin septation detected by chest US as an initial presentation may be of value in predicting the development or occurrence of RPT in TBPE following completion of anti-TB medication [6, 31]. A previous *in vivo* study also demonstrated that angiogenesis was required in the development of pleural fibrosis [11, 12].

In this study, fourteen patients who developed RPT at the end of follow-up presented initially with fluid loculation and had greater effusion size, higher effusion levels of VEGF, IL-8, PAI-1, and PAI-1/tPA ratio, and lower effusion levels of pH and tPA. Furthermore, the multivariate analysis demonstrated that larger effusion size or higher effusion level of VEGF was the independent risk factor for development of RPT. Our results also revealed that effusion VEGF >842 pg/mL, followed by effusion CXR score >62%, had optimal sensitivity and specificity to predict RPT in TBPE. At variance with the previous reports [6, 30], our study indicated that the presence of loculation did not increase the risk of pleural fibrosis. The discrepancy may be explained in part by the fact that all loculated TBPE patients in the present study received chest US-guided drainage and streptokinase irrigation, which may minimize the effect of effusion loculation on the occurrence of RPT [15]. Collectively, in agreement with the previous *in vivo* reports [11–13], our study indicated that the increased angiogenic activity in the pleural fluid might contribute to subsequent development of pleural fibrosis and signified the role of VEGF-related impaired fibrinolytic activity in the formation of RPT in TBPE.

A previous study demonstrated that administration of corticosteroids, in conjunction with anti-TB therapy, resulted in more rapid improvement in symptoms of fever and chest pain and in resolution of effusions in patients with TBPE, suggesting the beneficial effect of anti-inflammatory agents on clinical outcome [32]. However, to date, no effective medical treatment is available for preventing pleural fibrosis in TBPE [33]. The reason may be that another critical factor in pleural fibrosis is the formation of fibrinous neomatrix which results from disorder in fibrin turnover [8]. Transforming growth factor (TGF)-β, like VEGF [11, 12], could cause PAI-1/tPA imbalance and disordered fibrin turnover, and intrapleural injection with anti-TGF-β antibody has been shown to decrease pleural fibrosis in experimental empyema in rabbits [34]. Accordingly, the previous studies [32–34] and our results may justify further researches on the usefulness of anti-VEGF therapy for TBPE.

Taken together, the present study highlighted the pivotal role of VEGF in orchestration of inflammation, formation of pleural fluid, impairment of fibrinolysis, and development of residual fibrosis in TBPE. As prompted by the promising effect of targeted therapy with antiangiogenic agents on outcome of patients with metastatic colorectal cancer [35] and neovascular age-related macular degeneration [36], further preclinical and clinical trials are required to investigate the potential use of targeting VEGF as a therapeutic strategy adjunct to standard anti-TB treatment for TBPE.

Abbreviations

CT: Computed tomography
CXR: Chest radiography
IL-8: Interleukin-8
PAI-1: Plasminogen activator inhibitor-1
PE: Pleural effusion
RPT: Residual pleural thickening
tPA: Tissue type plasminogen activator
TB: Tuberculosis
TBPE: Tuberculous pleural effusion
US: Ultrasonography
VEGF: Vascular endothelial growth factor.

Conflict of Interests

All the authors declare that there is no conflict of interests regarding the publication of this paper.

Acknowledgments

This work was supported by grants from the National Science Council, Taiwan (NSC 101-2314-B-038-044-MY3), and the Chi-Mei Medical Center-Taipei Medical University (102CM-TMU-08). Dr. Mauo-Ying Bien and Dr. Ming-Ping Wu contributed equally in this work and should be regarded as first authors together.

References

[1] C. Dye and B. G. Williams, "The population dynamics and control of tuberculosis," *Science*, vol. 328, no. 5980, pp. 856–861, 2010.

[2] J. M. Porcel, "Tuberculous pleural effusion," *Lung*, vol. 187, no. 5, pp. 263–270, 2009.

[3] V. B. Antony, "Immunological mechanisms in pleural disease," *European Respiratory Journal*, vol. 21, no. 3, pp. 539–544, 2003.

[4] K. A. Mohammed, N. Nasreen, J. Hardwick, C. S. Logie, C. E. Patterson, and V. B. Antony, "Bacterial induction of pleural mesothelial monolayer barrier dysfunction," *The American Journal of Physiology—Lung Cellular and Molecular Physiology*, vol. 281, no. 1, pp. L119–L125, 2001.

[5] V. C. Broaddus, A. M. Boylan, J. M. Hoeffel et al., "Neutralization of IL-8 inhibits neutrophil influx in a rabbit model of endotoxin-induced pleurisy," *Journal of Immunology*, vol. 152, no. 6, pp. 2960–2967, 1994.

[6] C. L. Chung, C. H. Chen, J. R. Sheu, Y. C. Chen, and S. C. Chang, "Proinflammatory cytokines, transforming growth factor-β1, and fibrinolytic enzymes in loculated and free-flowing pleural exudates," *Chest*, vol. 128, no. 2, pp. 690–697, 2005.

[7] T. C. Bithell, *Wintrobe's Clinical Hematology*, Lea & Febiger, Philadelphia, Pa, USA, 1993.

[8] S. Idell, W. Girard, K. B. Koenig, J. McLarty, and D. S. Fair, "Abnormalities of pathways of fibrin turnover in the human pleural space," *The American Review of Respiratory Disease*, vol. 144, no. 1, pp. 187–194, 1991.

[9] S. Idell, A. P. Mazar, P. Bitterman, S. Mohla, and A. L. Harabin, "Fibrin turnover in lung inflammation and neoplasia," *The American Journal of Respiratory and Critical Care Medicine*, vol. 163, no. 2, pp. 578–584, 2001.

[10] M. S. Pepper, N. Ferrara, L. Orci, and R. Montesano, "Vascular endothelial growth factor (VEGF) induces plasminogen activators and plasminogen activator inhibitor-1 in microvascular endothelial cells," *Biochemical and Biophysical Research Communications*, vol. 181, no. 2, pp. 902–906, 1991.

[11] Y. B. Guo, I. Kalomenidis, M. Hawthorne, K. S. Parman, K. B. Lane, and R. W. Light, "Pleurodesis is inhibited by anti-vascular endothelial growth factor antibody," *Chest*, vol. 128, no. 3, pp. 1790–1797, 2005.

[12] L. R. Teixeira, F. S. Vargas, M. M. P. Acencio et al., "Blockage of vascular endothelial growth factor (VEGF) reduces experimental pleurodesis," *Lung Cancer*, vol. 74, no. 3, pp. 392–395, 2011.

[13] S. C. C. Ribeiro, F. S. Vargas, L. Antonangelo et al., "Monoclonal anti-vascular endothelial growth factor antibody reduces fluid volume in an experimental model of inflammatory pleural effusion," *Respirology*, vol. 14, no. 8, pp. 1188–1193, 2009.

[14] C. L. Chung, S. H. Hsiao, G. Hsiao, J. R. Sheu, W. L. Chen, and S. C. Chang, "Clinical Importance of Angiogenic Cytokines, Fibrinolytic Activity and Effusion Size in Parapneumonic Effusions," *PLoS ONE*, vol. 8, no. 1, Article ID e53169, 2013.

[15] C. L. Chung, C. H. Chen, C. Y. Yeh, J. R. Sheu, and S. C. Chang, "Early effective drainage in the treatment of loculated tuberculous pleurisy," *European Respiratory Journal*, vol. 31, no. 6, pp. 1261–1267, 2008.

[16] D. Jiménez Castro, G. Díaz, E. Pérez-Rodríguez, and R. W. Light, "Prognostic features of residual pleural thickening in parapneumonic pleural effusions," *European Respiratory Journal*, vol. 21, no. 6, pp. 952–955, 2003.

[17] D. S. Cheng, R. M. Rodriguez, E. A. Perkett et al., "Vascular endothelial growth factor in pleural fluid," *Chest*, vol. 116, no. 3, pp. 760–765, 1999.

[18] F. Economidou, K. M. Antoniou, N. Tzanakis, K. Sfiridaki, N. M. Siafakas, and S. E. Schiza, "Angiogenic molecule Tie-2 and VEGF in the pathogenesis of pleural effusions," *Respiratory Medicine*, vol. 102, no. 5, pp. 774–779, 2008.

[19] T. S. Kiropoulos, K. Kostikas, K. I. Gourgoulianis et al., "Vascular endothelial growth factor levels in pleural fluid and serum of patients with tuberculous pleural effusions," *Chest*, vol. 128, no. 1, article 128, pp. 468–469, 2005.

[20] F. Alatas, Ö. Alatas, M. Metintas, A. Özarslan, S. Erginel, and H. Yildirim, "Vascular endothelial growth factor levels in active pulmonary tuberculosis," *Chest*, vol. 125, no. 6, pp. 2156–2159, 2004.

[21] C. S. Grove and Y. C. G. Lee, "Vascular endothelial growth factor: the key mediator in pleural effusion formation," *Current Opinion in Pulmonary Medicine*, vol. 8, no. 4, pp. 294–301, 2002.

[22] Y. Wu, Q. Zhang, D. K. Ann et al., "Increased vascular endothelial growth factor may account for elevated level of plasminogen activator inhibitor-1 via activating ERK1/2 in keloid fibroblasts," *The American Journal of Physiology—Cell Physiology*, vol. 286, no. 4, pp. C905–C912, 2004.

[23] T. Fukumoto, A. Matsukawa, T. Yoshimura et al., "IL-8 is an essential mediator of the increased delayed-phase vascular permeability in LPS-induced rabbit pleurisy," *Journal of Leukocyte Biology*, vol. 63, no. 5, pp. 584–590, 1998.

[24] C. Alemán, J. Alegre, J. Monasterio et al., "Association between inflammatory mediators and the fibrinolysis system in infectious pleural effusions," *Clinical Science*, vol. 105, no. 5, pp. 601–607, 2003.

[25] A. Candela, J. Andujar, L. Hernández et al., "Functional sequelae of tuberculous pleurisy in patients correctly treated," *Chest*, vol. 123, no. 6, pp. 1996–2000, 2003.

[26] A. de Pablo, V. Villena, J. Echave-Sustaeta, and A. L. Encuentra, "Are pleural fluid parameters related to the development of residual pleural thickening in tuberculosis?" *Chest*, vol. 112, no. 5, pp. 1293–1297, 1997.

[27] C. C. Hua, L. C. Chang, Y. C. Chen, and S. C. Chang, "Proinflammatory cytokines and fibrinolytic enzymes in tuberculous and malignant pleural effusions," *Chest*, vol. 116, no. 5, pp. 1292–1296, 1999.

[28] E. Kunter, A. Ilvan, E. Kilic et al., "The effect of pleural fluid content on the development of pleural thickness," *International Journal of Tuberculosis and Lung Disease*, vol. 6, no. 6, pp. 516–522, 2002.

[29] F. C. Lin, Y. C. Chen, F. J. Chen, and S. C. Chang, "Cytokines and fibrinolytic enzymes in tuberculous and parapneumonic effusions," *Clinical Immunology*, vol. 116, no. 2, pp. 166–173, 2005.

[30] I. Gerogianni, M. Papala, P. Tsopa et al., "Could IFN-γ predict the development of residual pleural thickening in tuberculous pleurisy?" *Monaldi Archives for Chest Disease—Pulmonary Series*, vol. 69, no. 1, pp. 18–23, 2008.

[31] Y. F. Lai, M. C. Su, H. H. Weng, J. T. Wu, and C. T. Chiu, "Sonographic septation: a predictor of sequelae of tuberculous pleurisy after treatment," *Thorax*, vol. 64, no. 9, pp. 806–809, 2009.

[32] C. H. Lee, W. J. Wang, R. S. Lan, Y. H. Tsai, and Y. C. Chiang, "Corticosteroids in the treatment of tuberculous pleurisy. A double-blind, placebo-controlled, randomized study," *Chest*, vol. 94, no. 6, pp. 1256–1259, 1988.

[33] J. T. Huggins and S. A. Sahn, "Causes and management of pleural fibrosis," *Respirology*, vol. 9, no. 4, pp. 441–447, 2004.

[34] C. R. Kunz, M. R. Jadus, G. D. Kukes, F. Kramer, V. N. Nguyen, and S. A. Sasse, "Intrapleural injection of transforming growth factor-β antibody inhibits pleural fibrosis in empyema," *Chest*, vol. 126, no. 5, pp. 1636–1644, 2004.

[35] E. T. Pavlidis and T. E. Pavlidis, "Role of bevacizumab in colorectal cancer growth and its adverse effects: a review," *World Journal of Gastroenterology*, vol. 19, no. 31, pp. 5051–5060, 2013.

[36] A. Chiang and C. D. Regillo, "Preferred therapies for neovascular age-related macular degeneration," *Current Opinion in Ophthalmology*, vol. 22, no. 3, pp. 199–204, 2011.

Hindawi Publishing Corporation
The Scientific World Journal
Volume 2015, Article ID 492683, 9 pages
http://dx.doi.org/10.1155/2015/492683

Research Article

Static Magnetic Field Attenuates Lipopolysaccharide-Induced Inflammation in Pulp Cells by Affecting Cell Membrane Stability

Sung-Chih Hsieh,[1,2] Jeng-Ting Tsao,[3] Wei-Zhen Lew,[1] Ya-Hui Chan,[1] Lin-Wen Lee,[4] Che-Tong Lin,[1] Yung-Kai Huang,[5] and Haw-Ming Huang[1,6]

[1] *School of Dentistry, College of Oral Medicine, Taipei Medical University, Taipei 11031, Taiwan*
[2] *Department of Dentistry, Wan Fang Hospital, Taipei 11696, Taiwan*
[3] *Division of Allergy and Immunology, Department of Internal Medicine, Cathay General Hospital, Taipei 10630, Taiwan*
[4] *Department of Microbiology and Immunology, Taipei Medical University, Taipei 11031, Taiwan*
[5] *School of Oral Hygiene, College of Oral Medicine, Taipei Medical University, 250 Wu-Hsing Street, Taipei 11031, Taiwan*
[6] *Graduate Institute of Biomedical Materials and Tissue Engineering, College of Dental Medicine, Taipei Medical University, 250 Wu-Hsing Street, Taipei 11031, Taiwan*

Correspondence should be addressed to Yung-Kai Huang; ykhuang@tmu.edu.tw and Haw-Ming Huang; hhm@tmu.edu.tw

Received 17 July 2014; Accepted 28 August 2014

Academic Editor: Duen-Suey Chou

One of the causes of dental pulpitis is lipopolysaccharide- (LPS-) induced inflammatory response. Following pulp tissue inflammation, odontoblasts, dental pulp cells (DPCs), and dental pulp stem cells (DPSCs) will activate and repair damaged tissue to maintain homeostasis. However, when LPS infection is too serious, dental repair is impossible and disease may progress to irreversible pulpitis. Therefore, the aim of this study was to examine whether static magnetic field (SMF) can attenuate inflammatory response of dental pulp cells challenged with LPS. In methodology, dental pulp cells were isolated from extracted teeth. The population of DPSCs in the cultured DPCs was identified by phenotypes and multilineage differentiation. The effects of 0.4 T SMF on DPCs were observed through MTT assay and fluorescent anisotropy assay. Our results showed that the SMF exposure had no effect on surface markers or multilineage differentiation capability. However, SMF exposure increases cell viability by 15%. In addition, SMF increased cell membrane rigidity which is directly related to higher fluorescent anisotropy. In the LPS-challenged condition, DPCs treated with SMF demonstrated a higher tolerance to LPS-induced inflammatory response when compared to untreated controls. According to these results, we suggest that 0.4 T SMF attenuates LPS-induced inflammatory response to DPCs by changing cell membrane stability.

1. Introduction

Pulpitis is a disease caused by inflammation of dental pulp. When such inflammation occurs, pressure inside pulp cavity increases that cannot be dissipated by surrounding soft tissue because pulp is surrounded by hard tissue [1]. Since pulp contains blood vessels and nerves, pressure created by pulpitis causes pain and creates difficulties for blood and nutrient supply.

It is well known that pulp tissue is composed of immune cells, ectomesenchymal cells, fibroblasts, preodontoblasts, odontoblasts, and dental pulp stem cells (DPSCs) [2]. Of these cells, DPSCs exhibit multipotent differentiation ability; thus, tissue engineering study has gradually come to focus on DPSCs [3, 4]. In addition, DPSCs were reported to have excellent potential for dentin repair and tooth regeneration [5]. Given this potential use in tissue engineering, investigations into the treatment of bacterial induced pulpitis and tooth preservation are increasingly important for regenerative medicine. Until now, however, the only way to prevent pain is by removing the pulp via root canal treatment or tooth extraction. In this regard, several scholars have focused their aim on investigating the immunoresponse of DPSCs and dental pulp cells (DPCs) [5–9].

The gram-negative bacterial cell wall component lipopolysaccharide (LPS) is now well documented as an initiator of pulpitis. Among gram-negative bacteria, *Porphyromonas gingivalis* can be found in 48% of teeth with endodontic infection [10]. In addition, Botero et al. demonstrated that *Porphyromonas* endodontalis LPS induce cytokine expression in DPSCs and DPCs [7]. It is now known that the coreceptor of LPS formed by the Toll-like receptor 4 (TLR4) and CD14 is the binding site for signaling LPS-induced cytotoxicity [11, 12]. Even though DPSCs and DPCs express LPS receptors (TLRs) on their membrane surfaces [5, 7, 9], it is hard to bring medicines to the infected pulp tissue because these sites are surrounded by hard tissue. For the successful regeneration of pulp tissue in a root canal, neutralizing the adverse effects of residual LPS remains a challenge for scientists [5].

Static magnetic fields (SMFs) are physical stimulators that have anti-inflammatory effects on human macrophages and lymphocytes [13, 14] and on cytokine release by human peripheral blood mononuclear cells [15]. In an in vitro study, Lin et al. found that long-term SMF exposure inhibits LPS-induced cytotoxicity of fibroblasts [16]. Shen et al. also found that SMF attenuates lipopolysaccharide-induced neuroinflammatory response [17]. After an animal study, Lin's group showed for the first time that LPS-injected mice that had been preexposed to an SMF exhibited significantly better survival rates compared to unexposed control mice [18]. All these studies suggest that SMF has the potential to be an alternative stimulation source for controlling LPS-induced inflammatory response. Nevertheless, no study has yet investigated the anti-inflammatory effects of SMF on dental pulp cells. The aim of this study was to test whether or not SMF had attenuating effects on inflammatory response of LPS stimulated dental pulp cells.

2. Materials and Methods

2.1. DPCs Isolation and Culture. Human dental pulp was obtained from healthy wisdom teeth or orthodontically extracted premolars under the approval of the TMU-Joint Institutional Review Board. Freshly extracted teeth were immediately cleaned with Dulbecco's phosphate-buffered saline and sent to the lab for storage in a culture medium. The isolation method was modified from the outgrowth method discussed in previous studies [19–21]. The crown portions were separated using a sterile mortar and pestle after PBS irrigation. Pulp tissue was extirpated with forceps and sliced into small pieces with a scalpel. These small prices of minced pulp tissues were then cultured on 3.5 cm petri dishes using α-minimal essential medium (α-MEM; Gibco/Invitrogen, Grand Island, NY) supplemented with 15% FBS (Gibco/Invitrogen, Grand Island, NY), 100 μM L-ascorbic acid 2-phosphate (Sigma-Aldrich, St. Louis, MO), and 1% antibiotic-antimycotic (Gibco/Invitrogen, Grand Island, NY) at 37°C in 5% CO_2. Until reaching 70–80% confluence, DPCs were further cultured in new 10 cm petri dishes for further propagation.

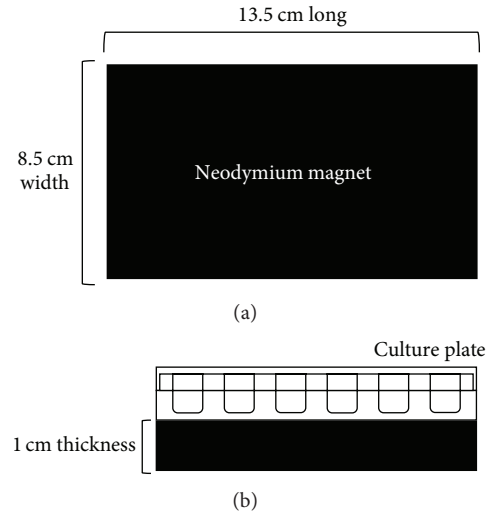

Figure 1: Schematic representation of the static magnetic field equipment setup. (a) Neodymium blocks 13.5 × 8.5 × 1 cm were used to provide a 0.4 T static magnetic field. (b) The 24-well culture plate was placed directly on the north pole (on the base) of the magnetic block.

2.2. SMF Equipment Setup and Exposure. A rectangular neodymium magnetic block 8.5 cm wide, 13.5 cm long, and 1 cm thick (Figure 1) with a 0.4 T flux density was used in our experiment to generate the SMF exposure environment. For the experimental group, DPCs were seeded on 24-well plates and placed on the north-pole surface of the neodymium magnet block for SMF stimulation. For sham groups, the cell culture dishes were placed on another similar but nonmagnetized neodymium block.

2.3. DPSC Identification. To identify the DPSCs population of the cultured DPCs, a set of surface markers were determined and differential stimulation was performed. Cell surface markers were labeled with corresponding antibodies and analyzed by flow cytometry. The DPCs numbering 1×10^5 were cultured on 10 cm petri dishes and placed on the 0.4 T magnetic block for a period of 5 days. Then cells were collected and fixed with 75% ethanol at −20°C overnight. The fixed cells were incubated with the following fluorescent-conjugated antibodies in PBS at 4°C for 30 minutes: CD14 (AbD Serotec, NC, USA), CD34 (Santa Cruz Biotechnology, Santa Cruz, CA, USA), CD29 (Exbio, Praha, Czech Republic), CD73 (BD, Biosciences, Heidelberg, Germany), CD90, CD105 (Biolegend, San Diego, CA, USA), and CD146 (Santa Cruz). The cell suspension was then analyzed by flow cytometry (Guava EasyCyte Mini Base System, Guava Technologies, Millipore, Hayward, CA, USA) and raw data were analyzed by FlowJo software (TreeStar Inc., Ashland, USA).

The differentiation induction method was performed according to a previous published report [22]. Briefly, dental pulp cell solutions with a concentration of 2×10^4

cells/mL were cultured in 24-well plates for further differential induction. The 24-well plates were placed on the magnetized block or sham block for the whole culturing period. At the same time, basal medium was changed to osteogenesis, adipogenesis, and chondrogenesis induction medium, respectively, and cultured for 1 month. During this induction period, the cultured cell medium was changed twice a week. For the osteogenesis stimulus, 1.8 mM KH_2PO_4 and 0.01 μM dexamethasone were supplemented into the complete culture medium. For the adipogenesis stimulus, 10 μg/mL insulin, 0.5 μM hydrocortisone, 500 μM IBMX, and 60 μM indomethacin were supplemented into the culture medium. For the chondrogenesis stimulus, 0.1 μM dexamethasone, 10 ng/mL TGF-β, and 1 mM sodium pyruvate were added to the serum-free complete medium. Control cells were cultured with basal medium on the magnetized or nonmagnetized neodymium magnet for the whole experimental period. At the end of the period, cells were fixed with 4% paraformaldehyde and stained with 2% Alizarin Red S, Oil Red O, and 1% Safranin O for calcium deposition, intracellular lipid droplet, or glycosaminoglycan observation, respectively. Stained cells were then washed with PBS several times and observed under an optical microscope (Nikon Eclipse TS100, Japan).

2.4. The Effect of 0.4 T SMF on DPC Proliferation. MTT assays were performed to determine the effect of 0.4 T SMF on DPC proliferation. Cell solutions with a concentration of 2×10^4 cells/mL were seeded in two identical 24-well plates and placed on the surface of either the magnetized or nonmagnetized magnetic block for 5 days. Fifty μL of tetrazolium salt (MTT) was added according to the supplier's instructions (MTT kit, Roche Applied Science, Mannheim, Germany) every 24 hours. After standing for 4 hours, formazan dye was solubilized by the addition of 500 μL dimethyl sulfoxide (DMSO) and quantitated using a microplate reader (Model 2020, Anthos Labtec Instruments, Wals, Austria) at 570/690 nm. The optical density (OD) absorbance value was directly correlated to DPC number.

2.5. LPS Challenge to SMF-Exposed DPCs. To test the effect of the SMF on LPS-induced inflammatory response of DPCs, cells were starved in a serum-free medium for 12 hours. After being washed with PBS, cells were incubated with commercial *Pseudomonas aeruginosa* derived LPS (Sigma) at serial diluted concentrations ranging from 600 μg/mL to 0 μg/mL. After 12 hours, the MTT assay was performed to evaluate the viability of SMF-exposed and sham-exposed cells. Further, the cell morphology of SMF-exposed or sham-exposed LPS-challenged DPCs was observed with an optical microscope (Nikon Eclipse TS100, Japan).

2.6. Membrane Fluidity Measurement by Fluorescent Anisotropy. For the membrane fluidity test, 100 μL cell solutions with a concentration of 5×10^4 cells/mL were cultured in 96-well black plates for 24 hours. Then the cells were placed in the magnetic environments for an additional 8 hours. After discarding the culturing medium, 100 μL of 1 μM TMA-DPH or DPH was added to each well to label the cell membrane. Then cells were analyzed with a multilabel plate reader. Excitation and emission wavelengths were set at 355 nm and 430 nm, respectively. Fluorescent anisotropy was calculated using the following equation [23]:

$$r = \frac{(I_{\parallel} - I_{\perp})}{(I_{\parallel} + 2I_{\perp})}, \quad (1)$$

where $I_{\parallel}$ is fluorescence intensity measured through vertical excitation and vertical emission polarization filters and $I_{\perp}$ is the analog measured through vertical excitation and horizontal emission polarization filters. Higher levels of fluorescent anisotropy indicate a decrease in dye mobility and increase in membrane structural order.

2.7. Statistical Analysis. The cell proliferation, cell viability, and cell membrane fluorescent anisotropy data were presented using descriptive statistics. Comparisons of means between SMF-exposed group and sham-exposed groups were performed using unpaired Student's t-test. The significance level was set at $P < 0.05$.

3. Results

Cell surface markers were labeled with fluorescent-conjugated antibodies and analyzed by flow cytometry. The results demonstrated that the CD markers of SMF-exposed group were not different from previous published studies. It is positive for CD29, CD73, CD90, CD105, and CD146 and negative for CD14 and CD34 (Figure 2). There were high expression in CD29 (87.2%) and CD90 (95.7%) and moderate expression in CD73 (48.3%), CD105 (30.9%), and CD146 (30.1%), indicating that cells exhibit mesenchymal stem cell-like phenotypes even after prolonged culturing in SMF environment.

After culturing DPCs with the differentiation induction medium, the cells were stained with Alizarin Red, Oil Red O, and Safranin O. Observed under an optical microscope, sporadic calcified nodules in osteogenesis cells (Figure 3), intracellular lipid droplets in adipogenesis cells (Figure 4), and glycosaminoglycan matrix around the chondrogenesis cells (Figure 5) were found. The differentiation capability of SMF-exposed group showed no obvious superiority to the sham-exposed group, in neither osteogenesis, adipogenesis, nor chondrogenesis induction.

The MTT assay showed significantly higher cell viability ($P < 0.001$) for SMF-exposed DPCs compared to sham-exposed cells (Figure 6). Cell viability increased up to 15% in SMF-exposed groups during day 3 and day 4. That is, DPCs exposed to a 0.4 T SMF demonstrated a higher proliferation rate compared with the sham-exposed DPCs (Figure 7). Cell viability of DPCs incubated with serial diluted LPS concentrations for 12 hours was also measured by MTT assay. When DPCs were incubated with LPS with concentrations of 400 μg/mL and 600 μg/mL, the tested optical densities decreased to 96.66% and 68.32% of the control values, respectively (Figure 7). However, the results showed that cell

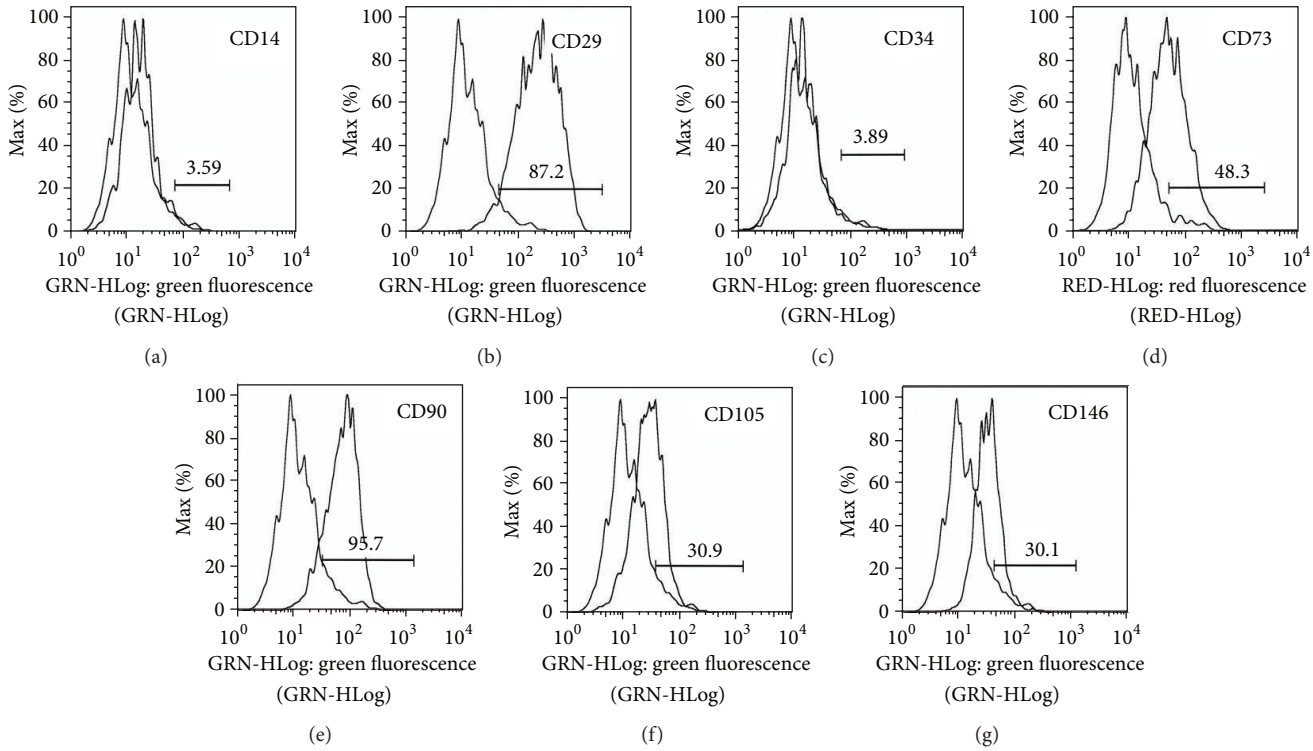

Figure 2: Flow cytometry histograms showed the DPSCs surface marker expressions after 0.4 T SMF exposure. Unstained control cells and cells stained with antibodies against the surface proteins were overlapped. Brackets indicate the positive cell populations in percent.

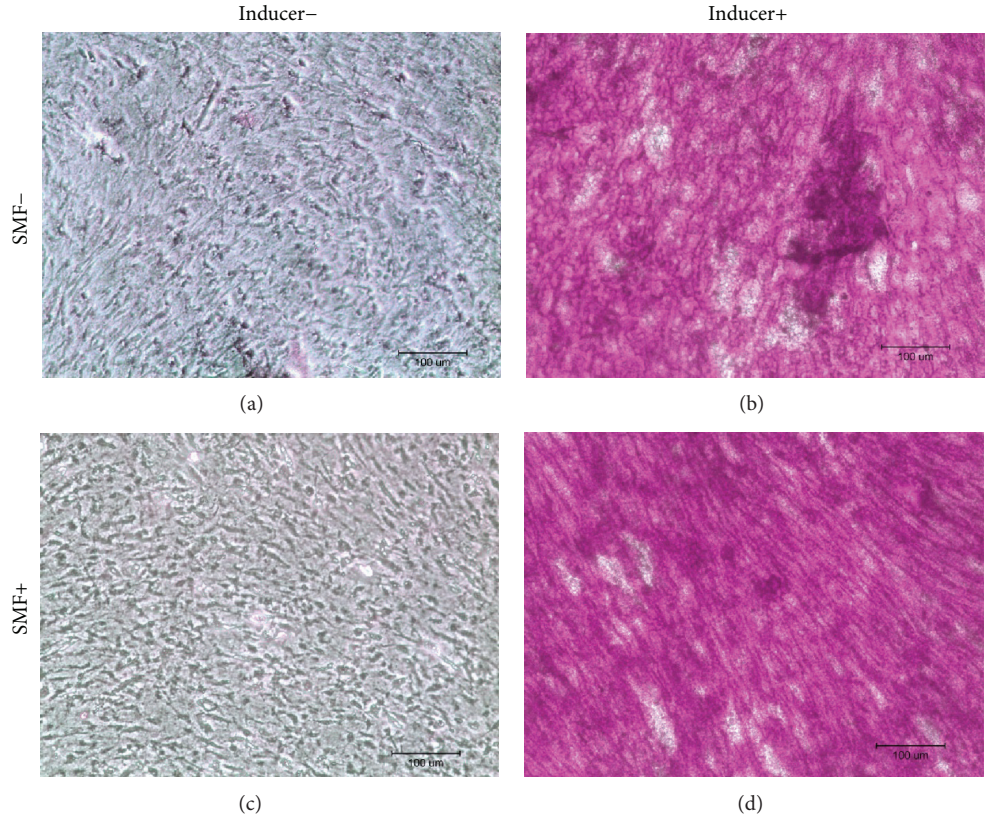

Figure 3: Results of Alizarin Red staining showed the calcified deposition in red. There were no significant differences between SMF-exposed and sham-exposed cells after osteogenesis induction. Neither of noninduction controls had calcified deposition present.

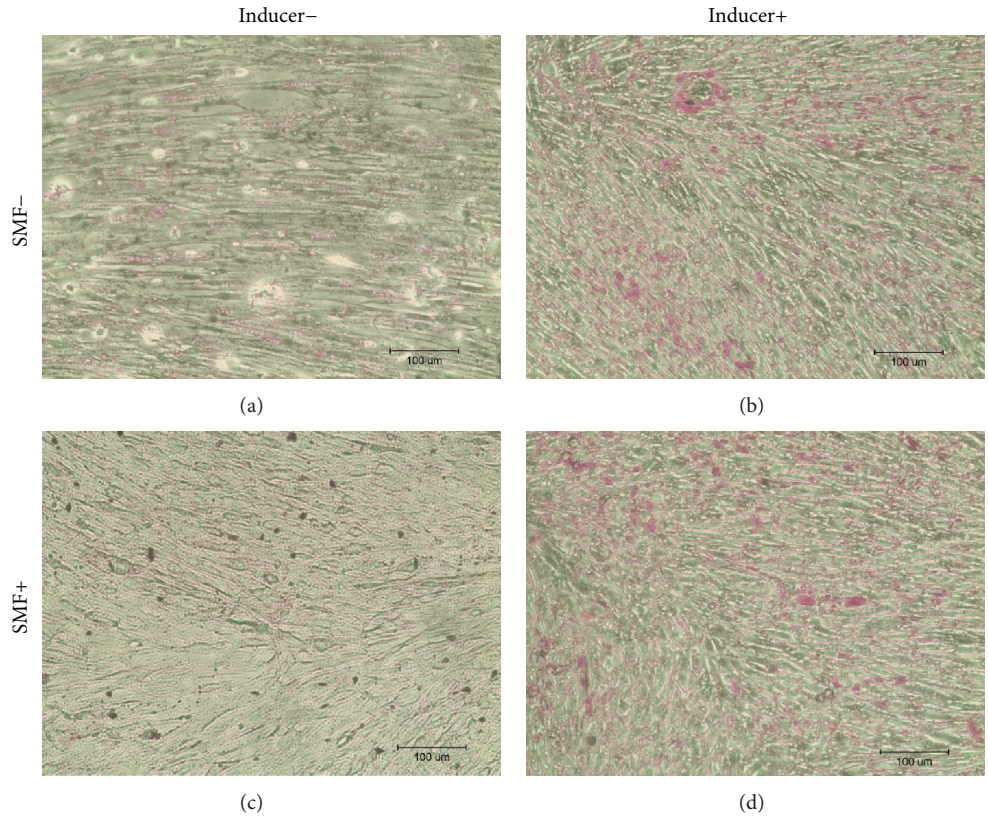

Figure 4: Oil Red O staining results showed the intracellular lipid droplets stained in red after adipogenesis induction. No significant differences could be observed between SMF-exposed and sham-exposed DPCs after adipogenesis induction.

viability of LPS-challenged DPCs had significantly higher OD value when cotreated with the 0.4 T SMF ($P < 0.001$). When treated with 400 μg/mL and 600 μg/mL LPS, the optical densities of SMF treated groups were 1.25 and 1.34 times higher than sham-exposed DPCs.

The morphological changes in each experimental group are presented in Figure 8. Sham-exposed DPCs were evenly distributed and formed a continuous monolayer throughout each well (Figure 8(a)). The SMF-exposed DPCs had no obvious changes when compared with control group (Figure 8(b)). Otherwise, more-rounded shape in cell form and suspended debris was observed in the LPS-challenged group (Figure 8(c)). Interestingly, LPS treatment caused less cell pattern change and debris emergence when cells were cotreated with 0.4 T SMF (Figure 8(d)).

There was no significant difference in fluorescent anisotropy between SMF-exposed and sham-exposed cells when labeled with TMA-DPH (Figure 9). However, the average DPH fluorescent anisotropy of the exposed cells (0.14) was significantly higher ($P < 0.001$) than the sham-exposed group (0.11). The higher fluorescent anisotropy represents the limited orientation of intercalated DPH. This result suggests that 0.4 T SMF increased the order of hydrophilic region of cell membrane and enhanced the rigidity of lipid bilayer.

4. Discussion

It was reported that approximately 1% of pulp cells have the potential to differentiate into odontoblast-like cells and secrete proteins for forming dentin [24]. In this study, immunostaining of various surface markers was performed by flow cytometry. The identity of the DPSCs was confirmed by negative expression of hematopoietic markers CD14 and CD34 and positive expression of CD29, CD73, CD 105, and CD146. In addition, the high expression of CD29, CD73, CD90, and CD105 coincides with other studies [22, 25]. Thus, the DPC sample contain cells meeting criteria of DPSCs.

In 2010, Hsu and Chang reported that the response in proliferation rates of rat dental pulp cells to SMF is insensitivity [26]. They exposed these cells to a 290 mT SMF and found no visible change in cell proliferation rates. However, their results showed that SMF can be an adjuvant to accelerate the osteogenic differentiation and mineralization of cells when rat dental pulp cells were cultured with an osteogenic induction medium combined with SMF exposure [27]. In this study, we found that continuous exposure to a 0.4 T SMF does not affect the multidifferentiation capability of stem cells (Figures 3–5). However, an increase in osteogenic differentiation was not observed in this study. This is because the SMFs were not provided during the osteogenic induction

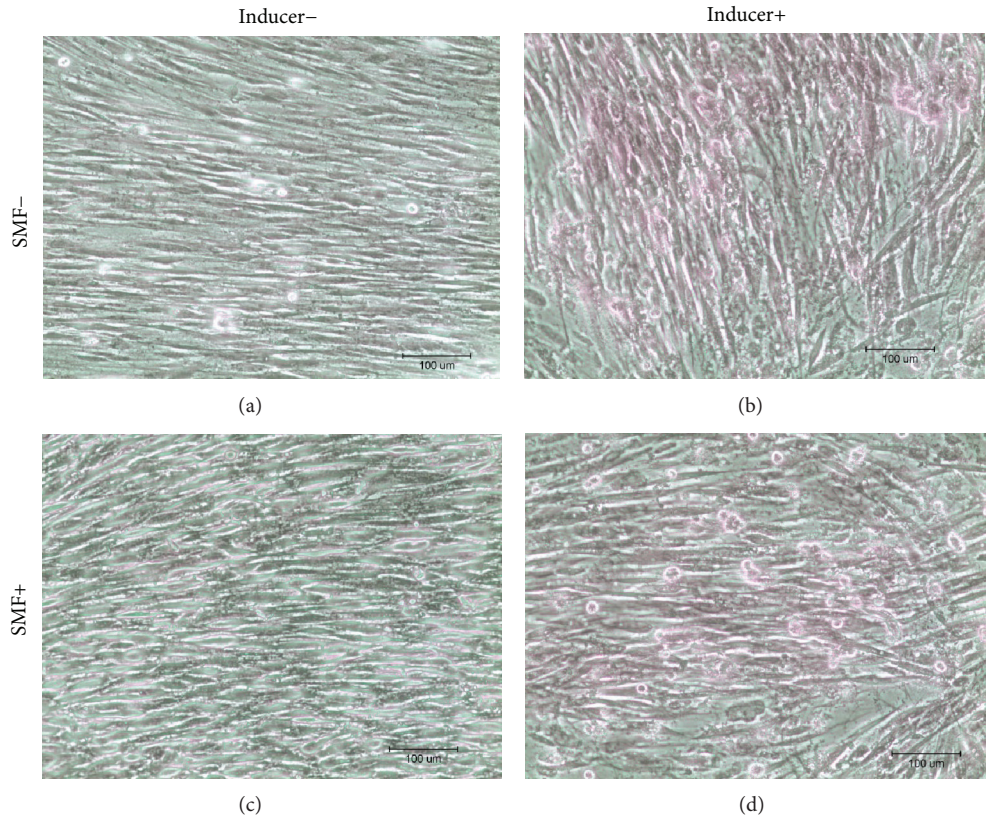

Figure 5: Safranin O staining results showed the glycosaminoglycan extracellular matrix around the cells in pink to red after chondrogenesis induction. No significant differences could be observed between SMF-exposed and sham-exposed DPCs after adipogenesis induction.

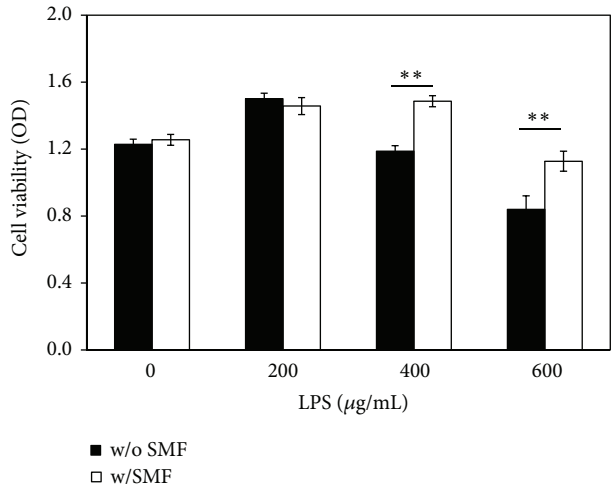

Figure 6: DPC cell grown after prolonged culturing in an SMF environment was enhanced. Cell viability of the SMF-exposed group was significantly higher than the sham-exposed group ($P < 0.001$) at day 3 and day 4.

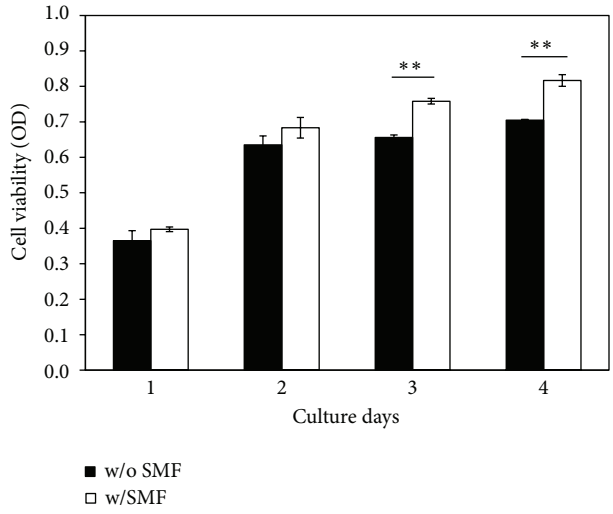

Figure 7: The effect of SMF on the LPS-induced cell viability changes to DPCs. Pretreatment with a 0.4 T SMF significantly attenuated the inflammatory response of LPS.

process. Again, enhancement of the proliferation of SMF-exposed human DPCs was found in this study; viability of SMF-exposed cells was 15% higher when compared with sham-exposed cells after 3 days of culturing.

The aim of this study was to investigate whether or not SMFs reduced the toxicity effect of LPS when added to DPCs. LPS was found in apical tissues as well as root canals during endodontic infection [27, 28]. Previous studies reported that

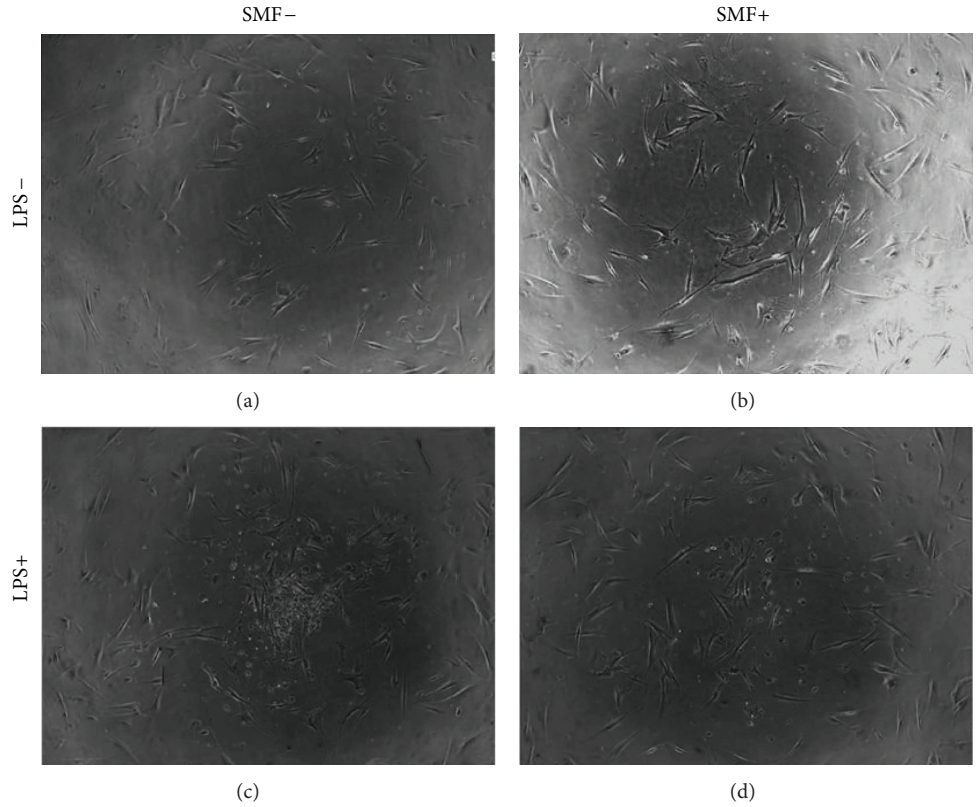

Figure 8: Representation of the optical microscope images of DPC cultures. (a) Sham-exposed DPCs showed fusiform to polygonal shape in a monolayer distribution. (b) There was no difference in cell shape or growth pattern in DPCs exposed to 0.4 T SMF. (c) When challenged with LPS, cell shape changed from fusiform to round, and much suspended debris appeared. (d) However, LPS-challenged DPCs cotreated with 0.4 T SMF had a lower level of shape disorder and suspended debris.

this molecule is potentially harmful to host cells as a toxin and as an immune stimulant [5, 28]. Our data also shows that LPS has a toxic effect on DPCs in a dose-dependent manner (Figure 7). Interestingly, however, cell viability of the LPS-challenged DPCs exposed to a 0.4 T SMF was 25% higher than that of the sham-exposed group (Figure 7). These results can be compared with the microscopic observations (Figure 8), which show that development of endotoxin tolerance in the dental pulp cells occurred after 12 hours of continuous 0.4 T SMF exposure. This effect may result from the reduction of proinflammatory cytokine release and increase of anti-inflammatory cytokine release by fibroblasts.

Several studies suggest that DPCs are involved in immune response during pulpal infection through the activation of IL-1 [5–7, 29]. Lin et al. found that long-term continuous exposure to a static magnetic field reduces lipopolysaccharide-induced inflammatory response of fibroblasts by increasing the production of IL-1 receptor antagonist [18]. It was reported that the plasma membrane is the primary site where SMF effect is seen [30, 31]. This effect can also be found in DPCs. Lin et al. used SMFs to improve DPC membrane stability which resulted in a reduction in damage caused by ice crystals during a freezing procedure [32]. In this study, after exposure to a 0.4 T SMF, the DPC membrane fluorescence anisotropy was significantly higher than in the sham-exposed group (Figure 9). These results are consistent with previous studies which also found that 0.4 T SMF increases cell membrane rigidity of MG-63, microglia cells, and red blood cells [17, 33–35]. Since phospholipids can be oriented by external magnetic fields when they are exposed

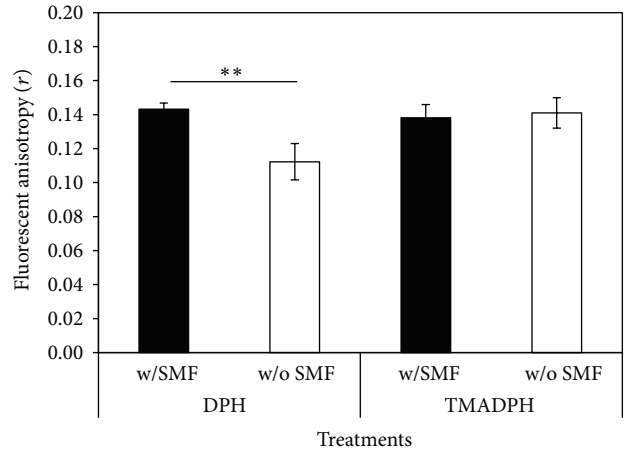

Figure 9: Comparison of fluorescent anisotropy change in DPCs exposed to 0.4 T SMF. Higher fluorescent anisotropy of SMF-exposed cells was found when labeled with DPH.

to flux densities exceeding a certain threshold [36–38], dental pulp cell membranes can be altered and the binding capability between LPS and its cross membrane receptor, Toll-like receptor 4, can also be changed.

Based on these findings, it appears reasonable to suggest that SMF stimulation inhibits LPS-induced inflammatory response of dental pulp cells. Moreover, SMF exposure can also enhance the proliferation of dental pulp cells in the later days. Therefore, although more advanced studies are needed, we suggested that SMF can be a possible choice to be used in clinical practice to treat LPS infected dentine-pulp complex.

Conflict of Interests

The authors declare that they have no conflict of interests.

Authors' Contribution

Sung-Chih Hsieh and Jeng-Ting Tsao contributed equally to this work.

Acknowledgments

This paper is supported by grants from the Cathay General Hospital-Taipei Medical University (102CGH-TMU-01-3) and National Science Council, Executive Yuan, Taiwan (NSC 102-2314-B-038-019 and NSC 101-2320-B-038-003).

References

[1] K. M. Hargreaves, H. E. Goodis, S. Seltzer, and I. B. Bender, *Seltzer and Bender's Dental Pulp*, Quintessence, Chicago, Ill, USA, 2002.

[2] J. V. Ruch, H. Lesot, and C. Begue-Kirn, "Odontoblast differentiation," *The International Journal of Developmental Biology*, vol. 39, no. 1, pp. 51–68, 1995.

[3] M. Gebhardt, P. E. Murray, K. N. Namerow, S. Kuttler, and F. Garcia-Godoy, "Cell survival within pulp and periodontal constructs," *Journal of Endodontics*, vol. 35, no. 1, pp. 63–66, 2009.

[4] L. Pierdomenico, L. Bonsi, M. Calvitti et al., "Multipotent mesenchymal stem cells with immunosuppressive activity can be easily isolated from dental pulp," *Transplantation*, vol. 80, no. 6, pp. 836–842, 2005.

[5] V. T.-K. Yamagishi, C. D. Torneck, S. Friedman, G. T.-J. Huang, and M. Glogauer, "Blockade of TLR2 inhibits *Porphyromonas gingivalis* suppression of mineralized matrix formation by human dental pulp stem cells," *Journal of Endodontics*, vol. 37, no. 6, pp. 812–818, 2011.

[6] J. Chang, C. Zhang, N. Tani-Ishii, S. Shi, and C.-Y. Wang, "NF-κB activation in human dental pulp stem cells by TNF and LPS," *Journal of Dental Research*, vol. 84, no. 11, pp. 994–998, 2005.

[7] T. M. Botero, J. S. Son, D. Vodopyanov, M. Hasegawa, C. E. Shelburne, and J. E. Nör, "MAPK signaling is required for LPS-induced VEGF in pulp stem cells," *Journal of Dental Research*, vol. 89, no. 3, pp. 264–269, 2010.

[8] W. He, T. Qu, Q. Yu et al., "LPS induces IL-8 expression through TLR4, MyD88, NF-kappaB and MAPK pathways in human dental pulp stem cells," *International Endodontic Journal*, vol. 46, no. 2, pp. 128–136, 2013.

[9] W. He, Z. Wang, Z. Zhou et al., "Lipopolysaccharide enhances Wnt5a expression through toll-like receptor 4, myeloid differentiating factor 88, phosphatidylinositol 3-OH kinase/AKT and nuclear factor kappa B pathways in human dental pulp stem cells," *Journal of Endodontics*, vol. 40, no. 1, pp. 69–75, 2014.

[10] J. F. Siqueira Jr., I. N. Rôças, and M. G. Silva, "Prevalence and clonal analysis of *Porphyromonas gingivalis* in primary endodontic infections," *Journal of Endodontics*, vol. 34, no. 11, pp. 1332–1336, 2008.

[11] R. Dziarski, R. I. Tapping, and P. S. Tobias, "Binding of bacterial peptidoglycan to CD14," *Journal of Biological Chemistry*, vol. 273, no. 15, pp. 8680–8690, 1998.

[12] Q. Jiang, S. Akashi, K. Miyake, and H. R. Petty, "Cutting edge: lipopolysaccharide induces physical proximity between CD14 and Toll-like receptor 4 (TLR4) prior to nuclear translocation of NF-κB," *The Journal of Immunology*, vol. 165, no. 7, pp. 3541–3544, 2000.

[13] C. Vergallo, L. Dini, Z. Szamosvölgyi et al., "In vitro analysis of the anti-Inflammatory effect of inhomogeneous static magnetic field-exposure on human macrophages and lymphocytes," *PLoS ONE*, vol. 8, no. 8, Article ID e72374, 2013.

[14] S. Salerno, A. Lo Casto, N. Caccamo et al., "Static magnetic fields generated by a 0.5 T MRI unit affects in vitro expression of activation markers and interleukin release in human peripheral blood mononuclear cells (PBMC)," *International Journal of Radiation Biology*, vol. 75, no. 4, pp. 457–463, 1999.

[15] C. Aldinucci, J. B. Garcia, M. Palmi et al., "The effect of strong static magnetic field on lymphocytes," *Bioelectromagnetics*, vol. 24, no. 2, pp. 109–117, 2003.

[16] C.-T. Lin, S.-Y. Lee, C.-Y. Chen, C.-A. Chen, C.-P. Lin, and H.-M. Huang, "Long-term continuous exposure to static magnetic field reduces popolysaccharide-induced cytotoxicity of fibroblasts," *International Journal of Radiation Biology*, vol. 84, no. 3, pp. 219–226, 2008.

[17] L.-K. Shen, H.-M. Huang, P.-C. Yang et al., "A static magnetic field attenuates lipopolysaccharide-induced neuro-inflammatory response via IL-6-mediated pathway," *Electromagnetic Biology and Medicine*, vol. 33, no. 2, pp. 132–138, 2014.

[18] S.-L. Lin, W.-J. Chang, Y.-S. Lin et al., "Static magnetic field attenuates mortality rate of mice by increasing the production of IL-1 receptor antagonist," *International Journal of Radiation Biology*, vol. 85, no. 7, pp. 633–640, 2009.

[19] G. T. J. Huang, W. Sonoyama, J. Chen, and S. H. Park, "In vitro characterization of human dental pulp cells: various isolation methods and culturing environments," *Cell and Tissue Research*, vol. 324, no. 2, pp. 225–236, 2006.

[20] J. Wang, X. Wei, J. Ling, Y. Huang, and Q. Gong, "Side population increase after simulated transient ischemia in human dental pulp cell," *Journal of Endodontics*, vol. 36, no. 3, pp. 453–458, 2010.

[21] M. Yan, Y. Yu, G. Zhang, C. Tang, and J. Yu, "A journey from dental pulp stem cells to a bio-tooth," *Stem Cell Reviews and Reports*, vol. 7, no. 1, pp. 161–171, 2011.

[22] S.-Y. Lee, G.-W. Huang, J.-N. Shiung et al., "Magnetic cryopreservation for dental pulp stem cells," *Cells Tissues Organs*, vol. 196, no. 1, pp. 23–33, 2012.

[23] M. Przybylska, A. Koceva-Chyla, B. Rózga, and Z. Józwiak, "Cytotoxicity of daunorubicin in trisomic (+21) human fibroblasts: Relation to drug uptake and cell membrane fluidity," *Cell Biology International*, vol. 25, no. 2, pp. 157–170, 2001.

[24] J. Smith, M. Patel, L. Graham, A. J. Sloan, and P. R. Couper, "Dentine regeneration: key role for stem cells and molecular

signaling," *Oral Biosciences and Medicine*, vol. 2, no. 2-3, pp. 127–132, 2005.

[25] N. F. Lizier, A. Kerkis, C. M. Gomes et al., "Scaling-up of dental pulp stem cells isolated from multiple niches," *PLoS ONE*, vol. 7, no. 6, Article ID e39885, 2012.

[26] S.-H. Hsu and J.-C. Chang, "The static magnetic field accelerates the osteogenic differentiation and mineralization of dental pulp cells," *Cytotechnology*, vol. 62, no. 2, pp. 143–155, 2010.

[27] N. Horiba, Y. Maekawa, T. Matsumoto, and H. Nakamura, "A study of the distribution of endotoxin in the dentinal wall of infected root canals," *Journal of Endodontics*, vol. 16, no. 7, pp. 331–334, 1990.

[28] C. R. Barthel, L. G. Levin, H. M. Reisner, and M. Trope, "TNF-α release in monocytes after exposure to calcium hydroxide treated *Escherichia coli* LPS," *International Endodontic Journal*, vol. 30, no. 3, pp. 155–159, 1997.

[29] J. Coil, E. Tam, and J. D. Waterfield, "Proinflammatory cytokine profiles in pulp fibroblasts stimulated with lipopolysaccharide and methyl mercaptan," *Journal of Endodontics*, vol. 30, no. 2, pp. 88–91, 2004.

[30] A. D. Rosen, "Mechanism of action of moderate-intensity static magnetic fields on biological systems," *Cell Biochemistry and Biophysics*, vol. 39, no. 2, pp. 163–173, 2003.

[31] A. D. Rosen, "Studies on the effect of static magnetic fields on biological systems," *PIERS Online*, vol. 6, no. 2, pp. 133–136, 2010.

[32] S.-L. Lin, W.-J. Chang, C.-Y. Lin et al., "Static magnetic field increases survival rate of dental pulp stem cells during DMSO-free cryopreservation," *Electromagnetic Biology and Medicine*, vol. 23, pp. 1–7, 2014.

[33] C. Y. Lin, W. J. Chang, S. Y. Lee et al., "Influence of a static magnetic field on the slow freezing of human erythrocytes," *International Journal of Radiation Biology*, vol. 89, no. 1, pp. 51–56, 2013.

[34] C.-Y. Lin, P.-L. Wei, W.-J. Chang et al., "Slow freezing coupled static magnetic field exposure enhances cryopreservative efficiency—a study on human erythrocytes," *PLoS ONE*, vol. 8, no. 3, Article ID e58988, 2013.

[35] K.-H. Chiu, K.-L. Ou, S.-Y. Lee et al., "Static magnetic fields promote osteoblast-like cells differentiation via increasing the membrane rigidity," *Annals of Biomedical Engineering*, vol. 35, no. 11, pp. 1932–1939, 2007.

[36] A. Coots, R. Shi, and A. D. Rosen, "Effect of a 0.5-T static magnetic field on conduction in guinea pig spinal cord," *Journal of the Neurological Sciences*, vol. 222, no. 1-2, pp. 55–57, 2004.

[37] T. Suda and S. Ueno, "Magnetic orientation of red blood cell membranes," *IEEE Transactions on Magnetics*, vol. 30, no. 6, pp. 4713–4715, 1994.

[38] H. Aoki, H. Yamazaki, T. Yoshino, and T. Akagi, "Effects of static magnetic fields on membrane permeability of a cultured cell line," *Research Communications in Chemical Pathology and Pharmacology*, vol. 69, no. 1, pp. 103–106, 1990.

Hindawi Publishing Corporation
The Scientific World Journal
Volume 2015, Article ID 289647, 7 pages
http://dx.doi.org/10.1155/2015/289647

Research Article

Change of Scaling-Induced Proinflammatory Cytokine on the Clinical Efficacy of Periodontitis Treatment

Kou-Gi Shyu,[1,2] Cheuk-Sing Choy,[3,4] Daniel Chung-Lang Wang,[5] Wei-Chen Huang,[6] Shyuan-Yow Chen,[6] Chien-Hsun Chen,[6] Che-Tong Lin,[7] Chao-Chien Chang,[2,8] and Yung-Kai Huang[9]

[1]*Division of Cardiology, Shin Kong Wu Ho-Su Memorial Hospital, Taipei 111, Taiwan*
[2]*Graduate Institute of Clinical Medicine, Taipei Medical University, Taipei 110, Taiwan*
[3]*Department of Medicine, School of Medicine, College of Medicine, Taipei Medical University, Taipei 110, Taiwan*
[4]*Department of Emergency, Min-Sheng General Hospital, Taoyuan 330, Taiwan*
[5]*Department of Obstetrics and Gynecology, Min-Sheng General Hospital, Taoyuan 330, Taiwan*
[6]*Dental Department, Cathay General Hospital, Taipei 106, Taiwan*
[7]*School of Dentistry, College of Oral Medicine, Taipei Medical University, Taipei 110, Taiwan*
[8]*Department of Cardiology, Cathay General Hospital, Taipei 106, Taiwan*
[9]*School of Oral Hygiene, College of Oral Medicine, Taipei Medical University, Taipei 110, Taiwan*

Correspondence should be addressed to Chao-Chien Chang; change@seed.net.tw and Yung-Kai Huang; ykhuang@tmu.edu.tw

Received 3 October 2014; Revised 17 February 2015; Accepted 23 February 2015

Academic Editor: Philip Aloysius Thomas

Proinflammatory cytokines are key inflammatory mediators in periodontitis. This study aimed to investigate the relationship between proinflammatory cytokines in saliva and periodontal status. To investigate the usefulness of cytokines in the therapeutic approach for periodontal disease, the relationship between stimulated cytokine changes and the periodontitis treatment outcome was investigated in this study. Saliva was obtained from 22 patients diagnosed by dentists as having chronic periodontitis. The proinflammatory cytokine (interleukin-1α (IL-1α), interleukin-1β (IL-1β), interleukin-6 (IL-6), interleukin-8 (IL-8), tumor necrosis factor α (TNF-α), and tumor necrosis factor β (TNF-β)) levels were determined using a commercially available kit. The IL-1β and IL-6 levels increased, whereas the TNF-β levels decreased with the severity of periodontitis (4 mm pocket percentage). Poststimulation IL-1α, IL-6, and IL-8 levels were higher in patients who had an improved treatment outcome. The differences of IL-6 levels (cut point: 0.05 μg/g) yielded a sensitivity and specificity of 90.0% and 81.82%, respectively, for predicting the periodontitis treatment outcome. Among the proinflammatory cytokines, stimulated IL-6 was an excellent marker for predicting the periodontitis treatment outcome.

1. Introduction

Periodontal disease is a localized inflammatory disorder in which periodontal pathogens escape the host immunological defense system, leading to tissue destruction and bone loss [1, 2]. Current knowledge suggests that periodontal pathogenesis is a mixed host response to dental bacterial biofilms and proinflammatory mediators [3]. A balance of these proinflammatory mediators and the host immune response can determine the effectiveness of a clinical treatment for periodontal disease.

These proinflammatory mediators are activated when bacterial biofilms accumulate in the gingival area of the teeth. In vitro studies have shown that proinflammatory cytokines (interleukin-1α (IL-1α), interleukin-1β (IL-1β), interleukin-6 (IL-6), interleukin-8 (IL-8), tumor necrosis factor α (TNF-α), and tumor necrosis factor β (TNF-β)) production increased when human gingival fibroblasts were stimulated by *Porphyromonas gingivalis* (*P. gingivalis*) [4], which also stimulated periodontal ligament stem cells to produce IL-1β, IL-6, and IL-8 [5]. These proinflammatory cytokines can both potentially influence the progression of periodontal disease

and be a novel therapeutic target for chronic periodontitis treatment.

Periodontitis is a type of inflammatory disease with risk factors including periodontal pathogens, the lifestyle, psychosocial factors, chronic diseases, and genetic factors [6]. Recent epidemiological studies have reported that proinflammatory cytokines are associated with periodontitis [7, 8]. Salivary IL-1β levels increase with the severity of periodontitis [9]. Interleukin-6 correlates with the presence of periodontitis; however, the TNF-α levels do not differ between periodontitis cases and healthy subjects [10]. Although proinflammatory cytokines are related to periodontitis, no study has yet investigated whether these cytokines interact or influence periodontitis outcomes.

Osteoclastogenesis is a key process leading to clinical periodontitis outcomes. Proinflammatory cytokines (IL-1α, IL-1β, IL-6, IL-8, TNF-α, and TNF-β) are associated with osteoclastogenesis [11]. These proinflammatory cytokines decreasing had reflected the clinical efficacy of periodontitis treatment [12]. The levels of these proinflammatory cytokines decrease when patients show clinical improvements during periodontal treatment [10].

Scaling is a part of periodontal disease treatment. Scaling, involving the thorough mechanical debridement of dental calculus, not only is a treatment for periodontal disease but also stimulates gingival tissue. Studies have shown that low intensity pulsed ultrasound activates the cell growth signaling pathway and stimulates human circulating angiogenic cells, which release endothelial nitric oxide synthase [13, 14]. The proinflammatory cytokine expression in gingival tissues increases with the severity of inflammation [15]. This study hypothesized that a scaling-stimulated change in the proinflammatory cytokine profile is related to periodontitis treatment effectiveness. The study aimed to investigate the relationship between salivary proinflammatory cytokines and periodontal status. The relationship between scaling-stimulated changes in proinflammatory cytokines and periodontal treatment effectiveness is evaluated in this study.

2. Material and Methods

2.1. Saliva and Clinical Data Collection. Saliva was collected from 22 systemically healthy patients with chronic periodontitis (at least 6 pockets with pocket depths (PDs) of >5 mm and more than 16 functional teeth) over a 6-month period (October 2011 to March 2012) at Cathay General Hospital Dental Department. Before conducting interviews and collecting samples, written informed consent was obtained from all subjects. Structured questionnaires were distributed by an experienced assistant who obtained data related to socioeconomic, demographic, and lifestyle characteristics through personal interviews. The study complied with the World Medical Association *Declaration of Helsinki* and was approved by the Cathay General Hospital Institutional Review Board.

Periodontal diagnostic criteria were based on the classification of the American Academy of Periodontology [16]. Each patient received periodontal examination and treatment from the same dental clinician. The PD was evaluated as the distance between the gingival margin and the bottom of the sulcus/pocket and was assessed at 6 sites. Salivary samples were collected before and after patients received scaling. Subsequently, the patients completed the nonsurgical periodontal treatment procedure. Patients were regarded as part of the nonprogress (NP) treatment group when differences in >7 mm PD percentage increased between the initial clinical treatment and after the completion of 4 weeks of clinical treatment ($N = 12$). The remaining 10 patients were regarded as part of the effective treatment (ET) group ($N = 10$).

2.2. Saliva Preparation and Proinflammatory Cytokine Determination. We described the details of saliva collection in a previous paper [17]. In brief, saliva was collected using sterilized gauze pieces from the buccal and sublingual areas and recovered through centrifugation (1000 rpm, 3 min). At least 2 mL of unstimulated saliva was collected in each tube. The tubes were stored at −20°C and analyzed within 2 months. Proinflammatory cytokine (IL-1α, IL-1β, IL-6, IL-8, TNF-α, and TNF-β) levels were determined using a Human 22-plex multicytokine detection system (catalog number 48-011; Millipore, Billerica, MA, USA) and analyzed using a Luminex 100 system (Luminex Inc.). To consider changes in the salivary volume, we used the total protein level for adjustment while expressing the proinflammatory cytokines. The total protein level was evaluated using the Bradford test and spectrophotometric methods. The differences in proinflammatory cytokines were calculated by subtracting baseline salivary cytokine levels from scaling-stimulated salivary cytokines levels.

2.3. Statistical Analysis. Data were analyzed using SAS 9.3 software (SAS, Cary, NC, USA). Because the salivary proinflammatory cytokines in this study were not normally distributed, a nonparametric test was used for the data analysis. Demographic characteristics and baseline clinical data for the NP and ET groups were analyzed using Fisher's exact test. Differences in continuous parameters between the NP and ET groups were analyzed using the Mann-Whitney U test. The correlation strength of proinflammatory cytokines before and after the scaling stimulation was determined using Spearman's rank correlation. To evaluate the accuracy of detecting periodontitis treatment effectiveness, receiver operating characteristic (ROC) curves and areas under the curve (AUC), based on the levels of these proinflammatory cytokines, were calculated. Probability levels of <0.05 were considered significant.

3. Results

Baseline clinical parameters, demographics, and conventional periodontitis risk factors of the treatment outcome group are shown in Table 1. No statistical differences existed in demographic characteristics or conventional periodontitis risk factors between the NP and ET groups. Table 2 shows a comparison of the baseline cytokine levels between the

Table 1: Demographic characteristics and conventional periodontitis risk factors of study subjects by treatment outcome strata.

	NP group ($N = 12$)	ET group ($N = 10$)	P value
	Median (Q1–Q3)		
Age, years	61.5 (46–71)	56.0 (44–60)	0.37[a]
Distribution of subjects	N (%)	N (%)	
Gender			0.63[b]
Male	5 (41.67)	4 (40.00)	
Female	7 (58.33)	6 (60.00)	
Education			0.41[b]
High school	4 (33.33)	2 (20.00)	
University or above	8 (66.67)	8 (80.00)	
Smoking			0.22[b]
Nonsmokers	10 (83.33)	6 (60.00)	
Smokers	2 (16.67)	4 (40.00)	
Alcohol consumption			0.71[b]
Never or occasional	11 (91.67)	9 (90.00)	
Regular	1 (8.33)	1 (10.00)	
Betel nut chewing			0.19[b]
Nonchewer	12 (100.00)	8 (80.00)	
Chewer	0 (0.00)	2 (20.00)	
Dental visiting pattern			0.96[b]
Regular visits (<1 year)	8 (66.37)	9 (90.00)	
Irregular visits (≥1 year)	4 (33.33)	1 (10.00)	
Tooth cleaning frequency			0.97[b]
<2 times/day	1 (8.33)	3 (30.00)	
≥2 times/day	11 (91.67)	7 (70.00)	

[a]Mann-Whitney U test.
[b]Fisher's exact test.
NP group: nonprogress treatment group.
ET group: effective treatment group.

Table 2: Baseline proinflammatory cytokine profiles of study subjects by treatment outcome strata.

	NP group ($N = 12$)	ET group ($N = 10$)	P value[a]
	Median (Q1–Q3)		
IL-1α	120.18 (12.58–167.16)	67.97 (52.3–190.12)	0.97
IL-1β	28.55 (3.15–119.49)	5.99 (0.18–14.8)	0.07
IL-6	5.21 (1–9.46)	1.24 (0.78–4.24)	0.15
IL-8	125.68 (50.05–184.49)	50.8 (16.9–138.74)	0.19
TNF-α	0.00 (0.00–0.11)	0.10 (0.00–0.12)	0.18
TNF-β	0.18 (0.16–0.21)	0.21 (0.17–0.23)	0.19

[a]Mann-Whitney U test.

NP and ET groups. No statistical differences existed in the baseline cytokine levels between the 2 groups. Table 3 shows the correlations between baseline salivary proinflammatory cytokines in patients with periodontitis. Baseline salivary IL-1β was significantly correlated with baseline IL-1α, IL-6, IL-8, and TNF-β; the correlation coefficients were 0.46, 0.72, 0.60, and −0.46, respectively.

The scatter plots in Figure 1 show that proinflammatory cytokines and 4–6 mm pocket percentages are representative of the severity of periodontitis. The β values of IL-1β and IL-6 were 2.04 and 0.34, respectively, indicating that these 2 proinflammatory cytokines significantly increased with the severity of periodontitis. TNF-β significantly decreased with the baseline percentages of 4–6 mm pockets (β value = −0.0057 and $P = 0.02$).

To investigate the correlation between baseline and scaling-stimulated proinflammatory cytokines, the correlation coefficients between baseline and stimulated salivary cytokines in patients with periodontitis were calculated (Table 4). A positive correlation existed between baseline IL-1α and stimulated IL-1α ($r = 0.66$ and $P < 0.01$). The correlation between baseline IL-1β and stimulated IL-1β was also positive ($r = 0.44$ and $P = 0.0.4$). Stimulated IL-6 was significantly correlated with baseline IL-1α, IL-1β, IL-6, and TNF-α; the correlation coefficients were 0.63, 0.47, 0.60, and −0.48, respectively.

The relationship between proinflammatory cytokine differences and the clinical treatment outcome is shown in Table 5. The differences in IL-1α, IL-6, and IL-8 were significantly higher in the ET group than in the NP group. The median IL-1β differences were −28.38 and −0.13 μg/g in the NP and ET groups, respectively. A negative median value means that the cytokine decreased after scaling. The IL-1β difference was larger in the ET group than that in the NP group.

To evaluate the accuracy of predicting the periodontitis treatment outcome, ROC curves and AUC, based on the difference in proinflammatory cytokines, were calculated (Figure 2). The AUCs of IL-1α, IL-1β, IL-6, IL-8, TNF-α, and TNF-β were 0.79, 0.76, 0.92, 0.79, 0.49, and 0.60, respectively. The differences of IL-6 levels (cut point: 0.05 μg/g) yielded a sensitivity and specificity of 90.0% and 81.82%, respectively, for predicting the periodontitis treatment outcome. Thus, the IL-6 difference is an effective marker for predicting the periodontitis treatment outcome.

4. Discussion

Inflammatory responses protect cells against periodontopathic bacteria [18, 19]. Bacterial DNA can activate inflammatory cytokine production [20]. Proinflammatory cytokines play a vital role in bone remodeling modulation [21]. High baseline cytokine levels could affect the effect of treatment. The baseline proinflammatory cytokines were not significantly different between the NP and ET groups in this study. Although differences in TNF-α and TNF-β were not correlated with the periodontal disease treatment outcome, differences in IL-1α, IL-1β, IL-6, and IL-8 were significantly higher in the ET group in this study. These results imply that scaling stimulated IL-1α, IL-6, and IL-8 and that IL-1β may be useful as a treatment progress biomarker of periodontitis.

Table 3: Correlation between baseline salivary proinflammatory cytokines in patients with periodontitis.

Baseline	Baseline					
	IL-1α	IL-1β	IL-6	IL-8	TNF-α	TNF-β
	Correlation coefficients (P value)					
IL-1α	1.00					
IL-1β	0.46* (0.03)	1.00				
IL-6	0.26 (0.26)	0.72** (0.0002)	1.00			
IL-8	0.32 (0.16)	0.60** (0.0043)	0.43 (0.05)	1.00		
TNF-α	−0.14 (0.55)	−0.38 (0.09)	−0.33 (0.14)	0.00 (1.00)	1.00	
TNF-β	−0.42 (0.06)	−0.46* (0.04)	−0.41 (0.07)	−0.07 (0.77)	0.56 (0.01)	1.00

* $P < 0.05$.
** $P < 0.01$.

Table 4: Correlation between baseline and stimulated salivary proinflammatory cytokines in patients with periodontitis.

Stimulated	Baseline					
	IL-1α	IL-1β	IL-6	IL-8	TNF-α	TNF-β
	Correlation coefficients (P value)					
IL-1α	0.66** (0.001)	0.37 (0.1)	0.38 (0.09)	0.02 (0.93)	−0.4 (0.08)	−0.35 (0.12)
IL-1β	0.42 (0.06)	0.44* (0.04)	0.31 (0.17)	0.08 (0.72)	−0.36 (0.1)	−0.28 (0.22)
IL-6	0.63** (0.002)	0.47* (0.03)	0.60** (0.004)	0.26 (0.26)	−0.48* (0.03)	−0.41 (0.07)
IL-8	0.38 (0.09)	0.22 (0.34)	0.14 (0.53)	0.25 (0.27)	−0.30 (0.18)	−0.18 (0.43)
TNF-α	0.29 (0.21)	0.25 (0.28)	0.03 (0.90)	−0.001 (1.00)	−0.26 (0.26)	−0.12 (0.61)
TNF-β	−0.02 (0.92)	−0.24 (0.29)	−0.46 (0.03)	−0.14 (0.54)	0.27 (0.24)	0.32 (0.16)

* $P < 0.05$.
** $P < 0.01$.

Table 5: Difference in proinflammatory cytokines between patients with and without clinical treatment progress.

Difference in proinflammatory cytokines	NP group ($N = 12$)		ET group ($N = 10$)		P value[a]
	Median	Q1–Q3	Median	Q1–Q3	
IL-1α	−11.97	−39.08–45.53	142.70	37.5–188.77	0.02
IL-1β	−28.38	−118.3–2.99	−0.13	−14.53–0.86	0.04
IL-6	−0.72	−7.19–0.05	3.33	2.76–10.18	0.0014
IL-8	−87.31	−133.23–−38.42	7.84	−51.79–64.65	0.02
TNF-α	0.11	0.00–1.02	0.41	−0.11–1.47	0.97
TNF-β	−0.01	−0.04–0.08	0.01	−0.02–0.16	0.45

[a]Mann-Whitney U test.
NP group: nonprogress treatment group.
ET group: effective treatment group.

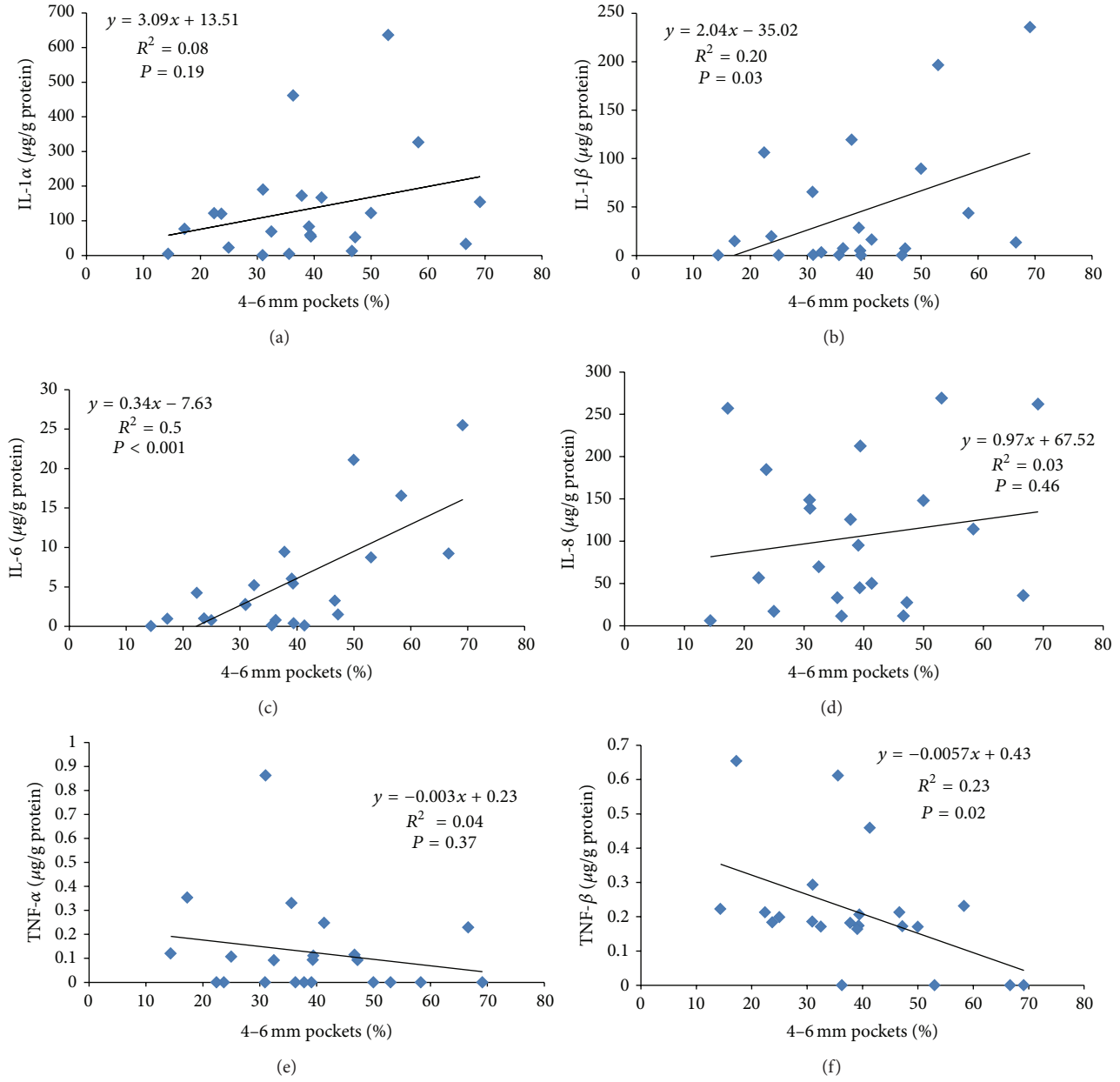

Figure 1: Scatter plots of baseline proinflammatory cytokines and 4–6 mm pocket percentages (before treatment) in patients with chronic periodontitis. (a) Interleukin-1α (IL-1α). (b) Interleukin-1β (IL-1β). (c) Interleukin-6 (IL-6). (d) Interleukin-8 (IL-8). (e) Tumor necrosis factor α (TNF-α). (f) Tumor necrosis factor β (TNF-β).

Biologically active pro-IL-1α and pro-IL-1β are both synthesized in the cytoplasm and cleaved by other proteins to generate IL-1α and IL-1β, respectively [22]. Interleukin-1α located in the membrane acts as an intracellular transcriptional regulator; IL-1β regulates innate immunity and stimulates connective tissue turnover [23]. *P. gingivalis* produced IL-1β in human periodontitis tissue and in a periodontitis activation animal model [24]. Salivary IL-1β is significantly higher in patients with severe periodontitis than in healthy controls; however, IL-1β does not differ between patients with mild periodontitis and healthy controls [9]. In this study, baseline salivary IL-1β increased significantly with the severity of periodontitis. The IL-1β difference was larger in the ET group than that in the NP group. For predicting periodontitis treatment outcomes, scaling-stimulated IL-1β is a superior biomarker than pretreatment salivary IL-1β.

Interleukin-6 has pleiotropic properties because it shares a common signaling pathway with the signal transducer glycoprotein 130 [25, 26]. For nonchallenged status, IL-6 was higher in gingival fibroblasts than in periodontal ligament fibroblasts; when challenged by *P. gingivalis*, the gingival fibroblasts of 4 of 6 subjects induced more IL-6 than did periodontal ligament fibroblasts [27]. Recent studies have shown that IL-6 is significantly higher in patients with chronic periodontitis than in healthy controls [8, 28]. Teles et al. showed that salivary IL-6 was lower in patients with

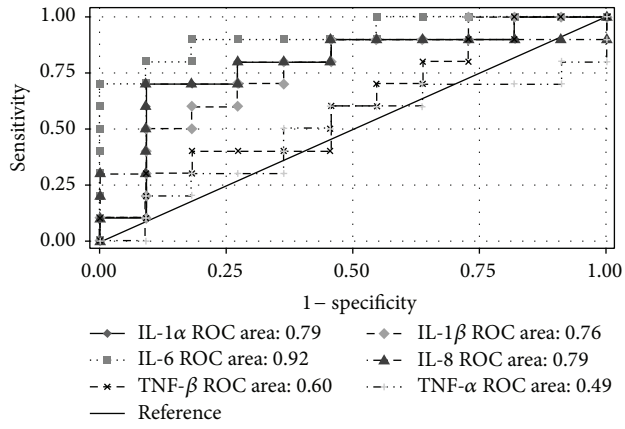

Figure 2: Receiver operating characteristic (ROC) curve and area under the curve (AUC) of proinflammatory cytokines for predicting the treatment outcome.

chronic periodontitis than in healthy subjects; however, no statistical differences were found between the patients with chronic periodontitis and healthy subjects [29]. According to these reports, IL-6 may not be used as a biomarker for the diagnosis of periodontitis. In this study, the AUC of the difference in IL-6 after scaling was 0.90, suggesting that the difference in IL-6 is an effective biomarker for predicting the periodontitis treatment outcome.

Compared with the gingival fibroblast tissue from healthy subjects, that from periodontal disease patients produced higher IL-1 before and after *P. gingivalis* challenge and pretreating gingival fibroblasts with IL-1α enhanced IL-6 production [30]. Previous studies have shown significant correlations between IL-6 and IL-1β ($r = 0.94$) or IL-8 ($r = 0.96$) in gingival fibroblasts and periodontal ligament fibroblasts ($r = 0.83$ for IL-6 and IL-1β; $r = 0.93$ for IL-6 and IL-1β) [27]. In this study, significant correlations were also observed between salivary IL-6 and IL-1β ($r = 0.72$ and $P < 0.01$) of patients with periodontitis. Salivary IL-1β and IL-6 significantly increased with the severity of periodontitis. These two proinflammatory cytokines are sensitive to pathogen infection and can reflect the severity of periodontitis.

Studies have also revealed that an increase in the gene expression of IL-1β, IL-6, IL-8, and TNF-α occurs in response to a *P. gingivalis* challenge in primary human gingival fibroblasts and periodontal ligament fibroblasts, whereas the normal T cell expression and secretion are regulated. The responsiveness of fibroblasts from different donors is similar; this may be useful in determining the vulnerability to periodontitis [27]. An in vitro study showed that a *P. gingivalis* challenge can enhance IL-8 but not IL-6 production in human gingival fibroblasts, suggesting that IL-6 and IL-8 are produced via different pathways [4]. Scaling-stimulated IL-6 was significantly correlated with baseline IL-1α, IL-1β, IL-6, IL-8, and TNF-α. Interleukin-6 has proinflammatory properties and is involved in numerous acute inflammatory and pathologic processes, such as the promotion of bone resorption [22]. Moreover, IL-6 is emerging as a crucial mediator and a novel therapeutic target for chronic inflammatory diseases and cancer [7].

The limitation of this study is that saliva specimens after treatment could not be collected for all of the subjects; the specimens of only 15 subjects were collected after completion of the periodontal treatment. Hence, the collection of specimens after treatment was incomplete and those specimens had not been used to determine the proinflammatory cytokines because of financial reasons. In this study, the significance of the cytokine changes after treatment could not be investigated in depth. In addition, proinflammatory cytokines significantly increased with the severity of periodontitis, and stimulated IL-6 was found to be an effective marker for predicting the periodontitis treatment outcome. It would be useful to further investigate IL-6 as a novel therapeutic target for improving periodontitis treatment efficacy in future studies.

Conflict of Interests

The authors declare that there is no conflict of interests.

Acknowledgments

This study was supported by research grants from Shin Kong Wu Ho-Su Memorial Hospital, Taipei Medical University (SKH-TMU-101-03), Cathay General Hospital, Taipei Medical University Joint Research Program (100CGH-TMU-05), and Taipei Medical University Hospital (102TMU-TMUH-02).

References

[1] M. Battino, P. Bullon, M. Wilson, and H. Newman, "Oxidative injury and inflammatory periodontal diseases: the challenge of anti-oxidants to free radicals and reactive oxygen species," *Critical Reviews in Oral Biology and Medicine*, vol. 10, no. 4, pp. 458–476, 1999.

[2] M. Battino, M. S. Ferreiro, I. Gallardo, H. N. Newman, and P. Bullon, "The antioxidant capacity of saliva," *Journal of Clinical Periodontology*, vol. 29, no. 3, pp. 189–194, 2002.

[3] J. A. C. de Souza, C. Rossa Jr., G. P. Garlet, A. V. B. Nogueira, and J. A. Cirelli, "Modulation of host cell signaling pathways as a therapeutic approach in periodontal disease," *Journal of Applied Oral Science*, vol. 20, no. 2, pp. 128–138, 2012.

[4] T. Imatani, T. Kato, and K. Okuda, "Production of inflammatory cytokines by human gingival fibroblasts stimulated by cell-surface preparations of *Porphyromonas gingivalis*," *Oral Microbiology and Immunology*, vol. 16, no. 2, pp. 65–72, 2001.

[5] H. Kato, Y. Taguchi, K. Tominaga, M. Umeda, and A. Tanaka, "Porphyromonas gingivalis LPS inhibits osteoblastic differentiation and promotes pro-inflammatory cytokine production in human periodontal ligament stem cells," *Archives of Oral Biology*, vol. 59, no. 2, pp. 167–175, 2014.

[6] R. J. Genco and W. S. Borgnakke, "Risk factors for periodontal disease," *Periodontology 2000*, vol. 62, no. 1, pp. 59–94, 2013.

[7] L. Nibali, S. Fedele, F. D'Aiuto, and N. Donos, "Interleukin-6 in oral diseases: a review," *Oral Diseases*, vol. 18, no. 3, pp. 236–243, 2012.

[8] S. Prakasam and M. Srinivasan, "Evaluation of salivary biomarker profiles following non-surgical management of chronic periodontitis," *Oral Diseases*, vol. 20, no. 2, pp. 171–177, 2014.

[9] G. A. Sánchez, V. A. Miozza, A. Delgado, and L. Busch, "Salivary IL-1β and PGE2 as biomarkers of periodontal status, before and after periodontal treatment," *Journal of Clinical Periodontology*, vol. 40, no. 12, pp. 1112–1117, 2013.

[10] Y. Shimada, Y. Komatsu, I. Ikezawa-Suzuki, H. Tai, N. Sugita, and H. Yoshie, "The effect of periodontal treatment on serum leptin, interleukin-6, and C-reactive protein," *Journal of Periodontology*, vol. 81, no. 8, pp. 1118–1123, 2010.

[11] Y.-C. G. Liu, U. H. Lerner, and Y.-T. A. Teng, "Cytokine responses against periodontal infection: protective and destructive roles," *Periodontology 2000*, vol. 52, no. 1, pp. 163–206, 2010.

[12] F. D'Aiuto, M. Parkar, G. Andreou et al., "Periodontitis and systemic inflammation: control of the local infection is associated with a reduction in serum inflammatory markers," *Journal of Dental Research*, vol. 83, no. 2, pp. 156–160, 2004.

[13] Y. Toyama, K.-I. Sasaki, K. Tachibana et al., "Ultrasound stimulation restores impaired neovascularization-related capacities of human circulating angiogenic cells," *Cardiovascular Research*, vol. 95, no. 4, pp. 448–459, 2012.

[14] R. Takeuchi, A. Ryo, N. Komitsu et al., "Low-intensity pulsed ultrasound activates the phosphatidylinositol 3 kinase/Akt pathway and stimulates the growth of chondrocytes in three-dimensional cultures: a basic science study," *Arthritis Research and Therapy*, vol. 10, no. 4, article R77, 2008.

[15] Y. Tokoro, Y. Matsuki, T. Yamamoto, T. Suzuki, and K. Hara, "Relevance of local Th2-type cytokine mRNA expression in immunocompetent infiltrates in inflamed gingival tissue to periodontal diseases," *Clinical and Experimental Immunology*, vol. 107, no. 1, pp. 166–174, 1997.

[16] C. B. Wiebe and E. E. Putnins, "The periodontal disease classification system of the American Academy of Periodontology—an update," *Journal of the Canadian Dental Association*, vol. 66, no. 11, pp. 594–597, 2000.

[17] P.-S. Yang, W.-C. Huang, S.-Y. Chen et al., "Scaling-stimulated salivary antioxidant changes and oral-health behavior in an evaluation of periodontal treatment outcomes," *The Scientific World Journal*, vol. 2014, Article ID 814671, 8 pages, 2014.

[18] G. Hajishengallis and S. E. Sahingur, "Novel inflammatory pathways in periodontitis," *Advances in Dental Research*, vol. 26, no. 1, pp. 23–29, 2014.

[19] I. Tomás, P. Diz, A. Tobías, C. Scully, and N. Donos, "Periodontal health status and bacteraemia from daily oral activities: systematic review/meta-analysis," *Journal of Clinical Periodontology*, vol. 39, no. 3, pp. 213–228, 2012.

[20] P. Dahiya, R. Kamal, R. Gupta, R. Bhardwaj, K. Chaudhary, and S. Kaur, "Reactive oxygen species in periodontitis," *Journal of Indian Society of Periodontology*, vol. 17, no. 4, pp. 411–416, 2013.

[21] G. E. Salvi and N. P. Lang, "Host response modulation in the management of periodontal diseases," *Journal of Clinical Periodontology*, vol. 32, no. supplement 6, pp. 108–129, 2005.

[22] P. M. Preshaw and J. J. Taylor, "How has research into cytokine interactions and their role in driving immune responses impacted our understanding of periodontitis?" *Journal of Clinical Periodontology*, vol. 38, supplement 11, pp. 60–84, 2011.

[23] W. P. Arend, G. Palmer, and C. Gabay, "IL-1, IL-18, and IL-33 families of cytokines," *Immunological Reviews*, vol. 223, no. 1, pp. 20–38, 2008.

[24] R. Jotwani, A. K. Palucka, M. Al-Quotub et al., "Mature dendritic cells infiltrate the T cell-rich region of oral mucosa in chronic periodontitis: in situ, in vivo, and in vitro studies," *The Journal of Immunology*, vol. 167, no. 8, pp. 4693–4700, 2001.

[25] T. Kishimoto, "Interleukin-6: from basic science to medicine—40 years in immunology," *Annual Review of Immunology*, vol. 23, pp. 1–21, 2005.

[26] F. Blanchard, L. Duplomb, M. Baud'huin, and B. Brounais, "The dual role of IL-6-type cytokines on bone remodeling and bone tumors," *Cytokine and Growth Factor Reviews*, vol. 20, no. 1, pp. 19–28, 2009.

[27] N. Scheres, M. L. Laine, T. J. de Vries, V. Everts, and A. J. van Winkelhoff, "Gingival and periodontal ligament fibroblasts differ in their inflammatory response to viable *Porphyromonas gingivalis*," *Journal of Periodontal Research*, vol. 45, no. 2, pp. 262–270, 2010.

[28] F. Javed, H. B. Ahmed, A. Saeed, A. Mehmood, and C. Bain, "Whole salivary interleukin-6 and matrix metalloproteinase-8 levels in patients with chronic periodontitis with and without prediabetes," *Journal of Periodontology*, vol. 85, no. 5, pp. e130–e135, 2014.

[29] R. P. Teles, V. Likhari, S. S. Socransky, and A. D. Haffajee, "Salivary cytokine levels in subjects with chronic periodontitis and in periodontally healthy individuals: a cross-sectional study," *Journal of Periodontal Research*, vol. 44, no. 3, pp. 411–417, 2009.

[30] L. W. Kent, F. Rahemtulla, and S. M. Michalek, "Interleukin (IL)-1 and Porphyromonas gingivalis lipopolysaccharide stimulation of IL-6 production by fibroblasts derived from healthy or periodontally diseased human gingival tissue," *Journal of Periodontology*, vol. 70, no. 3, pp. 274–282, 1999.

Hindawi Publishing Corporation
The Scientific World Journal
Volume 2014, Article ID 745802, 8 pages
http://dx.doi.org/10.1155/2014/745802

Research Article

Effect of *Antrodia camphorata* on Inflammatory Arterial Thrombosis-Mediated Platelet Activation: The Pivotal Role of Protein Kinase C

Wan-Jung Lu,[1,2] Shih-Chang Lin,[1,3,4,5] Chang-Chou Lan,[6] Tzu-Yin Lee,[1] Chih-Hsuan Hsia,[1] Yung-Kai Huang,[7] Hsiu-Chuan Lee,[2,8] and Joen-Rong Sheu[1]

[1] *Graduate Institute of Medical Sciences and Department of Pharmacology, College of Medicine, Taipei Medical University, 250 Wu-Hsing St., Taipei 11031, Taiwan*
[2] *School of Nutrition and Health Sciences, Taipei Medical University, Taipei 11031, Taiwan*
[3] *Division of Allergy and Immunology, Department of Internal Medicine, Cathay General Hospital, Taipei 10630, Taiwan*
[4] *The Laboratory of Allergy and Immunology, Cathay Medical Research Institute, New Taipei City 22171, Taiwan*
[5] *Department of Medicine, School of Medicine, Fu Jen Catholic University, New Taipei City 24205, Taiwan*
[6] *Sheen Chain Biotechnology, Co. Ltd., Taipei 11503, Taiwan*
[7] *School of Oral Hygiene, College of Oral Medicine, Taipei Medical University, Taipei 11031, Taiwan*
[8] *Program for Translation Medicine, Taipei Medical University, 250 Wu-Hsing St., Taipei 11031, Taiwan*

Correspondence should be addressed to Hsiu-Chuan Lee; hcjoyce.lee@gmail.com and Joen-Rong Sheu; sheujr@tmu.edu.tw

Received 5 August 2014; Accepted 11 September 2014; Published 14 October 2014

Academic Editor: Duen-Suey Chou

Antrodia camphorata is a rare Taiwanese medicinal mushroom. *Antrodia camphorata* extract has been reported to exhibit antioxidant, anti-inflammation, antimetastasis, and anticancer activities and plays a role in liver fibrosis, vasorelaxation, and immunomodulation. Critical vascular inflammation leads to vascular dysfunction and cardiovascular diseases, including abdominal aortic aneurysms, hypertension, and atherosclerosis. Platelet activation plays a crucial role in intravascular thrombosis, which is involved in a wide variety of cardiovascular diseases. However, the effect of *Antrodia camphorata* on platelet activation remains unclear. We examined the effects of *Antrodia camphorata* on platelet activation. In the present study, *Antrodia camphorata* treatment (56–224 μg/mL) inhibited platelet aggregation induced by collagen, but not U46619, an analogue of thromboxane A_2, thrombin, and arachidonic acid. *Antrodia camphorata* inhibited collagen-induced calcium (Ca^{2+}) mobilization and phosphorylation of protein kinase C (PKC) and Akt. In addition, *Antrodia camphorata* significantly reduced the aggregation and phosphorylation of PKC in phorbol-12, 13-dibutyrate (PDBu) activated platelets. In conclusion, *Antrodia camphorata* may inhibit platelet activation by inhibiting of Ca^{2+} and PKC cascade and the Akt pathway. Our study suggests that *Antrodia camphorata* may be a potential therapeutic agent for preventing or treating thromboembolic disorders.

1. Introduction

Antrodia camphorata is a rare Taiwanese medicinal mushroom that is popularly known as "niu cheng zhi" in Taiwan [1]. *Antrodia camphorata* has been used in traditional Chinese medicine to treat food poisoning, drug intoxication, diarrhea, abdominal pain, hypertension, skin irritation, and cancer [2]. Studies have identified bioactive compounds of *Antrodia camphorata*, including polysaccharides, maleic/succinic acid derivatives, triterpenoids, benzenoids, and benzoquinone derivatives [3, 4]. In addition, *Antrodia camphorata* was reported to induce apoptosis in SKOV-3 cells through ROS generation, loss of HER-2/neu activation, and suppression of its downstream signaling pathways, including the PI3K/Akt cascade [5]. In addition, *Antrodia camphorata* inhibited lipopolysaccharide- (LPS-)

induced NO production in macrophages [6]. Recent studies have reported that *Antrodia camphorata* is involved in various biological activities, including antioxidant, anti-inflammation, antimetastasis, and anticancer activities as well as liver fibrosis, vasorelaxation, and immunomodulation [7–9].

Critical vascular inflammation leads to vascular dysfunction and cardiovascular diseases, including abdominal aortic aneurysms, hypertension, and atherosclerosis. Intravascular thrombosis is involved in a wide variety of cardiovascular diseases (CVDs). Intraluminal thrombosis is believed to be initiated by platelet adherence and aggregation. Thus, in addition to mediating hemostasis, platelet aggregation may play a crucial role in atherothrombotic processes [10].

Blood platelet activation and aggregation constitute a common denominator in atherothrombotic events and various inflammatory diseases. Platelets have been viewed exclusively as mediators of thrombosis and hemostasis, but a study recently indicated that they play key roles in inflammation and immunity [11]. Therefore, the use of antiplatelet agents to treat thromboembolic diseases (myocardial infarction, ischaemic stroke, and vascular death) warrants investigation. During a preliminary study, we observed that *Antrodia camphorate* at 224 μg/mL inhibited the collagen-induced aggregation of washed human platelets. The influence of *Antrodia camphorata* on platelet activation has yet to be investigated thoroughly. We systematically examined the effects of *Antrodia camphorata* on human platelets and characterized the detailed mechanisms of *Antrodia camphorata*-mediated inhibition of platelet activation.

2. Materials and Methods

2.1. Plant Material. Crude extracts of *Antrodia camphorata* (70%) were provided by Well Shine Biotechnology Development Co., Pvt. Ltd., Taipei, Taiwan.

2.2. Materials. Type I collagen and phorbol-12, 13-dibutyrate (PDBu) were purchased from Sigma (St Louis, MO). Fura 2-AM was purchased from Molecular Probe (Eugene, OR). The anti-Akt (pan) (40D4) monoclonal antibody (mAb), anti-phospho-Akt (Ser^{473}) polyclonal antibody (pAb), anti-phospho-(Ser) protein kinase C (PKC) substrate pAb, anti-phospho-p38 mitogen-activated protein kinase (MAPK) (Thr^{180}/Tyr^{182}) pAb, anti-p38 MAPK (5F11) mAb, anti-phospho-p44/42 MAPK (ERK1/2) (Thr^{202}/Tyr^{204}) pAb, anti-p44/42 MAPK (137F5) mAb, anti-phospho-c-Jun N-terminal kinse (JNK) (Thr^{183}/Tyr^{185}) mAb, and anti-JNK pAb were purchased from Cell Signaling (Beverly, MA). The anti-α-tubulin mouse mAb was purchased from Thermo Scientific (Waltham, MA). The Hybond-P polyvinylidene difluoride (PVDF) membrane, an enhanced chemiluminescence (ECL) western blotting detection reagent, a horseradish-peroxidase (HRP)-conjugated donkey anti-rabbit IgG, and a sheep anti-mouse IgG were purchased from Amersham (Buckinghamshire, UK).

2.3. Platelet Aggregation Assay. Our study was approved by the Institutional Review Board of Taipei Medical University and conformed to the directives of the Helsinki Declaration. All human volunteers provided informed consent. Human platelet suspensions were prepared as described in a previous report [10]. Blood was collected from healthy human volunteers who had taken no medication during the preceding 2 weeks, and the blood samples were mixed with acid-citrate-dextrose solution. After centrifugation at 120 g for 10 min, the supernatant (platelet-rich plasma; PRP) was supplemented with PGE_1 (0.5 μM) and heparin (6.4 IU/mL) and then incubated for 10 min at 37°C and centrifuged at 500 g for 10 min. The platelet pellets were suspended in 5 mL of Tyrode's solution, pH 7.3 [containing (mM) NaCl 11.9, KCl 2.7, $MgCl_2$ 2.1, NaH_2PO_4 0.4, $NaHCO_3$ 11.9, and glucose 11.1]; then apyrase (1.0 U/mL), PGE_1 (0.5 μM), and heparin (6.4 IU/mL) were added, and the mixture was incubated for 10 min at 37°C. After centrifugation of the suspensions at 500 g for 10 min, the washing procedure was repeated. The washed platelets were suspended in Tyrode's solution containing 3.5 mg/mL of bovine serum albumin (BSA), and the final Ca^{2+} concentration in the solvent of the suspensions was adjusted to 1 mM.

A Lumi-Aggregometer (Payton Associates, Scarborough, ON, Canada) was used to measure platelet aggregation as described in a previous report [10]. Platelet suspensions (3.6×10^8 cells/mL) were preincubated with *Antrodia camphorata* at various concentrations or a solvent control (0.5% DMSO) for 3 min before agonists were added under a stirring condition. The reaction was allowed to proceed for 6 min, and the extent of aggregation was expressed in light transmission units.

2.4. Measurement of Platelet-Relative Ca^{2+} Mobilization by Using Fura 2-AM Fluorescence. After centrifugation of the citrated whole blood at 120 ×g for 10 min, the supernatant was incubated with 5 μM Fura 2-AM for 1 h with constant stirring condition. As described above, human platelets were then prepared. Finally, the external Ca^{2+} concentration of the platelet suspensions was adjusted to 1 mM. The relative Ca^{2+} mobilization was measured using a CAF 110 fluorescence spectrophotometer (Jasco, Tokyo, Japan) at excitation wavelengths of 340 and 380 nm and an emission wavelength of 500 nm as described in a previous report [12].

2.5. Immunoblotting. Washed platelets (1.2×10^9 cells/mL) were preincubated with 112, 224, or 448 μg/mL of *Antrodia camphorata* or a solvent control for 3 min, and agonists were added to trigger platelet activation under a stirring condition. After the reaction was stopped, platelets were immediately resuspended in 200 μL of lysis buffer. Samples containing 80 μg of protein were separated on a 12% acrylamide gel by performing sodium dodecyl sulfate polyacrylamide gel electrophoresis (SDS-PAGE), and the proteins were electrotransferred through semidry transfer (Bio-Rad, Hercules, CA). The blots were blocked with TBST (10 mM Tris-base, 100 mM NaCl, and 0.01% Tween 20) containing 5% BSA for 1 h and then probed with various primary antibodies. Membranes were incubated with an HRP-linked anti-mouse

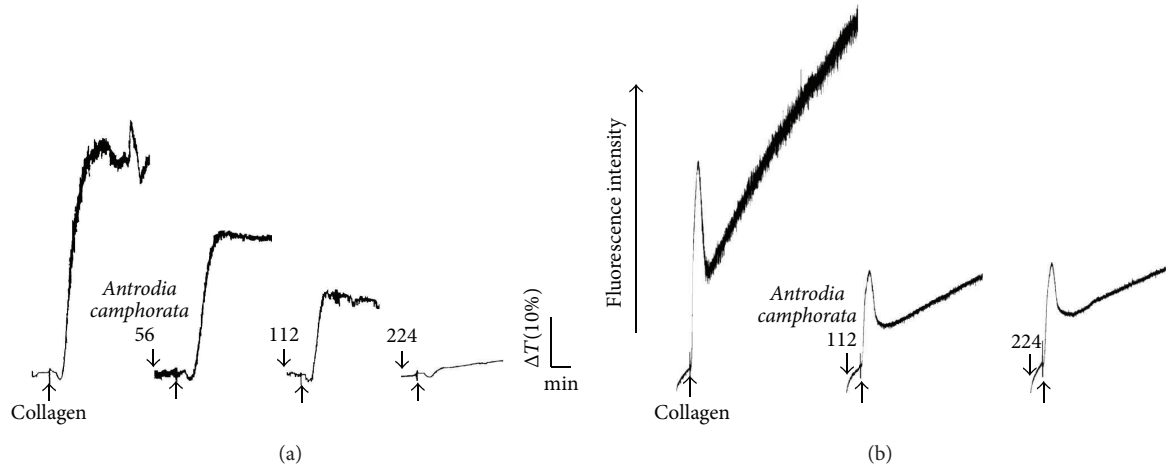

Figure 1: Effects of *Antrodia camphorata* on the regulation of platelet aggregation and calcium mobilization in washed human platelets. Washed platelets (3.6×10^8 cells/mL) were preincubated with a solvent control (DMSO, 0.05%) or 56–224 μg/mL of *Antrodia camphorata*, and 1 μg/mL of collagen was subsequently added to trigger (a) platelet aggregation and (b) relative Ca^{2+} mobilization. Profiles are representative examples of 3 independent experiments.

IgG, anti-goat IgG, or anti-rabbit IgG (diluted 1 : 3000 in TBST) for 1 h. Immunoreactive bands were detected using an enhanced ECL system. Ratios of the semiquantitative results were obtained by scanning the reactive bands and quantifying the optical density by using a video densitometer and the Biolight, Version V2000.01, computer software (Bioprofil,Vilber Lourmat, France).

2.6. Data Analysis. The experimental results are expressed as the mean ± SEM and are accompanied by the number of observations (n). Values of n refer to the number of experiments, each of which were conducted using different blood donors. The results of the experiments were evaluated using an analysis of variance (ANOVA). When the ANOVA indicated significant differences among the group means, each group was compared using the Student-Newman-Keuls method. The results of comparisons with a P value less than 0.05 were considered statistically significant. All statistical analyses were performed using the SAS, Version 9.2 software package (SAS Institute, Cary, NC).

3. Results

3.1. Effects of Antrodia camphorata on Platelet Aggregation and Intracellular Calcium Mobilization. As shown in Figure 1(a), *Antrodia camphorata* (56–224 μg/mL) inhibited platelet aggregation following treatment with 1 μg/mL of collagen. In subsequent experiments, 1 μg/mL of collagen was used as an agonist to stimulate platelet aggregation. As shown in Figure 1(b), calcium mobilization in human platelets stimulated with 1 μg/mL of collagen was inhibited by 112 or 224 μg/mL of *Antrodia camphorata* in a concentration-dependent manner. However, at a concentration of 448 μg/mL, *Antrodia camphorata* did not significantly inhibit platelet aggregation stimulated by 1 μM U46619, 0.01 U/mL of thrombin, or 60 μM AA (data not shown).

3.2. Effects of Antrodia camphorata on Mitogen-Activated Protein Kinases Activation. The MAPKs control major cellular responses in eukaryotic organisms and contribute to cell proliferation, migration, and differentiation as well as apoptosis. *Antrodia camphorata* did not inhibit collagen-mediated phosphorylation of p38 (Figure 2(a)), ERK (Figure 2(b)), or JNK (Figure 2(c)). These results suggest that *Antrodia camphorata* does not antagonize collagen-mediated MAPKs intracellular signaling events that occur during platelet activation.

3.3. Effects of Antrodia camphorata on Protein Kinase C Activation. Activation of platelets by various agonists could lead to the induction of PKC activation and subsequent phosphorylation of p47 proteins [13]. As compared to the protein profile of nonactivated platelets, a protein with an apparent molecular weight similar to that of p47 (47 kDa) was predominately phosphorylated in collagen- (Figure 3(a)) and PDBu- (150 nM; Figures 3(b) and 3(c)) activated human platelets. *Antrodia camphorata* treatments reduced apparent p47 phosphorylation in both collagen- and PDBu-activated platelets (Figures 3(a) and 3(c)). In addition, 448 μg/mL of *Antrodia camphorata* significantly reduced the aggregation of PDBu-activated platelets (Figure 3(b)), indicating that *Antrodia camphorata* directly affects PKC activation in human platelets.

3.4. Effects of Antrodia camphorata on Akt Activation. As shown in Figure 4(a), *Antrodia camphorata* concentration (112 or 224 μg/mL) dependently attenuated Akt phosphorylation stimulated by 1 μg/mL of collagen. In addition, *Antrodia camphorata* did not affect MAPKs phosphorylation in collagen-activated human platelets (Figure 2). These results revealed that *Antrodia camphorata* may prevent collagen-induced platelet activation through the inhibition of PKC and Akt phosphorylation (Figure 4(b)).

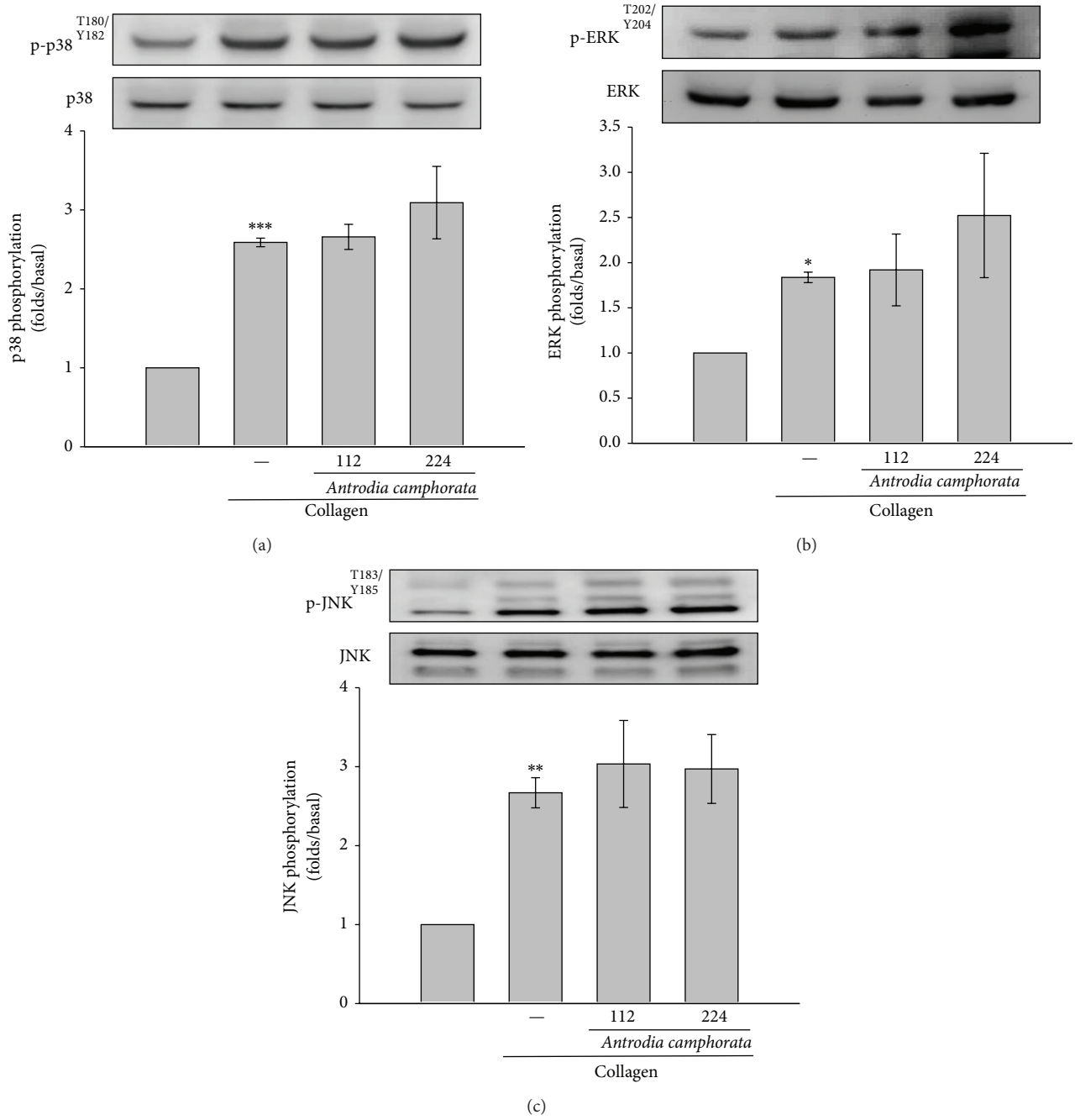

Figure 2: Effects of *Antrodia camphorata* on MAPK activation in collagen-activated platelets. Washed platelets (1.2×10^9 cells/mL) were preincubated with 112 or 224 μg/mL of *Antrodia camphorate* and subsequently treated with 1 μg/mL of collagen to induce platelet activation. The platelets were collected, and the phosphorylation of (a) p38, (b) ERK, or (c) JNK in the subcellular extracts was analyzed. Data are presented as the mean ± SEM ($n = 3$; $^*P < 0.05$, $^{**}P < 0.01$, and $^{***}P < 0.001$, compared with solvent control platelets).

4. Discussion

This study demonstrated for the first time that *Antrodia camphorata* exhibits potent antiplatelet activity via inhibiting both PKC and Akt activation in washed human platelets (Figure 4(b)). *Antrodia camphorata* has been used in traditional Chinese medicine to treat food poisoning, drug intoxication, diarrhea, abdominal pain, hypertension, skin irritation, and cancer [2]. Recent studies have reported that *Antrodia camphorata* induces substantial apoptosis in human promyelocytic leukemia (HL-60) cells [14]. Another study proved that *Antrodia camphorata* extracts may be used as an adjuvant antitumor agent for human hepatoma cells, which are resistant to most other antitumor agents. Our previous study demonstrated that *Antrodia camphorata* provides effective protection against carbon tetrachloride (CCl_4)

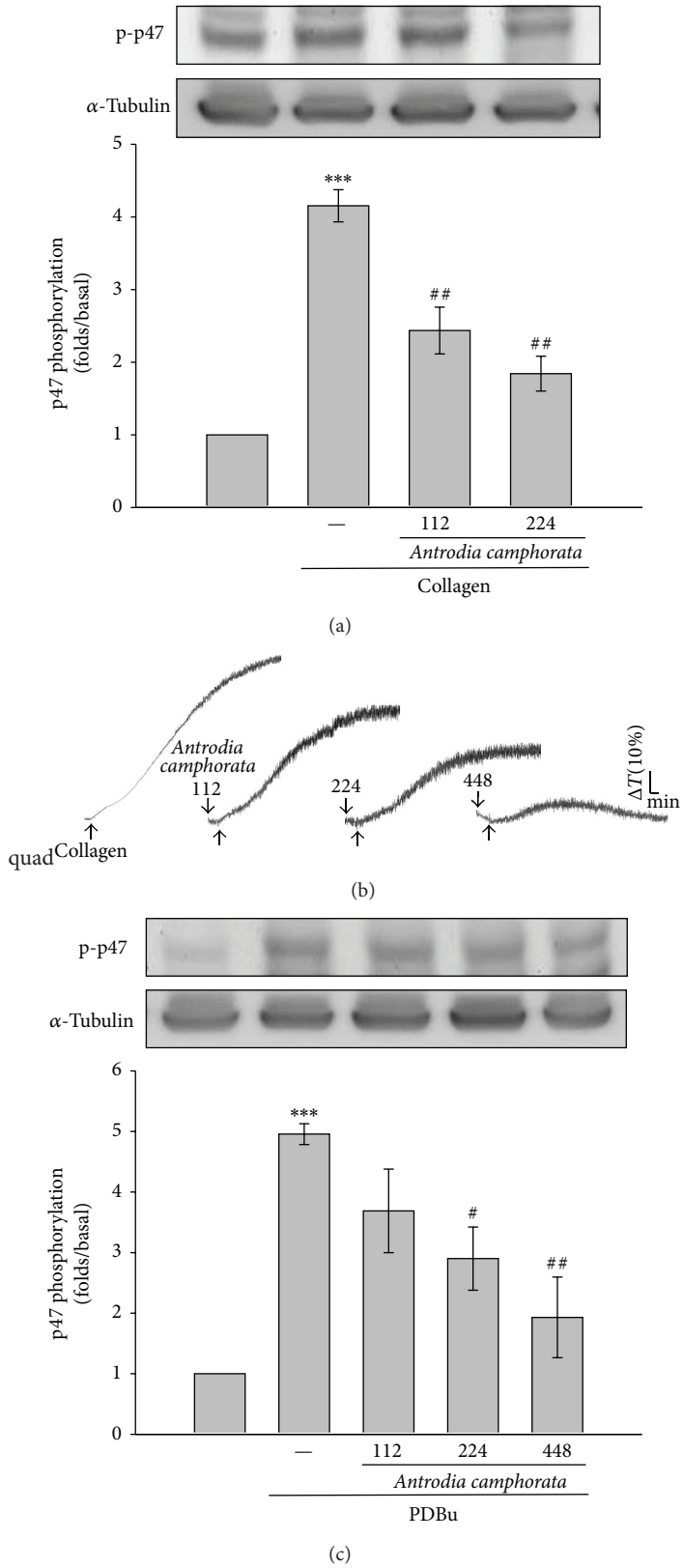

Figure 3: Influence of *Antrodia camphorata* on PKC activation in activated platelets. ((a) and (c)) Washed platelets were preincubated with 112, 224, or 448 μg/mL of *Antrodia camphorata* and subsequently treated with 1 μg/mL of collagen or 150 nM PDBu to induce p47 phosphorylation, the PKC downstream ((a) and (c)), and (b) platelet aggregation. Data are presented as the mean ± SEM ($n = 3$; $^{***}P < 0.001$ compared with solvent control platelets; $^{\#}P < 0.01$ and $^{\#\#}P < 0.01$ compared with the collagen group). Profiles (b) are representative of 3 independent experiments.

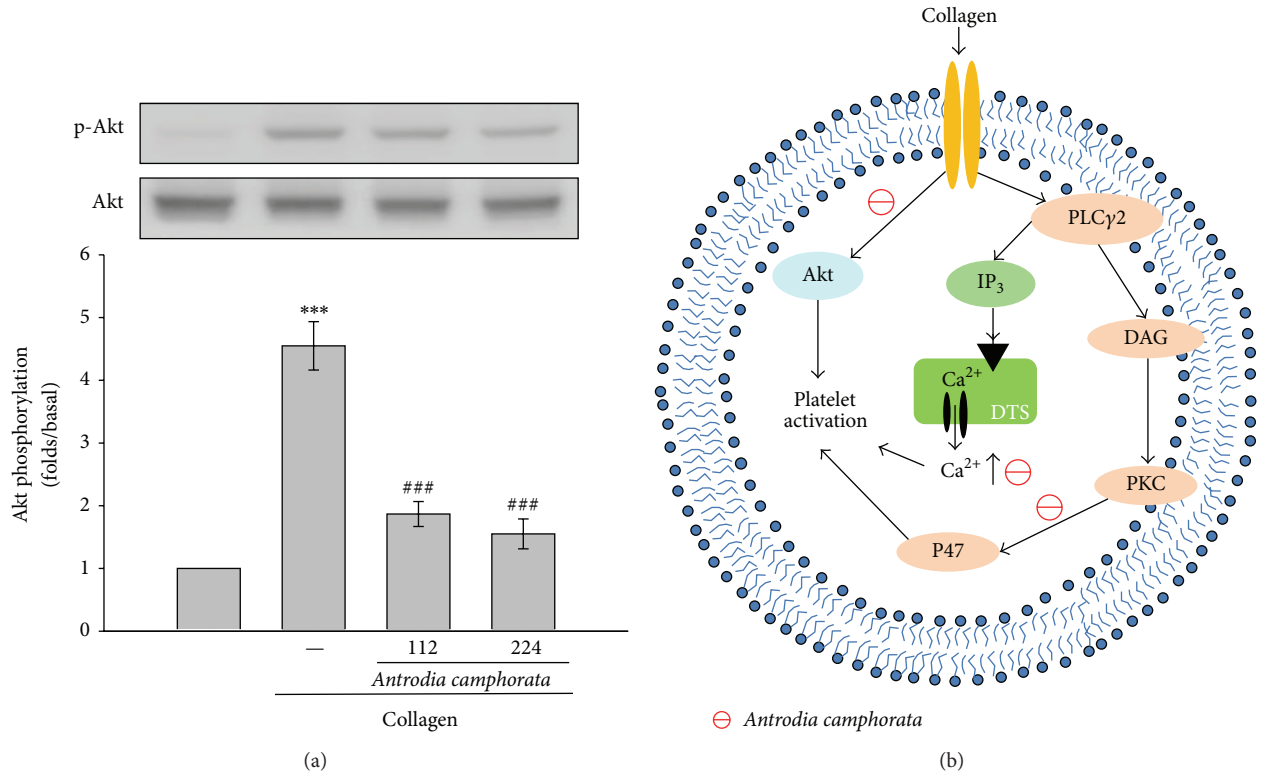

FIGURE 4: Effects of *Antrodia camphorata* on Akt phosphorylation in collagen-activated platelets. Washed platelets (1.2×10^9 cells/mL) were preincubated with 112 or 224 μg/mL of *Antrodia camphorata* and subsequently treated with 1 μg/mL of collagen to induce platelet activation. The platelets were collected, and the phosphorylation of (a) Akt in the subcellular extracts was analyzed. Data are presented as the mean ± SEM ($n = 3$; $^{***}P < 0.001$ compared with solvent control platelets; $^{###}P < 0.001$ compared with the collagen group). (b) Schematic illustration of *Antrodia camphorata*-mediated inhibition of platelet activation. Activated phospholipase Cγ2 (PLCγ2) catalyses the conversion of phosphatidylinositol 4,5-bisphosphate (PI4,5-P_2) into 1,2-diacylglycerol (DAG) and inositol 1,4,5-trisphosphate (IP_3). DAG activates protein kinase C (PKC) and, subsequently, phosphorylation of a 47-kDa protein (p47). IP_3induces the release of Ca^{2+} from the dense tubular system (DTS).

induced hepatic injury in vivo by mediating antioxidative and free radical scavenging activities [15], and it was shown to reduce H_2O_2-induced lipid peroxidation and upregulate the expression of hepatic glutathione-dependent enzymes, thereby protecting the rat liver from CCl_4-induced damage [16].

Phospholipidase (PL) activation may significantly alter by the occurrence of platelets activation by agonists, such as collagen. Inositol 1,4,5-trisphosphate (IP_3) and 1,2-diacylglycerol (DAG) are produced during the activation of phospholipidase C (PLC), which activates PKC, and subsequently induce the phosphorylation of p47 [17]. It has been proposed that activation of PKC may facilitate certain responses to specific activating signals in distinct cellular compartments [18]. The 6 families of PLC enzymes are found to be categorized: PLCβ, PLCγ, PLCδ, PLCε, PLCζ, and PLCη [18]. The PLCγ family comprises isozymes 1 and 2 and isoform 2 is found to associate in collagen-dependent signaling in platelets [19]. IP_3 triggers an increase in intracellular Ca^{2+} from Ca^{2+} storage sites (i.e., the dense tubular system, DTS) in platelets. DAG activates PKC-inducing protein phosphorylation (p47) (Figure 4(b)). PKC activation is a strategy adopted by cells to enable certain responses to specific activating signals in distinct cellular compartments [18]. In our study, the activation of both Ca^{2+} and PKC by collagen was diminished in the presence of *Antrodia camphorata*. *Antrodia camphorata* exerted direct effects on PKC activation because it reduced PDBu-induced PKC activation and PDBu-induced platelet aggregation, suggesting that *Antrodia camphorata*-mediated inhibition of platelet activity involves the Ca^{2+} and PKC cascade.

MAPKs include ERKs, p38, and JNKs which are involved in cell proliferation, migration, differentiation, and apoptosis. ERKs, JNKs, and p38 have consistently been identified in platelets [20] and they are activated in platelets stimulated by collagen and thrombin and are involved in thrombosis [21]. ERK and p38 play a vital role in stimulating granule secretion and facilitating clot retraction [22]. In addition, p38 plays a crucial role in activating cytosolic phospholipase A_2, which produces thromboxane A_2 by catalyzing AA release [23]. Moreover, JNK1 is reportedly involved in collagen-induced platelet aggregation and thrombus formation [24]. The time of thrombus formation was significantly prolonged in JNK1−/− arterioles in an *in vivo* model and platelet

secretion was impaired in JNK1−/− platelets *in vitro* [25]. Akt is a downstream effector of PI3-kinase [26], and previous studies found that Akt-knockout mice exhibited defects in agonist-induced platelet activation [27, 28]. In this study, we demonstrated that *Antrodia camphorata* inhibits the activation of Akt, but not MAPKs, suggesting that the *Antrodia camphorata*-mediated inhibition of platelet activation may involve inhibition of the Akt cell-signaling pathway.

In conclusion, we demonstrated that the antiplatelet activity of *Antrodia camphorata* may inhibit the Ca^{2+} and PKC cascades and Akt signaling pathway (Figure 4(b)). These alterations reduce platelet activity and ultimately inhibit platelet aggregation. Our findings suggest that *Antrodia camphorata* may be a potential therapeutic agent for preventing or treating thromboembolic disorders.

Conflict of Interests

The authors declare that they have no conflict of interests.

Authors' Contribution

Dr. Wan-Jung Lu and Dr. Shih-Chang Lin contributed equally to this work.

Acknowledgments

This work was supported by grants from the National Science Council, Taiwan (NSC100-2320-B-038-021-MY3, NSC102-2811-B-038-026, and MOST103-2811-B-038-023), and Cathay General Hospital-Taipei Medical University (103CGH-TMU-01-2).

References

[1] Y. C. Hseu, W. C. Chang, Y. T. Hseu et al., "Protection of oxidative damage by aqueous extract from *Antrodia camphorata* mycelia in normal human erythrocytes," *Life Sciences*, vol. 71, no. 4, pp. 469–482, 2002.

[2] H. L. Yang, K. J. S. Kumar, and Y. C. Hseu, "Multiple molecular targets of *Antrodia camphorata*: a suitable candidate for ovarian cancer chemoprevention," in *Breast Cancer Cells-2*, Intech Press, Rijeka, Croatia, 2012.

[3] Y.-C. Chen, H.-L. Chiu, C.-Y. Chao et al., "New anti-inflammatory aromatic components from Antrodia camphorata," *International Journal of Molecular Sciences*, vol. 14, no. 3, pp. 4629–4639, 2013.

[4] Y. U.-H. Hsieh, F.-H. Chu, Y. A.-S. Wang et al., "Antrocamphin A, an anti-inflammatory principal from the fruiting body of *Taiwanofungus camphoratus*, and its mechanisms," *Journal of Agricultural and Food Chemistry*, vol. 58, no. 5, pp. 3153–3158, 2010.

[5] H. L. Yang, K. Y. Lin, Y. C. Juan, and et al, "The anti-cancer activity of *Antrodia camphorata* against human ovarian carcinoma (SKOV-3) cells via modulation of HER-2/neu signaling pathway," *Journal of Ethnopharmacology*, vol. 148, no. 1, pp. 254–265, 2013.

[6] C. C. Liaw, Y. C. Chen, G. J. Huang, and et al, "Anti-inflammatory lanostanoids and lactone derivatives from *Antrodia camphorata*," *Journal of Natural Products*, vol. 76, no. 4, pp. 489–494, 2013.

[7] G. J. Huang, S. S. Huang, S. S. Lin, and et al, "Analgesic effects and the mechanisms of anti-inflammation of ergostatrien-3β-ol from *Antrodia camphorata* submerged whole broth in mice," *Journal of Agricultural and Food Chemistry*, vol. 58, no. 12, pp. 7445–7452, 2010.

[8] J.-S. Deng, S.-S. Huang, T.-H. Lin et al., "Analgesic and anti-inflammatory bioactivities of eburicoic acid and dehydroeburicoic acid isolated from antrodia camphorata on the inflammatory mediator expression in mice," *Journal of Agricultural and Food Chemistry*, vol. 61, no. 21, pp. 5064–5071, 2013.

[9] G.-J. Huang, J.-S. Deng, S.-S. Huang et al., "Hepatoprotective effects of eburicoic acid and dehydroeburicoic acid from *Antrodia camphorata* in a mouse model of acute hepatic injury," *Food Chemistry*, vol. 141, no. 3, pp. 3020–3027, 2013.

[10] J. R. Sheu, C. R. Lee, C. H. Lin, and et al, "Mechanisms involved in the antiplatelet activity of Staphylococcus aureus lipoteichoic acid in human platelets," *Thrombosis and Haemostasis*, vol. 83, no. 5, pp. 777–784, 2000.

[11] P. von Hundelshausen and C. Weber, "Platelets as immune cells: bridging inflammation and cardiovascular disease," *Circulation Research*, vol. 100, no. 1, pp. 27–40, 2007.

[12] J.-R. Sheu, W.-C. Hung, C.-H. Wu et al., "Reduction in lipopolysaccharide-induced thrombocytopenia by triflavin in a rat model of septicemia," *Circulation*, vol. 99, no. 23, pp. 3056–3062, 1999.

[13] W. D. Singer, H. A. Brown, and P. C. Sternweis, "Regulation of eukaryotic phosphatidylinositol-specific phospholipase C and phospholipase D," *Annual Review of Biochemistry*, vol. 66, pp. 475–509, 1997.

[14] Y.-C. Hseu, H.-L. Yang, Y.-C. Lai, J.-G. Lin, G.-W. Chen, and Y.-H. Chang, "Induction of apoptosis by *Antrodia camphorata* in human premyelocytic leukemia HL-60 cells," *Nutrition and Cancer*, vol. 48, no. 2, pp. 189–197, 2004.

[15] G. Hsiao, M.-Y. Shen, K.-H. Lin et al., "Antioxidative and hepatoprotective effects of *Antrodia camphorata* extract," *Journal of Agricultural and Food Chemistry*, vol. 51, no. 11, pp. 3302–3308, 2003.

[16] T.-Y. Song and G.-C. Yen, "Protective effects of fermented filtrate from *Antrodia camphorata* in submerged culture against CCl4-induced hepatic toxicity in rats," *Journal of Agricultural and Food Chemistry*, vol. 51, no. 6, pp. 1571–1577, 2003.

[17] P. Mangin, Y. Yuan, I. Goncalves et al., "Signaling role for phospholipase Cγ2 in platelet glycoprotein Ibα calcium flux and cytoskeletal reorganization: Involvement of a pathway distinct from FcRγ chain and FcγRIIA," *Journal of Biological Chemistry*, vol. 278, no. 35, pp. 32880–32891, 2003.

[18] A. Pascale, M. Amadio, S. Govoni, and F. Battaini, "The aging brain, a key target for the future: the protein kinase C involvement," *Pharmacological Research*, vol. 55, no. 6, pp. 560–569, 2007.

[19] A. Ragab, S. Séverin, M.-P. Gratacap et al., "Roles of the C-terminal tyrosine residues of LAT in GPVI-induced platelet activation: insights into the mechanism of PLCγ2 activation," *Blood*, vol. 110, no. 7, pp. 2466–2474, 2007.

[20] F. Bugaud, F. Nadal-Wollbold, S. Lévy-Toledano, J.-P. Rosa, and M. Bryckaert, "Regulation of c-Jun-NH2 terminal kinase and extracellular-signal regulated kinase in human platelets," *Blood*, vol. 94, no. 11, pp. 3800–3805, 1999.

[21] F. Adam, A. Kauskot, J.-P. Rosa, and M. Bryckaert, "Mitogen-activated protein kinases in hemostasis and thrombosis," *Journal of Thrombosis and Haemostasis*, vol. 6, no. 12, pp. 2007–2016, 2008.

[22] P. Flevaris, Z. Li, G. Zhang, Y. Zheng, J. Liu, and X. Du, "Two distinct roles of mitogen-activated protein kinases in platelets and a novel Rac1-MAPK-dependent integrin outside-in retractile signaling pathway," *Blood*, vol. 113, no. 4, pp. 893–901, 2009.

[23] L. Coulon, C. Calzada, P. Moulin, E. Véricel, and M. Lagarde, "Activation of p38 mitogen-activated protein kinase/cytosolic phospholipase A_2 cascade in hydroperoxide-stressed platelets," *Free Radical Biology and Medicine*, vol. 35, no. 6, pp. 616–625, 2003.

[24] A. Kauskot, F. Adam, A. Mazharian et al., "Involvement of the mitogen-activated protein kinase c-Jun NH_2-terminal kinase 1 in thrombus formation," *The Journal of Biological Chemistry*, vol. 282, no. 44, pp. 31990–31999, 2007.

[25] F. Adam, A. Kauskot, P. Nurden et al., "Platelet JNK1 is involved in secretion and thrombus formation," *Blood*, vol. 115, no. 20, pp. 4083–4092, 2010.

[26] T. F. Franke, S.-I. Yang, T. O. Chan et al., "The protein kinase encoded by the *Akt* proto-oncogene is a target of the PDGF-activated phosphatidylinositol 3-kinase," *Cell*, vol. 81, no. 5, pp. 727–736, 1995.

[27] D. Woulfe, H. Jiang, A. Morgans, R. Monks, M. Birnbaum, and L. F. Brass, "Defects in secretion, aggregation, and thrombus formation in platelets from mice lacking Akt2," *The Journal of Clinical Investigation*, vol. 113, no. 3, pp. 441–450, 2004.

[28] J. Chen, S. De, D. S. Damron, W. S. Chen, N. Hay, and T. V. Byzova, "Impaired platelet responses to thrombin and collagen in AKT-1-deficient mice," *Blood*, vol. 104, no. 6, pp. 1703–1710, 2004.

Hindawi Publishing Corporation
The Scientific World Journal
Volume 2014, Article ID 686109, 8 pages
http://dx.doi.org/10.1155/2014/686109

Research Article

Extract of *Antrodia camphorata* Exerts Neuroprotection against Embolic Stroke in Rats without Causing the Risk of Hemorrhagic Incidence

Ye-Ming Lee,[1,2,3] Chiu-Yun Chang,[4] Ting-Lin Yen,[3] Pitchairaj Geraldine,[5] Chang-Chou Lan,[6] Joen-Rong Sheu,[3] and Jie-Jen Lee[2,3,7,8]

[1] *Department of Surgery, Hsinchu Mackay Memorial Hospital, Hsinchu 300, Taiwan*
[2] *Department of Nursing, Mackay Medicine, Nursing and Management College, Taipei 112, Taiwan*
[3] *Graduate Institute of Medical Sciences, College of Medicine, Taipei Medical University, 250 Wu-Hsing Street, Taipei 110, Taiwan*
[4] *Department of Anatomy, School of Medicine, Taipei Medical University, Taipei 110, Taiwan*
[5] *Department of Animal Science, School of Life Sciences, Tiruchirappalli, Tamil Nadu 620 024, India*
[6] *Sheen Chain Biotechnology, Co., Ltd., Taipei 115, Taiwan*
[7] *Mackay Junior College of Medicine, Nursing, and Management, Mackay Memorial Hospital, Taipei 112, Taiwan*
[8] *Department of Surgery, Mackay Memorial Hospital, No. 92, Section 2, Zhongshan N. Road, Taipei 104, Taiwan*

Correspondence should be addressed to Joen-Rong Sheu; sheujr@tmu.edu.tw and Jie-Jen Lee; jjlee1957@gmail.com

Received 3 June 2014; Accepted 7 July 2014; Published 21 July 2014

Academic Editor: Duen-Suey Chou

In this study, the neuroprotective effect of an extract of *Antrodia camphorata* (*A. camphorata*), a fungus commonly used in Chinese folk medicine for treatment of viral hepatitis and cancer, alone or in combination with aspirin was investigated in a rat embolic stroke model. An ischemic stroke was induced in rats by a selective occlusion of the middle cerebral artery (MCA) with whole blood clots and then orally treated with *A. camphorata* (0.25 and 0.75 g/kg/day) alone and combined with aspirin (5 mg/kg/day). Sixty days later, the brains were removed, sectioned, and stained with triphenyltetrazolium chloride and analysed by a commercial image processing software program. Brain infarct volume, neurobehavioral score, cerebral blood perfusion, and subarachnoid and intracerebral hemorrhage incidence were perceived. In addition, potential bleeding side effect of the combinative therapy was assessed by measuring hemoglobin (Hb) content during intracerebral hemorrhage and gastric bleeding, prothrombin time (PT), and occlusion time (OT) after oral administration. Posttreatment with high dose *A. camphorata* significantly reduced infarct volume and improved neurobehavioral score ($P < 0.05$). Since *A. camphorata* alone or with aspirin did not alter the Hb level, this treatment is safe and does not cause hemorrhagic incident. Remarkably, the combination of *A. camphorata* and aspirin did not show a significant effect on the bleeding time, PT and OT increase suggesting that *A. camphorata* may have the neuroprotective effect without the prolongation of bleeding time or coagulation time. From these observations, we suggest that combinative therapy of *A. camphorata* and aspirin might offer enhanced neuroprotective efficacies without increasing side effects.

1. Introduction

Stroke is the second most leading cause of death and the first cause of major adult disability in the world [1, 2]. Among the stroke patients, 85–90% of the cases are ischaemic stroke with a major (75–80%) cause of cerebral arterial thrombosis, and majorities of ischaemic incidents ensue as a result of occlusion of the middle cerebral artery [3, 4]. Mortality and serious disability result if patients are not treated successfully within 30–90 min after onset of symptoms. Aspirin is the most widely used drug for the secondary prevention of thrombotic events, due to its antiplatelet action. It is effective for the prevention of secondary stroke and has been used in up to 89% of patients in China. Nevertheless, while

recurrent stroke is controlled by this treatment, the incidence of cerebral haemorrhage and other bleeding events is higher in Asian countries than in high-income countries [5]. Hence, combinations of antiplatelet drugs that act on different pathways have been used to overcome the risk of haemorrhage. These compounds have been shown to be used efficiently and safely in patients with unstable coronary heart disease. Recent studies have revealed that the combination of two antiplatelet drugs is disastrous to recover stroke prevention rates owing to the increased risk of bleeding events associated with their long-term use [6, 7]. Bleeding due to antiplatelet drugs is a vital clinical issue in primary and secondary stroke prevention, mostly in the Chinese population, which has a higher incidence of cerebral haemorrhage than other indigenous groups [8].

A. camphorata is one of the complementary alternative medicines. It is a parasitic fungus that only grows on the inner heartwood wall of *Cinnamomum kanehirai* Hay (Lauraceae). *A. camphorata* is usually used in Taiwanese folk medicine for abdominal pain, chemical intoxication, diarrhea, hypertension, itchy skin, and hepatoma [9]. Recent studies have demonstrated that *A. camphorata* induces significant apoptosis of human promyelocytic leukemia (HL-60) cells [10]. Another study proved that *A. camphorata* extracts may be used as an adjuvant antitumor agent for human hepatoma cells, which are resistant to most other antitumor agents. Our previous study demonstrated that *A. camphorata* owns effective protection against carbon tetrachloride- (CCl_4-) induced hepatic injury in vivo, by mediating antioxidative and free radical scavenging activities [11], and it has shown to reduce H_2O_2-induced lipid peroxidation and upregulating hepatic glutathione-dependent enzymes for protecting the rat liver from the CCl_4-induced damage [12].

The embolic model has been used previously in different experiments to induce experimental stroke in rodents [13], as this model mimics human stroke and is more relevant to the pathophysiological situation in patients. Besides, different sizes of lesion could be created in this model by injection of various volumes of clot into the middle cerebral artery [14]. Therefore, we investigated whether a combination of *A. camphorata* with the lowest effective dose of aspirin may provide more neuroprotection during the embolic model of stroke in rats without increasing the potential bleeding side effect and different hemorrhagic incidents.

2. Materials and Methods

2.1. Plant Material. The crude extracts of *A. camphorata* were offered by Well Shine Biotechnology Development Co., Pvt. Ltd., Taipei, Taiwan.

2.2. Animals. Male Wistar rats weighing 250–300 g were used to assess the effects of *A. camphorata* given alone or in combination with aspirin on MCAO-induced brain damage. Animal care and the general protocols for animal use were approved by the Institutional Animal Care and Use Committee (IACUC) of Taipei Medical University (no. LAC-101-0239). Before undergoing the experimental procedures, all animals were clinically normal, free of apparent infection or inflammation and showed no neurological deficits.

2.3. Middle Cerebral Artery Occlusion- (MCAO-) Induced Ischemia. Rats were subjected to MCAO-induced ischemia by administration of an autologous blood clot as described in our previous study [15]. Briefly, arterial blood (0.6 mL) was withdrawn from a femoral catheter in a 1 mL syringe. The blood was immediately injected into PE-10 tubes. The tubes were kept at 4°C for 22 h, and the thread-like clots were removed and placed in a saline-filled dish. The clots were then washed to remove blood cells. Washed portions of the clots were transferred to fresh dishes, and the washing process was repeated until the saline remained clear. These clot sections were cut into 30 mm long fragments and then drawn up with the saline solution into a PE-10 catheter.

On the day of surgery, animals were anesthetized with a mixture of 75% air and 25% O_2 gases containing 3% isoflurane. The common carotid artery (CCA) was identified, and approximately 1 cm of the external carotid artery (ECA) was ligated and cut. Subsequently, the pterygopalatine artery (PA) was clamped with a 10 mm microaneurysm clamp, and the CCA was similarly clamped before the carotid bifurcation. The internal carotid artery (ICA) was then clamped between the carotid bifurcation and the PA. Next, the PE-50 catheter containing the clot was introduced approximately 5 mm into the previously cut ECA and tied in place with sutures. The ICA clamp was removed, and the clot was flushed into the ICA over a period of approximately 5 s. The PA clamp was removed, and the rat was left in this condition for 1 h.

2.4. Experimental Design. In this study, at 1 hr after MCA occlusion, rats were randomly separated into six groups: (1) a sham-operated group; (2) a group orally treated with an isovolumetric solvent (distilled water) for 60 days, followed by thromboembolic occlusion; (3 and 4) groups orally treated with *A. camphorata* (0.25 and 0.75 g/kg/day) alone for 60 days, followed by thromboembolic occlusion, respectively; and (5 and 6) groups treated with *A. camphorata* (0.25 and 0.75 g/kg/day) and aspirin (5 mg/kg/day), followed by thromboembolic occlusion, respectively. An observer blinded to the identity of the groups assessed the neurological deficits after reperfusion (before being euthanized) by forelimb akinesia (also called the postural tail-hang) test.

2.5. Quantification of Brain Infarct Volume. Rats were euthanized by decapitation after 24 h of reperfusion. The brains were cut into 2 mm coronal slices starting 1 mm from the frontal pole. Each stained brain (2% 2,3,5-triphenyltetrazolium; TTC) slice was drawn using a computerized image analyzer (Image-Pro Plus). The calculated infarct areas were then compiled to obtain the infarct volume (mm^3) per brain. Infarct volumes were expressed as a percentage of the contralateral hemisphere volume using the formula (the area of the intact contralateral [left] hemisphere—the area of the intact region of the ipsilateral [right] hemisphere) to compensate for edema formation in the ipsilateral hemisphere [15].

2.6. Neurological Functional Tests. Sensorimotor integrity was measured in rats at 1 and 24 h after MCAO by an investigator blind to the experimental groups to assess the neurobehavior [16]. Scoring was as follows: 0: no observable deficit, 1: forelimb flexion, 2: forelimb flexion plus decreased resistance to lateral push, 3: unidirectional circling, and 4: unidirectional circling plus decreased level of consciousness.

2.7. Evaluation of Hemorrhagic Incidence. As previously published, hemoglobin content in the ischemic hemisphere and gastric luminal fluid was determined as an index of intracerebral hemorrhage and gastric bleeding using a colorimetric method as described by a kit (Haemoglobin, HG1539) purchased from Randox Lab Ltd., UK. The hemoglobin content in ischemic hemisphere and gastric luminal fluid was determined by using the optical density readings obtained from the known hemoglobin standards and reported in g/dL.

2.8. Grading System for Subarachnoid Hemorrhage (SAH). The rats were sacrificed under deep anesthesia at 60 days after surgery and the brains were removed rapidly. High resolution pictures of the base of the brain depicting the circle of Willis and basilar arteries were taken. In the photographs, the basal cistern was shown in Figure 1(a). This grading was done by a blinded observer.

2.9. Measurement of Prothrombin Time (PT). Measurement of prothrombin time (PT) was performed by using a kit (Instrumentation Laboratory, Milano, Italy) as described [17]. Briefly, just before ligation to form a snare in the rat Wessler model, arterial blood samples (3 mL) were withdrawn; then the artery was ligated immediately; 0.9 mL of each blood sample was transferred into a 0.109 M trisodium citrate solution (1 : 9, v/v) and then centrifuged at 2000 ×g for 10 min to obtain plasma. 100 μL plasma was mixed with 50 μL of cephalin in a process plate, and the coagulation was started by the addition of $CaCl_2$ (1 mM), 100 μL of thromboplastin, and 100 μL of bovine thrombin into the 100 μL of incubated plasma for PT assay.

2.10. Measurement of Occlusion Time (OT). As described previously [15], mice were anesthetized, and an external jugular vein was cannulated with PE-10 so that dye and medication could be administered by an intravenous (i.v.) bolus. A segment of the small intestine was placed onto a transparent culture dish for microscopic observation. Venules (30 to 40 μm) were selected for irradiation to produce a microthrombus. Using the epi-illumination system, light from a 100 W mercury lamp was passed through a B-2A filter (Nikon, Tokyo, Japan) with a DM 510 dichromic mirror (Nikon). Wavelengths below 520 nm had been eliminated from the filtered light, which was used to irradiate a microvessel; the area of irradiation was approximately 100 μm in diameter on the focal plane. A dose of 0.75 g/kg/dayof *A. camphorata* was administered 3 min after fluorescein sodium administration. Five minutes after administration of the fluorescein sodium, irradiation by filtered light and the video timer were simultaneously begun, and occlusion time was

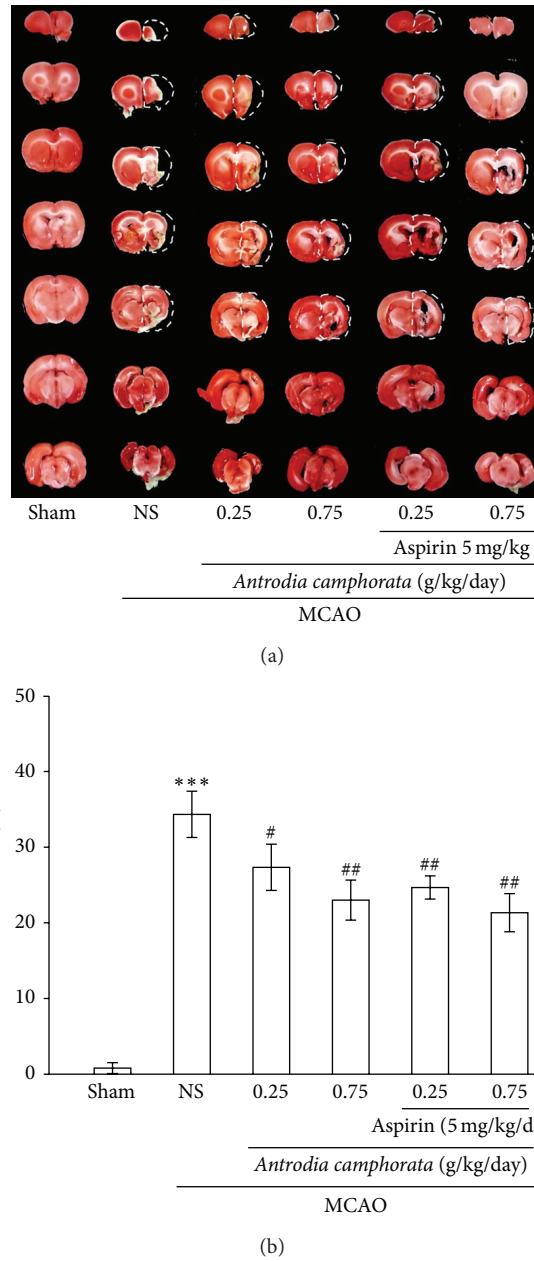

Figure 1: (a) Combination treatment of the extract of *A. camphorata* with aspirin against thromboembolic stroke in rats. Coronal sections of 2,3,5-triphenyltetrazolium- (TTC-) stained brains after thromboembolic occlusion-reperfusion rats were observed in a sham-operated group (sham), a group orally treated with an isovolumetric solvent (distilled water) for 60 days, followed by thromboembolic occlusion (MCAO group), groups orally treated with *A. camphorata* for 60 days alone, followed by thromboembolic occlusion, and groups orally treated with *A. camphorata* (0.25 and 0.75 g/kg/day) combined with aspirin (5 mg/kg/day) for 60 days, followed by thromboembolic occlusion as described in "Section 2." The results are representative examples of three similar experiments; (b) densitometric analysis of the combination treatment of the extract of *A. camphorata* with aspirin against thromboembolic stroke in rats. Data are presented as the infarct volume for each animal in the group as well as the means ± S.E.M. ($n = 5$). $^{***}P < 0.001$ compared to the sham-operated group, $^{\#}P < 0.05$ and $^{\#\#}P < 0.01$ compared to the MCAO group.

observed on a television monitor. The time lapse for inducing thrombus formation leading to the cessation of blood flow was measured.

2.11. Data Analysis. Experimental results are expressed as the mean ± S.E.M. and are accompanied by the number of observations. The experiments were assessed by the method of analysis of variance (ANOVA). If this analysis indicated significant differences among the group means, then each group was compared using the Newman-Keuls method. A P value of <0.05 was considered statistically significant.

3. Results

3.1. A. camphorata and Aspirin Combination Therapy Reduces Infarct Volume. The cerebral infarction was examined using 2 mm thick slices of the cerebrum 24 h after MCAO reperfusion in rats through TTC staining. Figure 1(a) shows typical photographs of coronal sections of sham-operated group, MCAO-treated group, *A. camphorata*-alone-treated groups (0.25 and 0.75 g/kg/day), and *A. camphorata* + aspirin (5 mg/kg/day) treated groups prior to the ischemic insult. At 24 h after MCAO, a high dose of *A. camphorata* treatment alone or combination treatment with aspirin reduced the infarct volume, both of which were more significantly reduced than the volume of MCAO-induced untreated group (Figure 1(b)). In addition, while even a high dose (0.75 g/kg/day) of *A. camphorata* combined with aspirin (5 mg/kg/day) did not show any significant effect on reducing the infarct volumes (Figure 1(b)), as it is found to be almost comparable to that of high dose *A. camphorata* treatment alone, the aspirin has been removed in the following studies.

3.2. A. camphorata Treatment Improves Neurological Outcome and Blood Perfusion Deficit. Variations of neurological deficits scores in different groups are shown in Figure 2(a). Before MCAO, the neurological score was zero in all animals. After MCAO, high-grade neurological deficits ($P < 0.001$) were present. Compared with vehicle-treated rats, treatment with *A. camphorata* significantly and dose-dependently improved the neurological score at 24 h after ischemia ($P < 0.05$). In addition, compared with other blood perfusion unit (BPU) or regional cerebral blood flow (rCBF) measuring methods, laser Doppler flowmeter (LDF; Oxford Array) provides a noninvasive and continuous measure of BPU. Figure 2(b) shows the relative changes of BPU by LDF after MCAO, 30 and 60 days of *A. camphorata* treatment alone. The results show that MCAO-induced animals sustained the most severe ($P < 0.001$) reduction in BPU. However, the low (0.25 g/kg/day) and high (0.75 g/kg/day) dose of *A. camphorata* treatment decreased the BPU compared with the vehicle, although there were no significant differences. All rats in the sham group maintained the baseline level of BPU.

3.3. Effects of A. camphorata on Subarachnoid Hemorrhage and Hemorrhagic Incidence. Representative photographs of the SAH can be seen in Figure 3(a). There is no significant

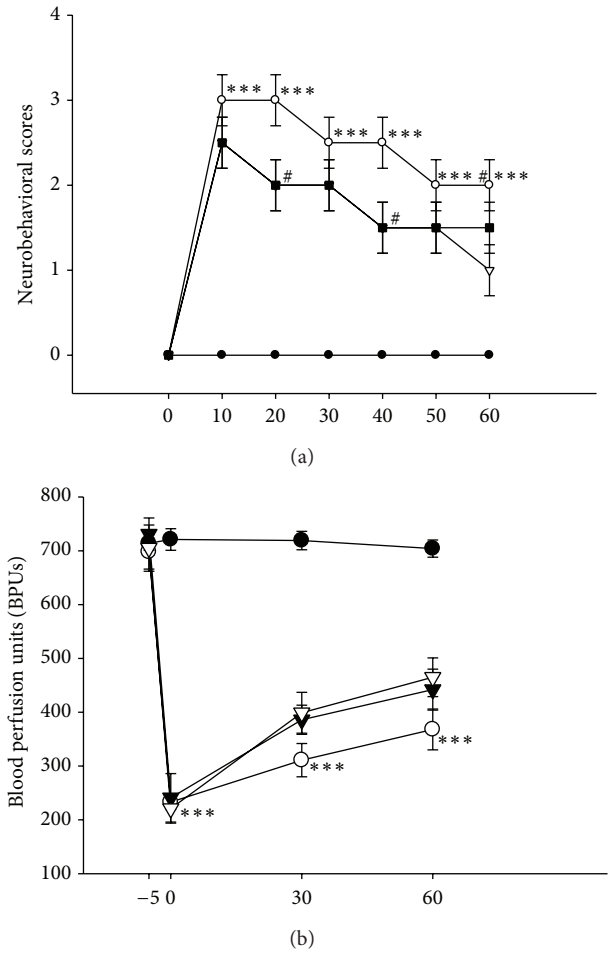

Figure 2: Effects of the extract of *A. camphorata* on (a) neurobehavioral deficits and (b) blood perfusion unit (BPU) in thromboembolic stroke-induced rats. (a) shows neurobehavioral deficits in 4 experimental groups; (b) shows BPU of solvent and *A. camphorata* or the aspirin treated rats were measured by laser Doppler flowmeter in the MCAO-supplied cortex. Data are presented as the means ± S.E.M. of three similar experiments. $^{***}P < 0.001$ compared to the sham-operated group; $^{\#}P < 0.05$ compared to the MCAO group.

difference among the groups of sham-operated, MCAO-induced, MCAO + *A. camphorata,* and MCAO + *A. camphorata* + aspirin treatment overall SAH grade. The arteries can be well recognized in the sham group. Although there is no severe effect in the SAH + MCAO group, a very little obliterated artery by the blood clot was seen. Furthermore, we found that treatment of *A. camphorata* (0.75 g/kg/day) alone or combination with aspirin (5 mg/kg/day) did not induce subarachnoid hemorrhage. In addition, the concentration of hemoglobin in the ischemic hemisphere and gastric luminal fluid in sham-operated and *A. camphorata* alone or combined with aspirin groups is almost similar (Figures 3(b) and 3(c)). Since there is no significant effect of *A. camphorata* at high dose alone or with aspirin on hemoglobin content, this treatment method is considered

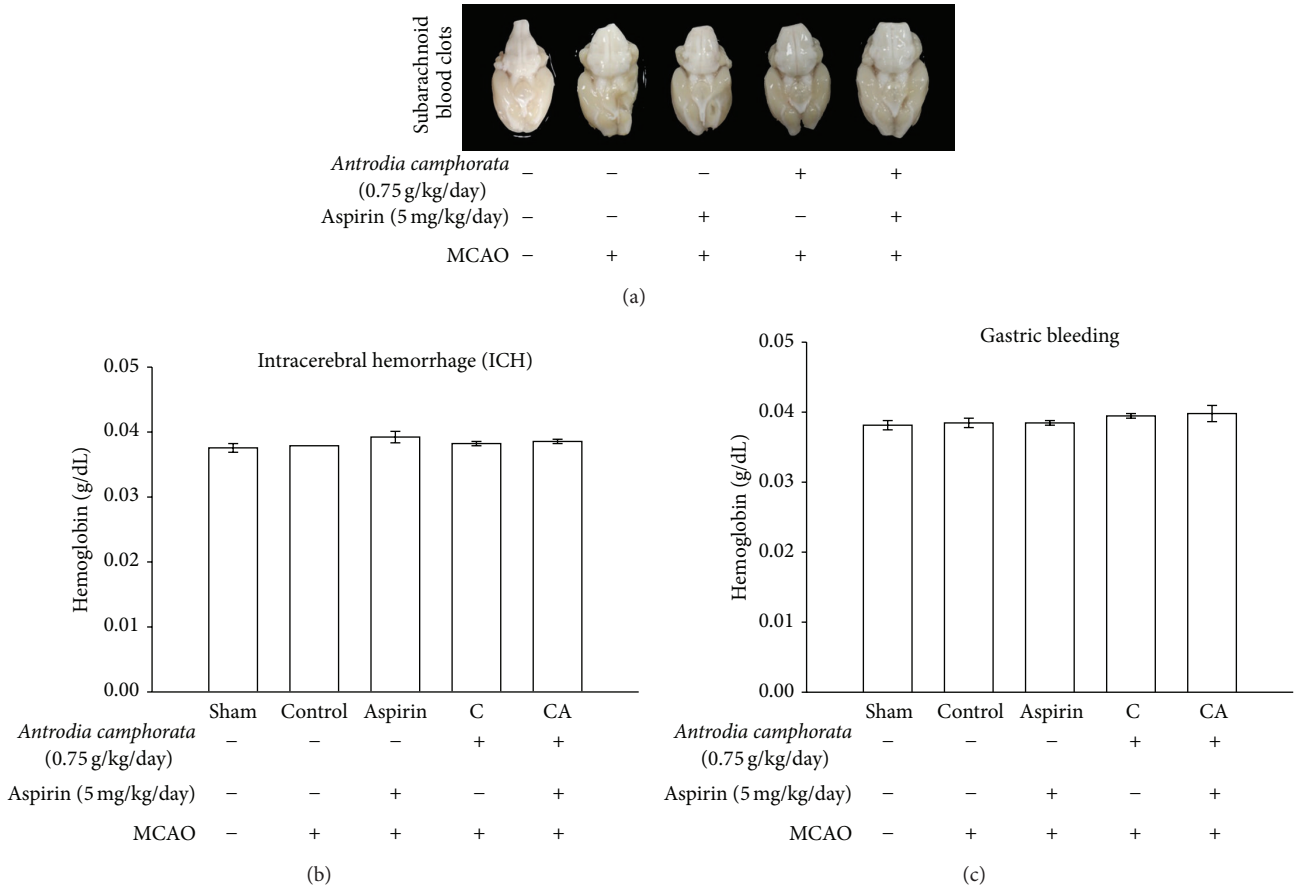

Figure 3: Effects of the extract of *A. camphorata* with aspirin on (a) subarachnoid hemorrhage (SAH), (b) intracerebral hemorrhage (ICH), and (c) gastric bleeding in thromboembolic stroke-induced rats. Data are presented as the means ± S.E.M. of seven similar experiments.

to be safer and does not cause any side effect. In addition, to check the intracerebral hemorrhage and gastric bleeding in studied animals hemoglobin content in the ischemic hemisphere and gastric luminal fluid was determined. The results revealed that the levels of hemoglobin were not altered in all the groups, which indicate that there are no side effects found during the treatment of *A. camphorata*, aspirin alone, or combination of both in MCAO-induced rats.

3.4. Effects of A. camphorata on Prothrombin Time (PT) and Occlusion Time (OT). To determine whether or not coagulation parameters are influenced by *A. camphorata* treatment alone or its combination with aspirin, PT and OT were measured in the present study. *A. camphorata* alone or with aspirin did not cause a prolongation of PT (Figure 4(a)), an observation which is at variance with a previously reported study [18]. Nevertheless, this treatment significantly ($P < 0.01$) increased prolongation of OT for inducing thrombus formation in mesenteric venules in mice when compared with fluorescein dye- (Sigma Aldrich, USA) induced untreated group (Figure 4(b)).

4. Discussion

There are numerous animal stroke models which were designated in the previous literature such as photochemically induced MCAO, surgical occlusion, and vessel occlusion which only simulated the aspect of vessel occlusion [18]; some aspects of human strokes can only be reproduced by these models. An ideal animal model, which resembles human embolic strokes as closely as possible, should be based on the thromboembolic occlusion of a large feeder artery. In the current study, the thromboembolic stroke model mimics human strokes more closely than do other models of cerebral ischemia [19]. Besides, animal thromboembolic strokes induced by blood clots simplify the investigation of the effects of thrombolytic therapy, which is currently the only available stroke treatment in humans. Cerebral ischemia restricted to the distribution of the thromboembolic occlusion gives rise to focal metabolic disturbances that result in infarction, neuronal necrosis, and brain edema [20]. In the present study, it is confirmed, for the first time, that oral treatment of an extract of *A. camphorata* suppresses thromboembolic stroke in rats by reducing infarct volume, improves neurological outcome, and provides neuroprotection.

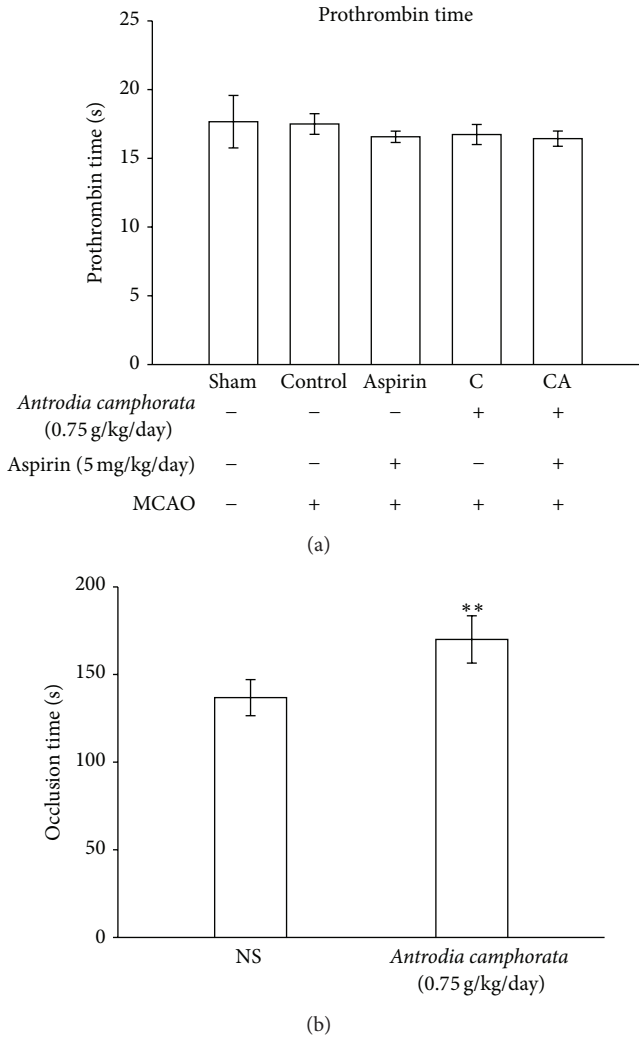

Figure 4: Effects of the extract of *A. camphorata* with aspirin on (a) prothrombin time (PT) and (b) occlusion time (OT) in thromboembolic stroke-induced rats. Data are presented as the means ± S.E.M. of three similar experiments.

Novel cellular and pharmacological therapeutic approaches are required to raise the capacity of the brain for neuroregeneration and neuroplasticity to reduce neurological deficits after stroke [21]. In the current study, we studied the neuroprotective effect of an extract of *A. camphorata* and aspirin combination treatment after an experimentally induced embolic stroke in rats. Notably, we found that administration of a combination treatment of *A. camphorata* in doses of 0.25 and 0.75 g/kg/day administered 24 h after MCAO significantly improved neurological functional outcome, reduced infarct volume, and kept sustained subarachnoid hemorrhagein rats at 60 days after MCAO. Our results also show that treatment with *A. camphorata* alone or with aspirin 24 h after MCAO resulted in no significant changes of hemorrhagic incidence, as there is no variation found in the levels of hemoglobin in cerebral hemorrhage and gastric bleeding of the ischemic hemisphere in sham, *A. camphorata* alone or in combination with aspirin groups. On the other hand, *A. camphorata* therapy alone or combined with aspirin had no effect on prothrombin time, whereas this treatment prolongs occlusion time. Together, our results demonstrate that combining *A. camphorata* with aspirin treatment has an additive effect on the treatment of this thromboembolic model of stroke.

The most commonly used tool for measuring the efficacy of neuroprotective compounds is TTC staining. Brain lesion identified by TTC staining indicates that tissues were irreversibly impaired in mitochondrial function and dehydrogenase activity [22]. Our study demonstrated that treatment with *A. camphorata* (0.25 and 0.75 g/kg/day) significantly decreased the volume of infarction following cerebral ischemia insult. It was implied that *A. camphorata* treatment could improve mitochondrial activity after brain ischemia. Behind stroke, animals consequently display a variety of neurological deficits. It is very imperative to assess neurological function outcome after stroke. The Bederson scale is a global neurological assessment that was developed to measure neurological impairments following stroke [23]. Our results revealed that *A. camphorata* alone at doses 0.25 and 0.75 g/kg/day could improve neurological behavior disturbance based on neurological deficit scores.

The duration of the ischemia and the degree of CBF or BPU reduction are the major factors to determine the severity of ischemic damage. It is generally accepted that >70% reductions in CBF are necessary to induce ischemic brain damage although some recent evidence suggests that more modest reductions may cause delayed neuronal death [24]. It was also reported that cortical injury was related to the duration of ischemia between 30 and 45 min, and beyond 37 min both magnitude and distribution of cortical injury increased markedly in a linear fashion [25]. In the present study, at 30 and 60 days MCAO induced an immediate reduction of BPU value. However, the BPU was improved in both low (0.25 mg/kg/day) and high (0.75 g/kg/day) dose groups of *A. camphorata* treatment. The increased BPU in the MCAO-induced rats may perhaps directly determine the volume of infarction. Therefore it is suggested that in our study the marked reductions of infarct volume in *A. camphorata*-treated groups may mainly result from the improved BPU in the brain during MCAO.

Increased risk of hemorrhage is a documented possible side effect of antithrombotic treatments [26]. To evaluate this aspect, the subarachnoid hemorrhage (SAH) grade was checked to know the possible side effect of *A. camphorata* alone or in combination with aspirin treatment on MCAO-induced rats. The results revealed that *A. camphorata* alone or in combination with aspirin treatment did not affect this parameter. On the other hand a literature about secondary intracerebral bleeding after stroke in rats is reported to be poor and hence bleeding rates in animals and humans may differ [27]. In this study, we focused on the efficacy of *A. camphorata* alone or with aspirin on hemoglobin content as a marker of bleeding and an important safety measure, and we found that there is no alteration in the hemoglobin level. To determine whether or not coagulation parameters and platelet functional marker are influenced by *A. camphorata*

or their combination with aspirin, PT and OT were measured in the present study. *A. camphorata* or aspirin alone did not cause a prolongation of PT, an observation which is at variance with a previously reported study [17]. However, *A. camphorata* at the dose of 0.75 mg/kg/day increased the prolongation of OT. This prompts the conclusion that coagulation cascade did not part the bleeding interaction with the combination of *A. camphorata* with aspirin.

In conclusion, the present study has demonstrated that pretreatment with *Antrodia camphorata* (0.25 and 0.75 g/kg/day) is beneficial in reducing infarct volume in the focal ischemic brain injury in the embolic model. *A. camphorata* treatment is also beneficial in reestablishing blood flow to the ischemic brain by reducing perfusion deficits following ischemia and it also provides added benefits, as it did not cause any hemorrhagic incidence when used in conjunction with aspirin therapy. This evidence suggests that *A. camphorata* has neuroprotective effect against ischemic insults in our MCAO model through a mechanism of blood perfusion regulation without increasing hemorrhagic transformation.

Conflict of Interests

The authors declare that they have no conflict of interests to disclose.

Authors' Contribution

Dr. Ye-Ming Lee and Dr. Chiu-Yun Chang contributed equally to this work.

Acknowledgments

This work was supported by Grants from the National Science Council of Taiwan (NSC97-2320-B-038-016-MY3 and NSC100-2320-B-038-021-MY3), the Hsinchu Mackay Memorial Hospital (MMH20130401), the Council of Agriculture, Executive Yuan (101AS-1.2.2-ST-aH and 102AS-1.2.3-ST-a8), and the Taipei Medical University (TMU-R-100-04).

References

[1] S. T. Carmichael, "Rodent models of focal stroke: size, mechanism, and purpose," *NeuroRx*, vol. 2, no. 3, pp. 396–409, 2005.

[2] M. P. Pereira, O. Hurtado, A. Cárdenas et al., "Rosiglitazone and 15-deoxy-Δ12,14-prostaglandin J 2 cause potent neuroprotection after experimental stroke through noncompletely overlapping mechanisms," *Journal of Cerebral Blood Flow and Metabolism*, vol. 26, no. 2, pp. 218–229, 2006.

[3] C. X. Wang, T. Yang, and A. Shuaib, "An improved version of embolic model of brain ischemic injury in the rat," *Journal of Neuroscience Methods*, vol. 109, no. 2, pp. 147–151, 2001.

[4] S. A. Lipton, "Failures and successes of NMDA receptor antagonists: molecular basis for the use of open-channel blockers like memantine in the treatment of acute and chronic neurologic insults," *NeuroRx*, vol. 1, no. 1, pp. 101–110, 2004.

[5] B. Jiang, W. Z. Wang, H. L. Chen et al., "Incidence and trends of stroke and its subtypes in China: results from three large cities," *Stroke*, vol. 37, no. 1, pp. 63–68, 2006.

[6] D. L. Bhatt, K. A. A. Fox, W. Hacke et al., "Clopidogrel and aspirin versus aspirin alone for the prevention of atherothrombotic events," *The New England Journal of Medicine*, vol. 354, no. 16, pp. 1706–1717, 2006.

[7] H. C. Diener, J. Bogousslavsky, and L. M. Brass, "Aspirin and clopidogrel compared with clopidogrel alone after recent ischaemic stroke or transient ischemic attack in high-risk patients (MATCH): randomized, double-blind, placebo controlled trial," *The Lancet*, vol. 364, no. 9431, pp. 331–337, 2004.

[8] Q. Yang, Q. Niu, Y. Zhou et al., "Incidence of cerebral hemorrhage in the Changsha community: a prospective study from 1986 to 2000," *Cerebrovascular Diseases*, vol. 17, no. 4, pp. 303–313, 2004.

[9] J. Liu, T. Huang, M. Hsu et al., "Antitumor effects of the partially purified polysaccharides from Antrodia camphorata and the mechanism of its action," *Toxicology and Applied Pharmacology*, vol. 201, no. 2, pp. 186–193, 2004.

[10] Y.-C. Hseu, H.-L. Yang, Y.-C. Lai, J.-G. Lin, G.-W. Chen, and Y.-H. Chang, "Induction of apoptosis by *Antrodia camphorata* in human premyelocytic leukemia HL-60 cells," *Nutrition and Cancer*, vol. 48, no. 2, pp. 189–197, 2004.

[11] G. Hsiao, M. Shen, K. Lin et al., "Antioxidative and hepatoprotective effects of Antrodia camphorata extract," *Journal of Agricultural and Food Chemistry*, vol. 51, no. 11, pp. 3302–3308, 2003.

[12] T. Y. Song and G. C. Yen, "Protective effects of fermented filtrate from Antrodia camphorata in submerged culture against CCl4-induced hepatic toxicity in rats," *Journal of Agricultural and Food Chemistry*, vol. 51, no. 6, pp. 1571–1577, 2003.

[13] A. Shuaib, C. X. Wang, T. Yang, and R. Noor, "Effects of nonpeptide V1 vasopressin receptor antagonist SR-49059 on infarction volume and recovery of function in a focal embolic stroke model," *Stroke*, vol. 33, no. 12, pp. 3033–3037, 2002.

[14] J. Lee, W. Hsu, T. Yen et al., "Traditional Chinese medicine, Xue-Fu-Zhu-Yu decoction, potentiates tissue plasminogen activator against thromboembolic stroke in rats," *Journal of Ethnopharmacology*, vol. 134, no. 3, pp. 824–830, 2011.

[15] G. Hsiao, K. H. Lin, Y. Chang et al., "Protective mechanisms of inosine in platelet activation and cerebral ischemic damage," *Arteriosclerosis, Thrombosis, and Vascular Biology*, vol. 25, no. 9, pp. 1998–2004, 2005.

[16] E. J. Lee, H. Chen, T. Wu, T. Chen, I. A. Ayoub, and K. I. Maynard, "Acute administration of Ginkgo biloba extract (EGb 761) affords neuroprotection against permanent and transient focal cerebral ischemia in Sprague-Dawley rats," *Journal of Neuroscience Research*, vol. 68, no. 5, pp. 636–645, 2002.

[17] H. Lu, D. X. Zhou, J. W. Yan, and W. H. Ge, "Anticoagulant activity of Danggui originated from four different places," *China Medical Technologies*, vol. 9, p. 225, 2002.

[18] K. Krueger and E. Busch, "Protocol of a thromboembolic stroke model in the rat: review of the experimental procedure and comparison of models," *Investigative Radiology*, vol. 37, no. 11, pp. 600–608, 2002.

[19] K. Overgaard, "Thrombolytic therapy in experimental embolic stroke," *Cerebrovascular and Brain Metabolism Reviews*, vol. 6, no. 3, pp. 257–286, 1994.

[20] M. D. Ginsberg and R. Busto, "Rodent models of cerebral ischemia," *Stroke*, vol. 20, no. 12, pp. 1627–1642, 1989.

[21] J. Chen and M. Chopp, " Neurorestorative treatment of stroke: cell and pharmacological approaches," *NeuroRx*, vol. 3, no. 4, pp. 466–473, 2006.

[22] A. Benedek, K. Móricz, Z. Jurányi et al., "Use of TTC staining for the evaluation of tissue injury in the early phases of reperfusion after focal cerebral ischemia in rats," *Brain Research*, vol. 1116, no. 1, pp. 159–165, 2006.

[23] A. Durukan and T. Tatlisumak, "Acute ischemic stroke: overview of major experimental rodent models, pathophysiology, and therapy of focal cerebral ischemia," *Pharmacology Biochemistry and Behavior*, vol. 87, no. 1, pp. 179–197, 2007.

[24] B. Ma and J. Zhang, "Nimodipine treatment to assess a modified mouse model of intracerebral hemorrhage," *Brain Research*, vol. 1078, no. 1, pp. 182–188, 2006.

[25] A. Riddle, N. L. Luo, M. Manese et al., "Spatial heterogeneity in oligodendrocyte lineage maturation and not cerebral blood flow predicts fetal ovine periventricular white matter injury," *Journal of Neuroscience*, vol. 26, no. 11, pp. 3045–3055, 2006.

[26] G. Helft, M. Gilard, C. Le Feuvre, and A. G. Zaman, "Drug Insight: Antithrombotic therapy after percutaneous coronary intervention in patients with an indication for anticoagulation," *Nature Clinical Practice Cardiovascular Medicine*, vol. 3, no. 12, pp. 673–680, 2006.

[27] G. Brinker, F. Pillekamp, and K.-A. Hossmann, "Brain hemorrhages after rt-PA treatment of embolic stroke in spontaneously hypertensive rats," *NeuroReport*, vol. 10, no. 9, pp. 1943–1946, 1999.

Hindawi Publishing Corporation
The Scientific World Journal
Volume 2014, Article ID 130381, 10 pages
http://dx.doi.org/10.1155/2014/130381

Research Article

Andrographolide Inhibits Nuclear Factor-κB Activation through JNK-Akt-p65 Signaling Cascade in Tumor Necrosis Factor-α-Stimulated Vascular Smooth Muscle Cells

Yu-Ying Chen,[1] Ming-Jen Hsu,[2] Cheng-Ying Hsieh,[1,2] Lin-Wen Lee,[3] Zhih-Cherng Chen,[1,2,4,5] and Joen-Rong Sheu[1,2]

[1] *Graduate Institute of Medical Sciences, College of Medicine, Taipei Medical University, Taipei 11031, Taiwan*
[2] *Department of Pharmacology, School of Medicine, Taipei Medical University, Taipei 11031, Taiwan*
[3] *Department of Microbiology and Immunology, Taipei Medical University, Taipei 11031, Taiwan*
[4] *Department of Cardiology, Chi-Mei Medical Center, Tainan City 71004, Taiwan*
[5] *Department of Pharmacy, Chia Nan University of Pharmacy & Science, Tainan City 71004, Taiwan*

Correspondence should be addressed to Zhih-Cherng Chen; z_cchen@yahoo.com.tw
and Joen-Rong Sheu; sheujr@tmu.edu.tw

Received 27 May 2014; Accepted 30 June 2014; Published 10 July 2014

Academic Editor: Duen-Suey Chou

Critical vascular inflammation leads to vascular dysfunction and cardiovascular diseases, including abdominal aortic aneurysms, hypertension, and atherosclerosis. Andrographolide is the most active and critical constituent isolated from the leaves of *Andrographis paniculata*, a herbal medicine widely used for treating anti-inflammation in Asia. In this study, we investigated the mechanisms of the inhibitory effects of andrographolide in vascular smooth muscle cells (VSMCs) exposed to a proinflammatory stimulus, tumor necrosis factor-α (TNF-α). Treating TNF-α-stimulated VSMCs with andrographolide suppressed the expression of inducible nitric oxide synthase in a concentration-dependent manner. A reduction in TNF-α-induced c-Jun N-terminal kinase (JNK), Akt, and p65 phosphorylation was observed in andrographolide-treated VSMCs. However, andrographolide affected neither IκBα degradation nor p38 mitogen-activated protein kinase or extracellular signal-regulated kinase 1/2 phosphorylation under these conditions. Both treatment with LY294002, a phosphatidylinositol 3-kinase/Akt inhibitor, and treatment with SP600125, a JNK inhibitor, markedly reversed the andrographolide-mediated inhibition of p65 phosphorylation. In addition, LY294002 and SP600125 both diminished Akt phosphorylation, whereas LY294002 had no effects on JNK phosphorylation. These results collectively suggest that therapeutic interventions using andrographolide can benefit the treatment of vascular inflammatory diseases, and andrographolide-mediated inhibition of NF-κB activity in TNF-α-stimulated VSMCs occurs through the JNK-Akt-p65 signaling cascade, an IκBα-independent mechanism.

1. Introduction

Coronary artery disease (CAD) represents the leading cause of mortality and morbidity in developed countries, and atherosclerosis is the hallmark of many critical events in the pathogenesis of CAD [1]. Consequently, developing novel therapeutic agents for atherosclerosis patients is a major research priority. One of the risk factors for atherosclerosis is chronic and mild inflammation of the arteries [2]. Therefore, the inhibition of vascular smooth muscle cell (VSMC) inflammation might be a major target for the treatment of cardiovascular diseases. Numerous studies have shown that several cytokines, including tumor necrosis factors (TNFs), interleukins, and interferons (IFNs), are important inflammatory stimulators of VSMCs in vitro and in vivo [3]. These inflammatory stimulators interact with specific receptors and activate signaling cascades, leading to inflammatory responses such as matrix metalloproteinase (MMP) expression; nitric oxide (NO); reactive oxygen species (ROS) production; and subsequent cell growth, adhesion, and migration [3].

Accumulating evidence has indicated that the induction of inducible nitric-oxide synthase (iNOS), a key enzyme for NO biosynthesis, contributes to the process of vascular diseases, such as atherosclerosis [4]. Vascular inflammatory responses induced by pathogens or cytokines are accompanied by the generation of peroxynitrite, a potent and vasotoxic molecule formed through the reaction of NO and superoxide [5]. In addition, a study showed that iNOS contributes to TNF-α-induced inflammation and regulates vascular endothelial functions [6]. Previous studies on TNF-α have reported a positive correlation through signal transduction pathways that converge at mitogen-activated protein kinases (MAPKs) [7] or nuclear factor-κB (NF-κB) [8]. Conversely, cellular responses to inflammatory stimuli mainly involve the activation of Akt signaling cascades. Akt is involved in the phosphatidylinositol 3-kinase (PI3K)/Akt signaling pathway, which regulates cellular processes, such as cell proliferation, survival, and inflammation [9], and was reported to be essential to TNF-α-induced NF-κB activation [10].

Andrographolide (Figure 1), a novel NF-κB inhibitor, is the most active and critical constituent isolated from the leaves of *Andrographis paniculata* [11]. *A. paniculata* has long been used as herbal medicine to prevent and treat upper respiratory tract infections, diarrhea, rheumatoid arthritis, and laryngitis in Asia and Scandinavia [11, 12]. Our previous studies have revealed that andrographolide enhances NF-κB subunit p65 Ser536 dephosphorylation and ROS formation by stimulating neutral sphingomyelinase-mediated ceramide formation in VSMCs [13, 14] and inhibits platelet aggregation by suppressing the p38MAPK/HO^--NF-κB-extracellular-signal-regulated-kinase (ERK) 2 cascade [15, 16]. Although andrographolide has exhibited anti-inflammatory activity in various cell types, its anti-inflammatory mechanism in VSMCs remains unclear. In the present study, by considering the pivotal role of VSMC inflammation in the development of atherosclerosis and restenosis [17], we investigated in detail the protective cellular signaling events associated with andrographolide in rat VSMCs stimulated by TNF-α, which represented vascular inflammatory conditions.

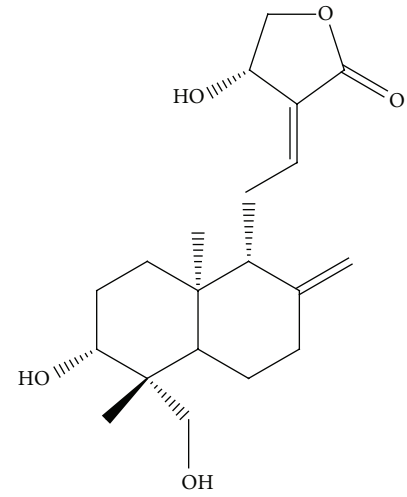

Figure 1: Chemical structure of andrographolide (Andro).

2. Materials and Methods

2.1. Materials. Dulbecco's modified Eagle's medium (DMEM), trypsin (0.25%), L-glutamine, penicillin/streptomycin, and fetal bovine serum (FBS) were purchased from Gibco (Gaithersburg, MD, USA). Andrographolide (≥98%), TNF-α, LY294002, SP600125, and dimethyl sulfoxide (DMSO) were obtained from Sigma-Aldrich (St. Louis, MO, USA). The anti-iNOS rabbit polyclonal antibody (pAb) and the anti-p65 antibody were purchased from Santa Cruz Biotechnology (Dallas, TX, USA); the anti-α-tubulin mouse monoclonal antibody (mAb) was purchased from Thermo Scientific (Waltham, MA, USA); and the anti-phospho-p38 MAPK Thr180/Tyr182 rabbit pAb, anti-p38 MAPK, anti-phospho-p44/p42 extracellular signal-regulated kinase (ERK1/2) Thr202/Tyr204 rabbit pAb, anti-ERK1/2 antibody, anti-phospho-JNK Thr183/Tyr185 rabbit mAb, anti-JNK antibody, anti-phospho-Akt Ser473 rabbit pAb, anti-Akt antibody, anti-phospho-p65 Ser536 rabbit pAb, and anti-IκBα antibody were purchased from Cell Signaling (Danvers, MA, USA). A hybond-P polyvinylidene difluoride (PVDF) membrane, an enhanced chemiluminescence (ECL) western blotting detection reagent and analysis system, the horseradish-peroxidase- (HRP-) conjugated donkey anti-rabbit immunoglobulin G (IgG), and the sheep anti-mouse IgG were acquired from Amersham (Buckinghamshire, UK). Andrographolide was dissolved in 0.1% DMSO and stored at 4°C until it was used.

2.2. Rat Aortic Smooth Muscle Cell Primary Culture. The male Wistar rats used in this study were purchased from BioLASCO (Taipei, Taiwan). The VSMCs were enzymatically dispersed from the male Wistar rats (250–300 g). Thoracic aortas from the Wistar rats were removed and stripped of the endothelium and adventitia. The VSMCs were obtained using a modification of the combined collagenase and elastase digestion method [18]. These cells were grown in DMEM supplemented with 20 mM HEPES, 10% FBS, 1% penicillin/streptomycin, and 2 mM glutamine at 37°C in a humidified atmosphere of 5% CO_2. The growth medium was changed every 2-3 d until the cells reached confluence. The growth medium was removed, and the monolayer was rinsed with phosphate-buffered saline (PBS). A trypsin-EDTA solution was added, and the monolayer was incubated at 37°C for 2 min. The culture dishes were observed under a phase-contrast microscope until the cells detached. The cells were removed using 10 mL of DMEM and centrifuged at 900 rpm for 7 min. The pellet was resuspended in DMEM in a culture dish, and cells from Passages 4–8 were used in all experiments. All protocols were approved by the Taipei Medical University Animal Care and Use Committee.

2.3. Cell Morphology. The VSMCs (5×10^5 cells/dish) were seeded in 60-mm dishes and cultured in DMEM containing 10% FBS for 24 h. Cell morphology was evaluated by phase

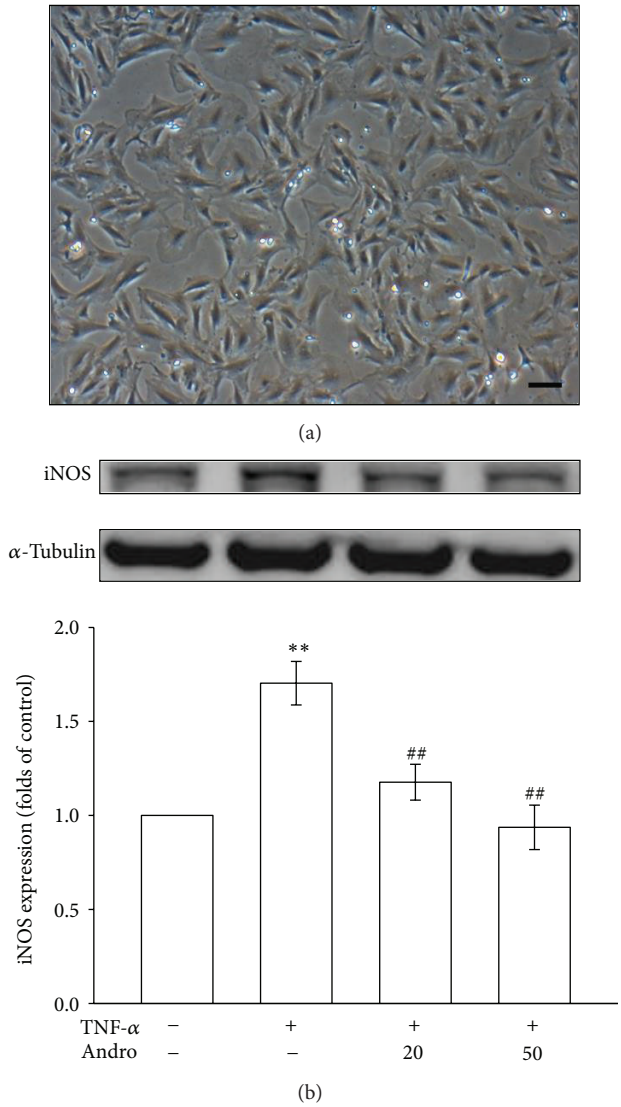

Figure 2: Effects of andrographolide on iNOS expression in TNF-α-stimulated VSMCs. (a) Photomicrograph showing the primary cultured rat aortic VSMCs (magnification ×100). (b) The VSMCs were treated with PBS (resting group) or pretreated with andrographolide (20 and 50 μM) or an equal volume of DMSO (solvent control) for 20 min, and TNF-α (10 ng/mL) was subsequently added for 24 h. The iNOS protein level was evaluated as described in Section 2. $^{**}P < 0.01$ compared with the resting group; $^{\#\#}P < 0.01$ compared with the TNF-α group. The data are presented as the mean ± SEM ($n = 3$).

contrast microscopy without preliminary fixation. The primary cultured rat aortic VSMCs exhibited "hills and valleys" pattern (Figure 2(a)), and the expression of α-smooth muscle actin was confirmed (data not shown). The micrographs were recorded using a Nikon phase-contrast microscope (Tokyo, Japan).

2.4. Immunoblot Analysis. Immunoblot analyses were performed as described previously [18]. Briefly, the VSMCs (5×10^5 cells/dish) were treated as the experimental design. After the experimental period, the proteins were extracted using a lysis buffer. Lysates were centrifuged, the supernatant protein (50 μg) was collected and subjected to sodium dodecyl sulfate-polyacrylamide gel electrophoresis, and the separated proteins were electrophoretically transferred onto 0.45-μm PVDF membranes by using semidry transfer (Bio-Rad, Hercules, CA, USA). The blots were blocked with TBST (10 mM Tris-base, 100 mM NaCl, and 0.01% Tween 20) containing 5% bovine serum albumin for 1 h and then probed with various primary antibodies. The membranes were incubated with HRP-linked anti-mouse IgG or anti-rabbit IgG (diluted 1 : 3000 in TBST) for 1 h. The immunoreactive bands were detected using an ECL system. Bar graphs depict the ratios of quantitative results obtained by scanning the reactive bands and quantifying the optical density by using video densitometry (Bio-Profil; Biolight Windows application Version 2000.01; Vilber Lourmat, France).

2.5. Statistical Analysis. The experimental results are expressed as the means ± standard error and are accompanied

by the number of observations. Data were assessed using an analysis of variance. If an analysis indicated significant differences among the group means, then each group was compared with the other groups by using the Newman-Keuls method. Values of $P < 0.05$ indicated statistical significance.

3. Results

3.1. Effects of Andrographolide on the Expression of Inducible Nitric Oxide Synthase in Tumor Necrosis Factor-α-Stimulated Vascular Smooth Muscle Cells. We examined whether andrographolide affects the protein level of iNOS, which catalyzes NO formation, in TNF-α-stimulated VSMCs. As shown in Figure 2(b), treatment with TNF-α increased iNOS expression 1.7 ± 0.1-fold compared with the iNOS expression observed in the control group ($P < 0.01$, $n = 3$). Concentration-dependent inhibition was observed in TNF-α-stimulated VSMCs in response to treatment with 20 μM and 50 μM andrographolide; specifically, iNOS expression decreased to 29.4% and 47.1%, respectively.

3.2. Effects of Andrographolide on p38 Mitogen-Activated Protein Kinase, Extracellular Signal-Regulated Kinase 1/2, c-Jun N-Terminal Kinase, and Akt Signaling Pathways in Tumor Necrosis Factor-α-Stimulated Vascular Smooth Muscle Cells. Vascular inflammation is intensively included in cardiovascular disease. In response to inflammatory stimuli, MAPK phosphorylation increases and subsequently promotes VSMC proliferation and migration [19]. To explore the mechanisms through which andrographolide inhibits TNF-α-induced vascular inflammation, we examined the effects of andrographolide on the status of p38MAPK, ERK1/2, and JNK activation in TNF-α-stimulated VSMCs. As shown in Figure 3(a), the increase in p38MAPK phosphorylation was 2.2 ± 0.2-fold ($P < 0.05$, $n = 3$) after the VSMCs were exposed to TNF-α for 10 min. In addition, 10-min TNF-α treatment caused 1.7 ± 0.1-fold and 1.9 ± 0.1-fold increases in ERK1/2 and JNK phosphorylation ($P < 0.01$, $n = 3$) (Figures 3(b) and 3(c)). Pretreating the cells with 20 and 50 μM andrographolide significantly reduced TNF-α-induced JNK phosphorylation (Figure 3(c)). However, pretreating the cells with 20 or 50 μM andrographolide did not significantly affect TNF-α-induced p38MAPK or ERK1/2 phosphorylation (Figures 3(a) and 3(b)). By contrast, a study reported that Akt is a crucial regulator involved in cell metabolism, cell growth, and vascular inflammation [20]. Figure 3(d) shows that Akt phosphorylation increased 1.5 ± 0.0-fold ($P < 0.01$, $n = 3$) after the VSMCs were exposed to TNF-α for 10 min. Pretreating the cells with 20 and 50 μM andrographolide significantly reduced TNF-α-induced Akt phosphorylation (Figure 3(d)). These results collectively suggested that andrographolide suppresses vascular inflammation by inhibiting JNK and Akt signaling cascades in TNF-α-stimulated VSMCs.

3.3. Effects of Andrographolide on IκBα Degradation and p65 Phosphorylation in Tumor Necrosis Factor-α-Stimulated Vascular Smooth Muscle Cells. Several studies have observed that NF-κB, a transcription factor, regulates the expression of numerous inflammatory proteins, including iNOS [21]. To clarify the mechanism through which andrographolide inhibits iNOS expression, we evaluated the effect of andrographolide on the level of IκBα, a cellular protein that masks the nuclear localization signals of NF-κB and keeps them sequestered in an inactive state [22], in the cytoplasm of TNF-α-stimulated VSMCs. However, as shown in Figure 4(a), pretreating the cells with 20 and 50 μM andrographolide did not reverse TNF-α-induced IκBα degradation. Several studies have indicated that p65 phosphorylation on serine 536 residue mediating its dimerization, DNA binding, and nuclear localization was not associated with or regulated by IκBα [23, 24]. As shown in Figure 4(b), pretreating VSMCs with 50 μM andrographolide significantly inhibited (47.7%) TNF-α-induced p65 phosphorylation compared with that in TNF-α-stimulated VSMCs that were not treated with andrographolide ($P < 0.05$, $n = 3$). These results suggested that p65 phosphorylation rather than IκBα degradation is responsible for the andrographolide-mediated inhibition of NF-κB activation in TNF-α-stimulated VSMCs.

3.4. Andrographolide Suppresses p65 Phosphorylation by Inhibiting the Akt and c-Jun N-Terminal Kinase Signaling Pathways in Tumor Necrosis Factor-α-Stimulated Vascular Smooth Muscle Cells. To clarify the correlations between Akt, JNK, and andrographolide-induced p65 de-phosphorylation in TNF-α-stimulated VSMCs, we used LY294002 (a PI3K/Akt inhibitor) and SP600125 (a JNK inhibitor) to confirm whether Akt or JNK signaling contributes to TNF-α-induced p65 phosphorylation in VSMCs. As shown in Figure 5(a), LY294002 at 10 μM significantly inhibited TNF-α-induced p65 phosphorylation. Similarly, a JNK inhibitor, SP600125 (10 μM), effectively attenuated TNF-α-induced p65 phosphorylation (Figure 5(a)). We further investigated the relationship between Akt and JNK phosphorylation and found that LY294002 (10 μM) and SP600125 (10 μM) obviously diminished TNF-α-induced Akt phosphorylation in VSMCs (Figure 5(b)), whereas LY294002 had no significant effects on TNF-α-induced JNK phosphorylation except SP600125 (Figure 5(c)). These results collectively suggested that andrographolide suppresses p65 phosphorylation by inhibiting the JNK-Akt signaling cascade in TNF-α-stimulated VSMCs.

4. Discussion

Our previous study suggested that andrographolide inhibits LPS/IFN-γ-induced iNOS and MMP-9 expression in rat VSMCs and revealed that andrographolide reduced neointimal formation in a rat carotid injury model [13]. Recent studies have indicated that andrographolide inhibits TNF-α-induced PI3K/Akt phosphorylation and subsequent NF-κB activation in vascular endothelial cells [25, 26]. In addition, in a mouse model of vascular injury, mice lacking functional TNF-α developed 14-fold less neointima than wild-type mice did [27]. We hypothesized that the anti-inflammatory effects of andrographolide in the rat model of vascular injury are related to the modulating effects of andrographolide in TNF-α-stimulated VSMCs. Therefore, the objective of this study

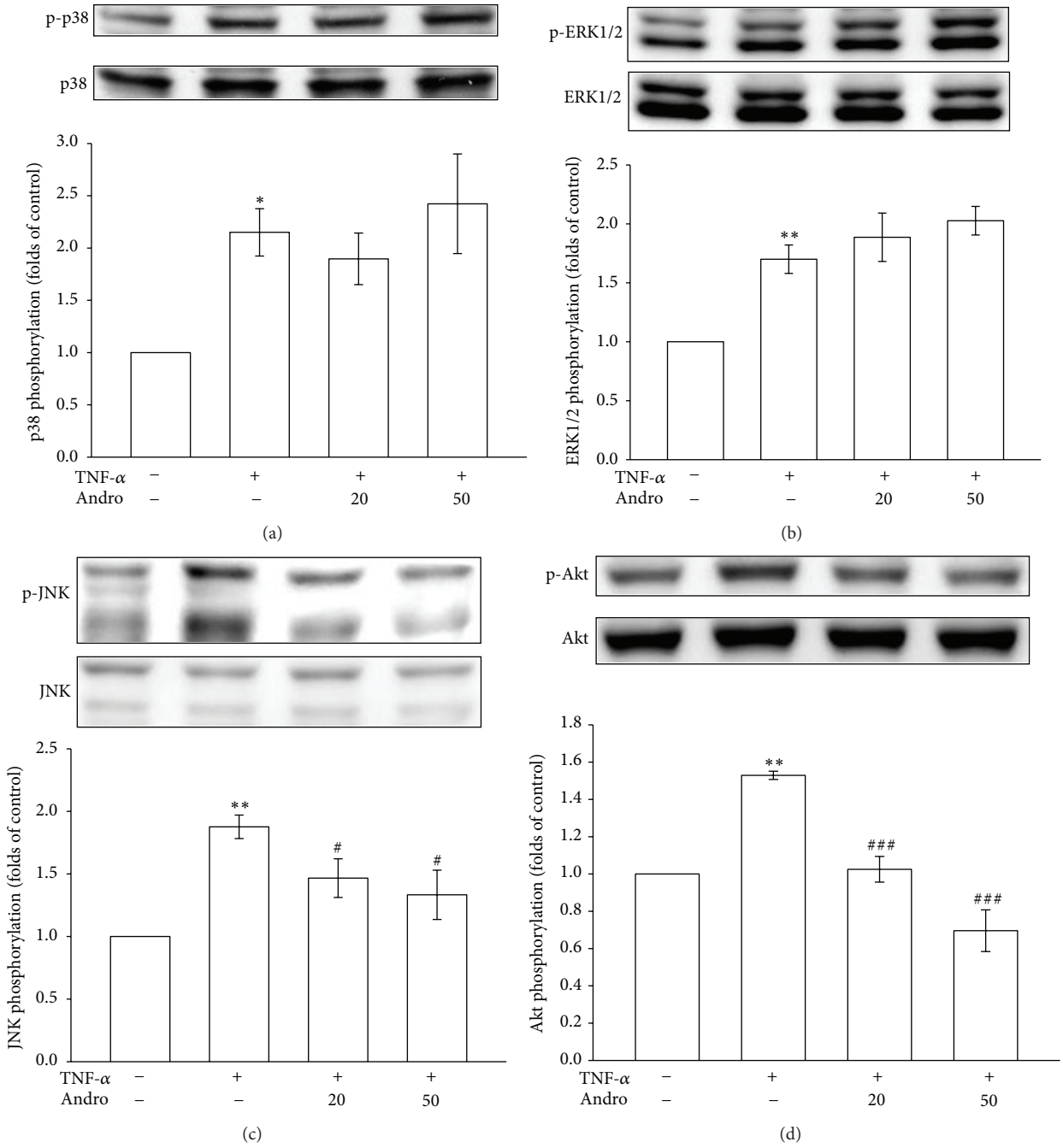

Figure 3: Effects of andrographolide on p38MAPK, ERK1/2, JNK, and Akt signaling pathways in TNF-α-stimulated VSMCs. The VSMCs were treated with PBS (resting group) or pretreated with andrographolide (20 and 50 μM) or an equal volume of DMSO (solvent control) for 20 min, and TNF-α (10 ng/mL) was subsequently added for 10 min. (a) p38MAPK phosphorylation, (b) ERK1/2 phosphorylation, (c) JNK phosphorylation, and (d) Akt phosphorylation were evaluated as described in Section 2. $^{*}P < 0.05$ and $^{**}P < 0.01$ compared with the resting group; $^{\#}P < 0.05$ and $^{\#\#\#}P < 0.001$ compared with the TNF-α group. The data are presented as the mean ± SEM ($n = 3$).

was to examine the effect of andrographolide on signaling molecules involved in TNF-α-stimulated VSMCs. During vascular inflammation, TNF-α gene transcription was time-dependently upregulated, indicating the active involvement of TNF-α in the development of cardiovascular disease [28]. TNF-α is a pleiotropic cytokine, and its receptor binding leads to the activation of MAPK, Akt, and NF-κB signaling cascades [29], thereby eliciting a broad spectrum of cellular responses involved in the control of VSMC proliferation, migration, apoptosis, and inflammation. In the present study,

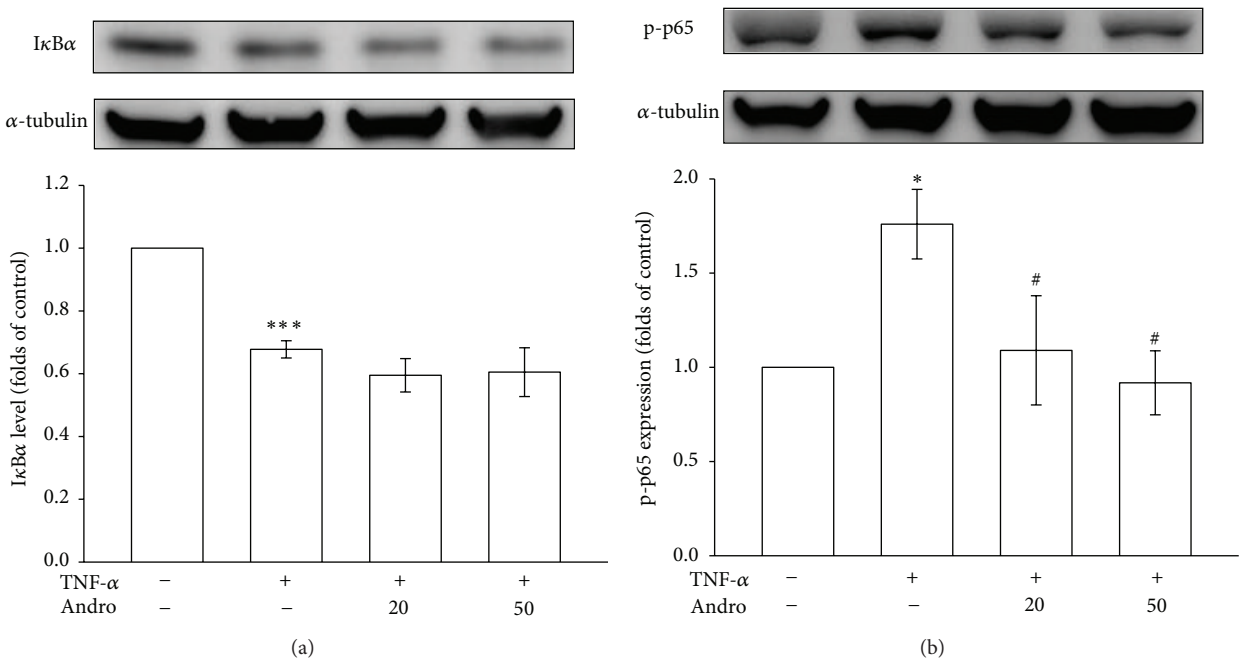

Figure 4: Effects of andrographolide on IκBα degradation and p65 activation in TNF-α-stimulated VSMCs. The VSMCs were treated with PBS (resting group) or pretreated with andrographolide (20 and 50 μM) or an equal volume of DMSO (solvent control) for 20 min, and TNF-α (10 ng/mL) was subsequently added for 30 min. (a) IκBα degradation and (b) p65 phosphorylation were evaluated as described in Section 2. $^{*}P < 0.05$ and $^{***}P < 0.001$ compared with the resting group; $^{\#}P < 0.05$ compared with the TNF-α group. The data are presented as the mean ± SEM ($n = 3$).

to increase the potential for using andrographolide to treat cardiovascular diseases, we showed that andrographolide inhibits TNF-α-induced iNOS expression in rat VSMCs.

TNF-α induces VSMC inflammation through signal transduction pathways that converge at MAPKs or NF-κB pathways [29]. MAPKs are activated in response to inflammatory and atherogenic stimuli, such as PDGF-BB, TNF-α, oxidative stress, hypertension, and balloon injury, and stimulate the expression of several inducible proteins [30]. Furthermore, cellular responses to inflammatory stimuli involve the activation of Akt signaling cascades. The results reported by Chen et al. [26] indicated that andrographolide reduced TNF-α-induced Akt phosphorylation in vascular endothelial cells. Whether MAPKs and Akt contribute to the anti-inflammatory property of andrographolide in VSMCs has not been determined. In the present study, we observed that andrographolide suppresses vascular inflammation by inhibiting JNK and Akt signaling cascades, but not p38MAPK and ERK1/2, in TNF-α-stimulated VSMCs.

NF-κB activation is securely controlled to ensure a functional host defense and prevent tumorigenesis and hyperinflammation [22]. The NF-κB common form in mainly cell types is the p65/p50 heterodimer, and NF-κB signaling is governed by the IKK complex, which consists of IKKα, IKKβ, IKKγ, and the downstream substrate IκBα. After stimulation, activated IKK phosphorylates IκBα, leading to IκBα degradation, enhanced NF-κB nuclear translocation and subsequent transcriptional activation [31]. However, andrographolide did not affect IκBα degradation in this study. Sasaki et al. have suggested that p65 phosphorylated on serine 536 is not associated with or regulated by IκBα, that it has a distinct set of target genes, and that it may represent a noncanonical NF-κB pathway that is independent of IκBα regulation [24]. In this study, we observed that the inhibition of p65 Ser536 phosphorylation may be related to the andrographolide-mediated inhibition of NF-κB in TNF-α-stimulated VSMCs.

Based on the data regarding the effects of andrographolide on MAPKs and Akt in the present study, we postulated that JNK and Akt must be inactivated to enable andrographolide to attenuate p65 phosphorylation. The prototype enzyme activated by PI3Ks is protein kinase B (PKB/Akt), a serine-threonine kinase. Three Akt isoforms are known, namely, Akt1, Akt2, and Akt3. Among these isoforms, Akt1 appears to be the enzyme that is the most relevant to cardiovascular functions [32]. Akt1, a crucial vascular effector of PI3K, plays a determinant role in atheroprotection. In double ApoE-Akt1 knockout mice, atherosclerotic lesions in the aorta and coronary vessels are more severe than those in ApoE-knockout controls. Loss of Akt1 in the vessel wall is associated with increased inflammatory signaling [33]. Thus, PI3Kg/Akt1 should be considered a fundamental molecular axis for the pathobiology of atherosclerosis. JNK is an inflammatory and stress-sensitive kinase. Because JNK plays contradictory roles in cell growth and death, the relative activation of these proteins is vital for the inflammatory status of the cell. As crucial upstream regulators in VSMC inflammation, Akt and JNK play key roles in the pathology of atherosclerosis [30,

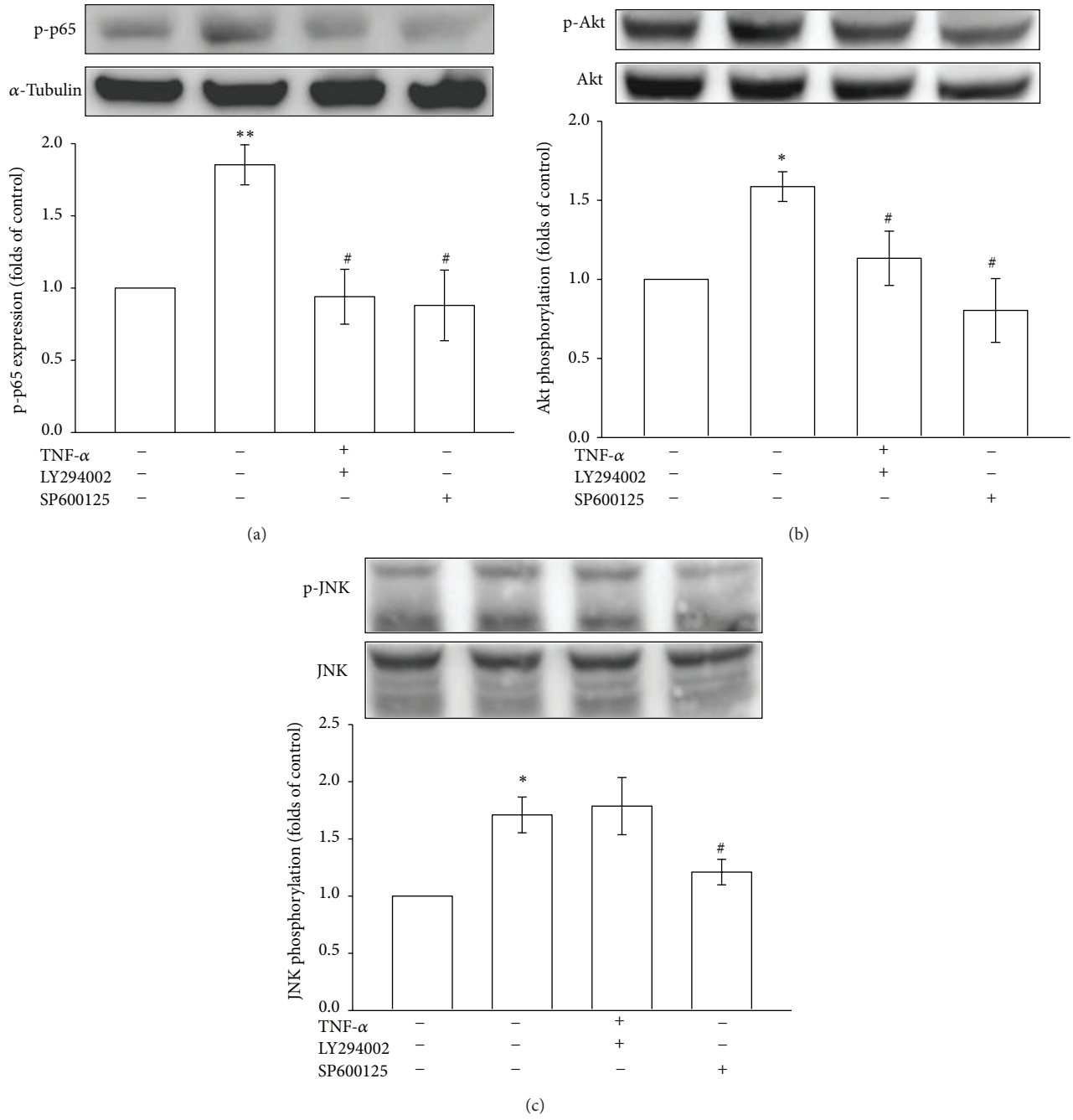

Figure 5: Regulatory effects of various signal inhibitors on p65 activation and Akt and JNK phosphorylation in TNF-α-stimulated VSMCs. The VSMCs were treated with PBS (resting group) or pretreated with LY294002 (10 μM), SP600125 (10 μM), or an equal volume of DMSO (solvent control) for 20 min, and TNF-α (10 ng/mL) was subsequently added for 10 min ((b) and (c)) or 30 min (a). (a) p65 phosphorylation, (b) Akt phosphorylation, and (c) JNK phosphorylation were evaluated as described in Section 2. $^{*}P < 0.05$ and $^{**}P < 0.01$ compared with the resting group; $^{\#}P < 0.05$ compared with the TNF-α group. The data are presented as the mean ± SEM ($n = 3$).

32]. Studies support the hypothesis that MAPK is required for the activation of several transcription factors, including NF-κB [34]. Bergmann et al. also demonstrated that the inhibitor of p38 MAPK SB203580 abolished TNF-α-induced cytokine synthesis and blocked NF-κB-mediated luciferase transactivation [35]. As shown in Figure 5, we observed that treatment with LY294002 (a PI3K/Akt inhibitor) and treatment with SP600125 (a JNK inhibitor) in TNF-α-stimulated VSMCs reversed the andrographolide-mediated inhibition of p65 phosphorylation; this observation is consistent with the results of a previous study that indicated that the PI3K/Akt and JNK signaling pathways regulate NF-κB activation [26, 36]. In addition, based on our results, LY294002 and SP600125 diminished Akt phosphorylation,

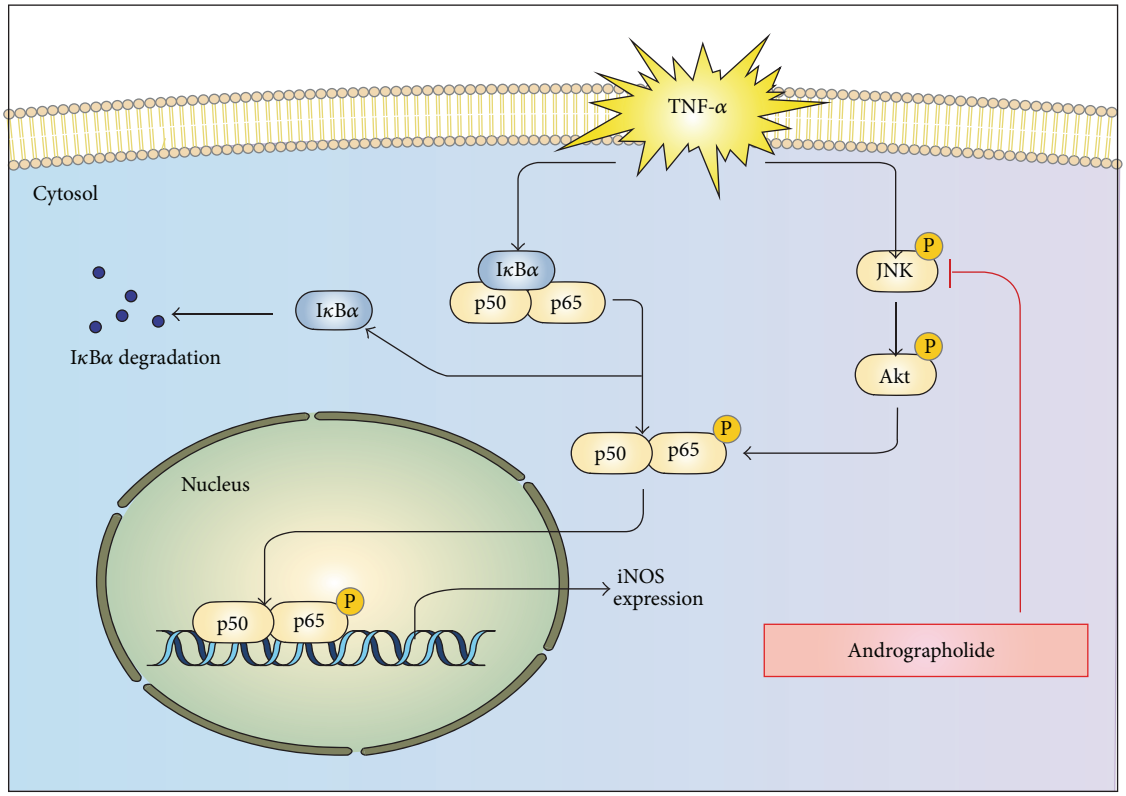

Figure 6: Diagram of the hypothetical inhibitory mechanism of andrographolide-induced effects in TNF-α-stimulated VSMCs. TNF-α triggers the expression of iNOS through IκBα-(IκBα-p65) and IκBα-independent (JNK-Akt-p65) pathways.

whereas LY294002 had no effects on JNK phosphorylation. Golden et al. have also found that combination of the MAPK Kinase-JNK1 signaling module with Akt represents a crucial stress-activated signalosome that may present protection to sustain cardiac contractility and maintain normal levels of Ca^{2+} [37]. These results may indicate that JNK, as a crucial upstream regulator, plays a key role to regulate the Akt phosphorylation in TNF-α-stimulated VSMCs.

Multiple lines of evidence have suggested that a NO-derived oxidant, peroxynitrite, contributes to inflammatory cardiovascular diseases, such as atherogenesis [5]. Our results indicated that andrographolide significantly diminished iNOS expression in TNF-α-stimulated VSMCs by attenuating the Akt and JNK signaling cascade. Moreover, our data suggested that the IκBα-independent inhibition of NF-κB activation occurs through the JNK-Akt signaling cascade to regulate the activation of p65 phosphorylation (Figure 6). In conclusion, andrographolide is a potential therapeutic agent that can be applied in treating and preventing inflammatory vascular diseases.

Conflict of Interests

The authors declare no conflict of interests.

Acknowledgments

This work was supported by Grants from the National Science Council, Taiwan (NSC98-2320-B-038-007-MY3, NSC100-2320-B-038-021-MY3, and NSC101-2320-B-038-034) and the Chi-Mei Medical Center-Taipei Medical University (102CM-TMU-11).

References

[1] G. E. McKellar, D. W. McCarey, N. Sattar, and I. B. McInnes, "Role for TNF in atherosclerosis? Lessons from autoimmune disease.," *Nature reviews. Cardiology*, vol. 6, no. 6, pp. 410–417, 2009.

[2] F. K. Swirski, M. Nahrendorf, M. Etzrodt et al., "Identification of splenic reservoir monocytes and their deployment to inflammatory sites," *Science*, vol. 325, no. 5940, pp. 612–616, 2009.

[3] Z. Yang, D. Gagarin, G. St. Laurent et al., "Cardiovascular inflammation and lesion cell apoptosis: a novel connection via the interferon-inducible immunoproteasome," *Arteriosclerosis, Thrombosis, and Vascular Biology*, vol. 29, no. 8, pp. 1213–1219, 2009.

[4] N. Cartwright, O. Murch, S. K. McMaster et al., "Selective NOD1 agonists cause shock and organ injury/dysfunction in vivo," *The American Journal of Respiratory and Critical Care Medicine*, vol. 175, no. 6, pp. 595–603, 2007.

[5] Y. Hattori, M. Matsumura, and K. Kasai, "Vascular smooth muscle cell activation by C-reactive protein," *Cardiovascular Research*, vol. 58, no. 1, pp. 186–195, 2003.

[6] J. Wang, W. Qian, and Q. Zhu, "Martentoxin, a large-conductance Ca^{2+}-activated K^+ channel inhibitor, attenuated TNF-alpha-induced nitric oxide release by human umbilical vein endothelial cells," *Journal of Biomedical Research*, vol. 27, no. 5, pp. 386–393, 2013.

[7] E. M. Rzucidlo, "Signaling pathways regulating vascular smooth muscle cell differentiation," *Vascular*, vol. 17, no. 1, pp. S15–S20, 2009.

[8] C.-H. Chung, K.-T. Lin, C.-H. Chang, H.-C. Peng, and T.-F. Huang, "The integrin $\alpha_2\beta_1$ agonist, aggretin, promotes proliferation and migration of VSMC through NF-κB translocation and PDGF production," *British Journal of Pharmacology*, vol. 156, no. 5, pp. 846–856, 2009.

[9] B. T. Hennessy, D. L. Smith, P. T. Ram, Y. Lu, and G. B. Mills, "Exploiting the PI3K/AKT pathway for cancer drug discovery," *Nature Reviews Drug Discovery*, vol. 4, no. 12, pp. 988–1004, 2005.

[10] O. N. Ozes, L. D. Mayo, J. A. Gustin, S. R. Pfeffer, L. M. Pfeffer, and D. B. Donner, "NF-κB activation by tumour necrosis factor requires tie Akt serine- threonine kinase," *Nature*, vol. 401, no. 6748, pp. 82–85, 1999.

[11] J. T. Coon and E. Ernst, "Andrographis paniculata in the treatment of upper respiratory tract infections: a systematic review of safety and efficacy," *Planta Medica*, vol. 70, no. 4, pp. 293–298, 2004.

[12] N. Poolsup, C. Suthisisang, S. Prathanturarug, A. Asawamekin, and U. Chanchareon, "Andrographis paniculata in the symptomatic treatment of uncomplicated upper respiratory tract infection: systematic review of randomized controlled trials," *Journal of Clinical Pharmacy and Therapeutics*, vol. 29, no. 1, pp. 37–45, 2004.

[13] C. Y. Hsieh, M. J. Hsu, G. Hsiao et al., "Andrographolide enhances nuclear factor-κB subunit p65 Ser536 dephosphorylation through activation of protein phosphatase 2A in vascular smooth muscle cells," *The Journal of Biological Chemistry*, vol. 286, no. 8, pp. 5942–5955, 2011.

[14] Y. Y. Chen, M. J. Hsu, J. R. Sheu, L. W. Lee, and C. Y. Hsieh, "Andrographolide, a novel NF- kappa B inhibitor, induces vascular smooth muscle cell apoptosis via a ceramide-p47phox-ROS signaling cascade," *Evidence-Based Complementary Alternative Medicine*, vol. 2013, Article ID 821813, 10 pages, 2013.

[15] W. Lu, J. Lee, D. Chou et al., "A novel role of andrographolide, an NF-kappa B inhibitor, on inhibition of platelet activation: the pivotal mechanisms of endothelial nitric oxide synthase/cyclic GMP," *Journal of Molecular Medicine*, vol. 89, no. 12, pp. 1261–1273, 2011.

[16] W. J. Lu, K. H. Lin, M. J. Hsu, D. S. Chou, G. Hsiao, and J. R. Sheu, "Suppression of NF-κB signaling by andrographolide with a novel mechanism in human platelets: Regulatory roles of the p38 MAPK-hydroxyl radical-ERK2 cascade," *Biochemical Pharmacology*, vol. 84, no. 7, pp. 914–924, 2012.

[17] S. Patel, D. S. Celermajer, and S. Bao, "Atherosclerosis-underlying inflammatory mechanisms and clinical implications," *The International Journal of Biochemistry and Cell Biology*, vol. 40, no. 4, pp. 576–580, 2008.

[18] G. Hsiao, M. Shen, W. Chang et al., "A novel antioxidant, octyl caffeate, suppression of LPS/IFN-γ-induced inducible nitric oxide synthase gene expression in rat aortic smooth muscle cells," *Biochemical Pharmacology*, vol. 65, no. 8, pp. 1383–1392, 2003.

[19] A. H. Sprague and R. A. Khalil, "Inflammatory cytokines in vascular dysfunction and vascular disease," *Biochemical Pharmacology*, vol. 78, no. 6, pp. 539–552, 2009.

[20] C. Dugourd, M. Gervais, P. Corvol, and C. Monnot, "Akt is a major downstream target of PI3-kinase involved in angiotensin II-induced proliferation," *Hypertension*, vol. 41, no. 4, pp. 882–890, 2003.

[21] Y. Hattori, K. Kasai, and S. S. Gross, "NO suppresses while peroxynitrite sustains NF-κB: a paradigm to rationalize cytoprotective and cytotoxic actions attributed to NO," *Cardiovascular Research*, vol. 63, no. 1, pp. 31–40, 2004.

[22] S. Ghosh and M. Karin, "Missing pieces in the NF-κB puzzle," *Cell*, vol. 109, no. 2, pp. S81–S96, 2002.

[23] Q. Li and I. M. Verma, "NF-κB regulation in the immune system," *Nature Reviews Immunology*, vol. 2, no. 10, pp. 725–734, 2002.

[24] C. Y. Sasaki, T. J. Barberi, P. Ghosh, and D. L. Longo, "Phosphorylation of Re1A/p65 on serine 536 defines an IκBα- independent NF-κB pathway," *The Journal of Biological Chemistry*, vol. 280, no. 41, pp. 34538–34547, 2005.

[25] C. Chao, C. Lii, I.-T. Tsai et al., "Andrographolide inhibits ICAM-1 expression and NF-κB activation in TNF-α-treated EA.hy926 cells," *Journal of Agricultural and Food Chemistry*, vol. 59, no. 10, pp. 5263–5271, 2011.

[26] H. Chen, A. Lin, H. Chu et al., "Inhibition of TNF-α-induced inflammation by andrographolide via down-regulation of the PI3K/Akt signaling pathway," *Journal of Natural Products*, vol. 74, no. 11, pp. 2408–2413, 2011.

[27] J. E. Rectenwald, L. L. Moldawer, T. S. Huber, J. M. Seeger, and C. K. Ozaki, "Direct evidence for cytokine involvement in neointimal hyperplasia," *Circulation*, vol. 102, no. 14, pp. 1697–1702, 2000.

[28] J. W. Gordon, J. A. Shaw, and L. A. Kirshenbaum, "Multiple facets of NF-κB in the heart: to be or not to NF-κB," *Circulation Research*, vol. 108, no. 9, pp. 1122–1132, 2011.

[29] D. Guo and D. B. Donner, "Tumor necrosis factor promotes phosphorylation and binding of insulin receptor substrate 1 to phosphatidylinositol 3-kinase in 3T3-L1 adipocytes," *The Journal of Biological Chemistry*, vol. 271, no. 2, pp. 615–618, 1996.

[30] S. Kim and H. Iwao, "Stress and vascular responses: mitogen-activated protein kinases and activator protein-1 as promising therapeutic targets of vascular remodeling," *Journal of Pharmacological Sciences*, vol. 91, no. 3, pp. 177–181, 2003.

[31] N. D. Perkins, "Integrating cell-signalling pathways with NF-κB and IKK function," *Nature Reviews Molecular Cell Biology*, vol. 8, no. 1, pp. 49–62, 2007.

[32] I. Shiojima and K. Walsh, "Role of Akt signaling in vascular homeostasis and angiogenesis," *Circulation Research*, vol. 90, no. 12, pp. 1243–1250, 2002.

[33] C. Fernández-Hernando, E. Ackah, J. Yu et al., "Loss of Akt1 leads to severe atherosclerosis and occlusive coronary artery disease," *Cell Metabolism*, vol. 6, no. 6, pp. 446–457, 2007.

[34] J. Garcia, B. Lemercier, S. Roman-Roman, and G. Rawadi, "A Mycoplasma fermentans-derived synthetic lipopeptide induces AP-1 and NF-κB activity and cytokine secretion in macrophages via the activation of mitogen-activated protein kinase pathways," *The Journal of Biological Chemistry*, vol. 273, no. 51, pp. 34391–34398, 1998.

[35] M. Bergmann, L. Hart, M. Lindsay, P. J. Barnes, and R. Newton, "IκBα degradation and nuclear factor-κB DNA binding are insufficient for interleukin-1β and tumor necrosis factor-α-induced κb-dependent transcription. Requirement for an additional activation pathway," *The Journal of Biological Chemistry*, vol. 273, no. 12, pp. 6607–6610, 1998.

[36] W. F. Chiou, C. C. Chen, and B. L. Wei, "3,4-Di-*O*-caffeoylquinic acid inhibits angiotensin-II-induced vascular smooth muscle cell proliferation and migration by downregulating the JNK and PI3k/AKT signaling pathways," *Evidence-Based Complementary and Alternative Medicine*, vol. 2011, Article ID 634502, 8 pages, 2011.

[37] H. B. Golden, L. E. Watson, D. Nizamutdinov et al., "Anthrax lethal toxin induces acute diastolic dysfunction in rats through disruption of the phospholamban signaling network," *International Journal of Cardiology*, vol. 168, no. 4, pp. 3884–3895, 2013.

Hindawi Publishing Corporation
The Scientific World Journal
Volume 2014, Article ID 423259, 10 pages
http://dx.doi.org/10.1155/2014/423259

Research Article

Sanguis draconis, a Dragon's Blood Resin, Attenuates High Glucose-Induced Oxidative Stress and Endothelial Dysfunction in Human Umbilical Vein Endothelial Cells

Yi Chang,[1,2,3] Ting-Chen Chang,[4] Jie-Jen Lee,[5,6,7] Nen-Chung Chang,[8] Yung-Kai Huang,[9] Cheuk-Sing Choy,[10,11] and Thanasekaran Jayakumar[3,5]

[1] *Department of Anesthesiology, Shin Kong Wu Ho-Su Memorial Hospital, 95 Wen-Chang Road, Taipei 101, Taiwan*
[2] *School of Medicine, Fu-Jen Catholic University, 510 Zhong-Zheng Road, Taipei 205, Taiwan*
[3] *Graduate Institute of Medical Sciences, College of Medicine, Taipei Medical University, Taipei 110, Taiwan*
[4] *Department of Lymphatic Vascular Surgery, Wan Fang Hospital, Taipei Medical University, Taipei 110, Taiwan*
[5] *Department of Pharmacology, Taipei Medical University, Taipei 110, Taiwan*
[6] *Department of Surgery, Mackay Memorial Hospital, Taipei 104, Taiwan*
[7] *Mackay Junior College of Medicine, Nursing, and Management, Taipei 112, Taiwan*
[8] *Department of Cardiology, School of Medicine, Taipei Medical University, Taipei 110, Taiwan*
[9] *School of Oral Hygiene, College of Oral Medicine, Taipei Medical University, Taipei 110, Taiwan*
[10] *Emergency and Intensive Care Department, Min-Sheng Hospital 168, Taoyuan 330, Taiwan*
[11] *Department of Medicine, Taipei Medical University, Taipei 110, Taiwan*

Correspondence should be addressed to Cheuk-Sing Choy; prof.choy@gmail.com
and Thanasekaran Jayakumar; tjaya_2002@yahoo.co.in

Received 11 April 2014; Accepted 10 May 2014; Published 2 June 2014

Academic Editor: Duen-Suey Chou

Hyperglycaemia, a characteristic feature of diabetes mellitus, induces endothelial dysfunction and vascular complications by limiting the proliferative potential of these cells. Here we aimed to investigate the effect of an ethanolic extract of *Sanguis draconis* (SD), a kind of dragon's blood resin that is obtained from *Daemonorops draco* (Palmae), on human umbilical vein endothelial cells (HUVEC) under high-glucose (HG) stimulation and its underlying mechanism. Concentration-dependent (0–50 μg/mL) assessment of cell viability showed that SD does not affect cell viability with a similar trend up to 48 h. Remarkably, SD (10–50 μg/mL) significantly attenuated the high-glucose (25 and 50 mM) induced cell toxicity in a concentration-dependent manner. SD inhibited high glucose-induced nitrite (NO) and lipid peroxidation (MDA) production and reactive oxygen species (ROS) formation in HUVEC. Western blot analysis revealed that SD treatments abolished HG-induced phosphorylation of extracellular signal-regulated kinase 1/2 (ERK 1/2), nuclear transcription factor, κB (NF-κB), VCAM-1, and E-selectin, and it also blocked the breakdown of PARP-116 kDa protein in a dose-dependent manner. Furthermore, we found that SD increased the expression of Bcl-2 and decreased Bax protein expression in HG-stimulated HUVEC. Thus, these results of this study demonstrate for the first time that SD inhibits glucose induced oxidative stress and vascular inflammation in HUVEC by inhibiting the ERK/NF-κB/PARP-1/Bax signaling cascade followed by suppressing the activation of VCAM-1 and E-selectin. These data suggest that SD may have a therapeutic potential in vascular inflammation due to the decreased levels of oxidative stress, apoptosis, and PARP-1 activation.

1. Introduction

Vascular disorders through overexpression of adhesion molecules are thought to play in the pathogenesis of atherosclerosis. Adhesion molecules are proteins which regulate the interaction between endothelium and leukocytes. An increase in their expression on the endothelial surface causes increased adhesion of leukocytes. Endothelial cells in human atherosclerotic lesions have been shown to overexpress intercellular adhesion molecule-1 (ICAM-1), vascular cell

adhesion molecule-1 (VCAM-1), and E-selectin [1], and adhesion molecules are reported to activate by nuclear transcription factor-κB (NF-κB). Previous studies have shown that high glucose activates NF-κB, one of the transcription factors for proinflammatory genes. NF-κB is present in the cytoplasm as an inactive form bound to its inhibitor molecule, inhibitory factor of NF-κB-α (IκB-α). Translocation of NF-κB from the cytoplasm to the nucleus is preceded by the phosphorylation, ubiquitination, and proteolytic degradation of IκB-α [2]. Moreover, during the oxidative stress, endothelial cells generate ROS, such as superoxides and peroxynitrite, leading to low-density lipo protein (LDL) oxidation, and the formation of ROS together with inflammatory factors including chemokines, cytokines, and adhesion molecules has been shown to be increased in atherosclerotic lesions [3]. Hyperglycemia induces mitochondrial superoxide production and prevents activity and expression of endothelial nitric oxide synthase (eNOS) in endothelial cells [4]. ROS can modify endothelial function by a variety of mechanisms, such as peroxidation of membrane lipids, activation of NF-κB, and decreasing the availability of nitric oxide (NO) [5].

Poly (ADP-ribose) polymerase (PARP), an abundant nuclear enzyme, initiates an energy consuming cellular metabolic cycle by transferring ADP-ribose units from NAD+ and ATP to nuclear proteins that leads to cellular metabolic disturbances and culminates in endothelial dysfunction [6]. It has been demonstrated that hyperglycemia induces PARP activation in endothelial cells in culture as well as in the vasculature of diabetic animals [6]. Recent studies have also established that activation of PARP plays a pivotal role in the overexpression of adhesion molecules and cytokines [7] and also on peroxynitrite formation [8]. In addition, a study has suggested that activation of PARP-1 is reported to be associated with hyperglycemia-induced ROS formation, as it is evidenced that PARP inhibitors blocked ROS production [9]. These observations lead to the suggestion that PARP-1, CAMs, ROS, and NF-κB inhibitors could be used as a therapeutic strategy in diabetic complications.

Sanguis draconis (SD) is a kind of red resin that is obtained from several botanical origins, and most SD that is traded internationally is from *Daemonorops* [10]. SD has long been used as a traditional Chinese medicine for improving blood circulation, stopping hemorrhages, and healing wounds and cuts and is also used as an antiseptic [11]. Hou et al. have reported that SD can ameliorate the progress of insulin resistance and enhance insulin sensitivity [12], and it has been elucidated that SD could efficiently reduce diabetics by inhibiting high plasma lipid level [13] and intestinal carbohydrate absorption [14]. On the other hand, SD has also found to inhibit platelet aggregation, thrombus formation, and myocardial ischemia [15]. Our previous studies have described that SD inhibits streptozotocin-induced iNOS protein expression, pancreatic injury, and lipid peroxidation via the inhibition of NF-κB activation [16], and it also inhibits the production of NO and prostaglandin E2 (PGE2) by downregulating iNOS and COX-2 gene expression via the suppression of NF-κB (p65) activation [17]. We postulated that SD can retreat the effects induced by high glucose concentration in endothelial cells; therefore, we evaluated the effect of SD on ROS, NO, and MDA production and expression of adhesion molecules NF-κB, PARP-1, ERK, and on Bax-Bcl2 in HUVEC treated with high concentrations of glucose.

2. Materials and Methods

2.1. Preparation of the Ethanolic Extract of S. draconis. Commercially available plant material (*Sanguis draconis*) was purchased from a traditional Chinese medicine drug store and the authenticity of SD was confirmed by Professor Ching-Chiung Wang of the School of Pharmacy, Taipei Medical University. A certificate of source and specimen is kept at our lab. Other details of preparation of SD are described in our previous paper [17].

2.2. Chemicals and Reagents. Cell culture reagents including M-199 medium, L-glutamine, penicillin, streptomycin, and fetal bovine serum were obtained from Gibco BRL (Grand Island, NY, USA). Anti-mouse and anti-rabbit immunoglobulin G-conjugated horseradish peroxidase (HRP) was purchased from Amersham Biosciences (Sunnyvale, CA, USA) and/or Jackson-ImmunoResearch (West Grove, PA, USA). Anti-eNOS, anti-p-NF-κB, anti-cleaved PARP, anti-VCAM-1, anti-Bax, and Bcl2 were all purchased from Santa Cruz Biotechnology (Santa Cruz, CA, USA). The anti-p42/p44 ERK (Thr202/Tyr204) was from Cell Signaling (Beverly, MA, USA). The Hybond-P polyvinylidene difluoride (PVDF) membrane, enhanced chemiluminescence (ECL) Western blotting detection reagent, and analysis system were obtained from Amersham (Buckinghamshire, UK). All other chemicals used in this study were of reagent grade.

2.3. Isolation and Culture of HUVEC. Human umbilical cords were obtained from the Hospital of National Taiwan University, Taipei, Taiwan, and human umbilical vein endothelial cells were isolated by enzymatic digestion as described previously [18]. After 15-min incubation with 0.1% collagenase at 37 ± 0.5°C, umbilical cord vein segments were perfused with 30 mL of medium 199 containing 10 U/mL penicillin and 100 μg/mL streptomycin for the collection of cells. After centrifugation for 8 min at 900 ×g, the cell pellet was resuspended in previous medium supplemented with 20% heat-inactivated fetal bovine serum, 30 μg/mL endothelial cell growth supplement, and 90 μg/mL heparin. Confluent primary cells were detached by trypsin, EDTA (0.05% : 0.02%, v/v), and passages between three and five were used in the experiments. Cultures had typical cobblestone morphology and stained uniformly for human von Willebrand factor (vWF) [19] as assessed by indirect immunofluorescence.

2.4. Cell Viability Assay. The viability of HUVECs upon treatment of glucose, SD alone, and combined together was measured by a colorimetric MTT assay. Briefly, HUVECs (2×10^5 cells/well) were seeded on 24-well plates and cultured in DMEM containing 10% FBS for 24 h. HUVECs were treated with glucose at concentrations of (5.5–150 μM)

and SD (10–50 μg/mL) alone and pretreated with SD (10–50 μM) in glucose (25 and 50 mM) induced cells or an isovolumetric solvent control (0.1% DMSO) for 24 or 48 h. The cell number was measured based on the ability of mitochondria in viable cells to reduce MTT as previously described [17]. The cell number index was calculated as the absorbance of treated cells/control cells × 100%.

2.5. Measurement of Intracellular ROS. Starved HUVECs (2×10^5 cells/well) were loaded with DCF-DA (20 μM) for 20 min. After treatment with SD (50 μg/mL) for 2 hr, cells were stimulated with glucose (25–75 mM) for 24 hr, washed with PBS, and then detached using trypsin. Levels of intracellular ROS were detected by flow cytometry (Beckman Coulter). All experiments were repeated at least four times to ensure reproducibility.

2.6. Determination of Nitrite Production. HUVECs cultured in 12-well plates were washed twice with Hanks balanced salt solution (HBSS) and then incubated at 37 ± 0.5°C in the same buffer for 30 min with various concentrations of SD. Acetylcholine (30 μM) was used as a positive control. Supernatants were collected and then injected into a nitrogen purge chamber containing vanadium(III) chloride in hydrochloric acid at 91 ± 0.5°C. All NO metabolites can be liberated as gaseous NO and reacted with ozone to form activated nitrogen dioxide that is luminescent in red and infrared spectra. The chemiluminescence was detected using a nitric oxide analyzer (NOA280, Sievers Instruments, Boulder, CO, USA) [20]. For calibration, the area under the curve was converted to nanomolar NO using a $NaNO_3$ standard curve, and the final data were expressed as *p*mol/mg protein.

2.7. Lipid Peroxidation Assay. Lipid peroxidation was assayed by the thiobarbituric acid (TBA) reaction method. The cells were homogenized in ice-cold 1.15% KCl. The samples were used to measure the malondialdehyde (MDA) formed in a peroxidizing lipid system. The amount of thiobarbituric acid reactive substance (TBARS) was determined using a standard curve of 1,1,3,3-tetramethoxypropane.

2.8. Western Blot Analysis. Western blot analysis was performed as previously described [21]. Lysates from each sample were mixed with 6× sample buffer (0.35 M Tris, 10% w/v SDS, 30% v/v glycerol, 0.6 M DTT, and 0.012% w/v bromophenol blue, pH 6.8) and heated to 95°C for 5 min. Proteins were separated by electrophoresis and transferred onto polyvinylidene difluoride (PVDF) membranes for pERK1/2, p-eNOS, pNF-κB, VCAM-1, PARP, Bax, and Bcl2. The membranes were blocked with 5% nonfat milk in TBS-0.1% Tween 20 and sequentially incubated with primary antibodies and HRP-conjugated secondary antibodies followed by enhanced chemiluminescence (ECL) detection (Amersham Biosciences). BIO-PROFIL Bio-1D light analytical software (Vilber Lourmat, Marne La Vallee, France) was used for the quantitative densitometric analysis. Data of specific protein levels are presented as relative multiples in relation to the control.

2.9. Statistical Analyses. The experimental results are expressed as the mean ± SEM and are accompanied by the number of observations. For analysis of the results, a one-way analysis of variance (ANOVA) test was performed using Sigma Stat v3.5 software. When group comparisons showed a significant difference, the Student-Newman-Keuls test was used. A P value of <0.05 was considered to be statistically significant.

3. Results

3.1. Effects of SD on HUVEC Cell Viability. The cytotoxic effect of various concentrations of SD and glucose on HUVECs cells was measured by MTT assay. The results indicated that SD did not affect the viability of HUVEC at the used concentrations of 0–50 μg/mL for 24 and 48 h (Figures 1(a) and 2(b)). However, treatment of cells with glucose (5.5–150 μM) decreased the cell viability of HUVEC in a concentration dependent manner. Interestingly, cells simultaneously incubated with glucose (25 and 50 mM) and SD (0–50 μg/mL) increased cell viability in a concentration dependent manner (Figures 1(c), 1(d), 1(e), and 1(f)).

3.2. SD Inhibited HG-Induced ROS and NO Production. To investigate the effectiveness of SD in inhibiting HG-induced ROS formation in HUVECs, a cell-permeative ROS-sensitive dye, DCFDA (nonfluorescent in a reduced state but fluorescent upon oxidation by ROS), was used. The intracellular level of ROS in HUVECs increased concentration dependently following incubation with high glucose (25–75 mM) compared with 5.5 mM glucose. Incubation of HUVECs with SD resulted in a marked reduction of HG-induced intracellular ROS generation (Figure 2(a)). Contrary to our expectations, glucose increased NO production instead of reducing it; however, when HUVECs were treated with SD plus glucose, SD completely abrogated the production of NO induced by glucose (Figure 2(b)).

3.3. SD Inhibited HG-Induced MDA Production. Studies have indicated that damaging cell membranes may cause a decrease of cell viability through peroxidation of membrane lipids. Therefore, we projected to estimate the levels of MDA in the present study. As shown in Figure 2(c), MDA, a marker of lipid peroxidation, was markedly elevated in HG-induced HUVEC. However, treatment of SD (50 μg/mL) significantly attenuated the elevation of MDA concentration in HG-stimulated HUVEC.

3.4. SD Enhanced the Phosphorylation of eNOS. The result showed that SD (30 and 50 μg/mL) alone had no influence on the protein expressions of phosphorylated eNOS at Ser1177, whereas high glucose leads to a significant decrease in the expression of eNOS (Figure 3(a)). Treatment with SD significantly attenuated the decreased level of eNOS expression.

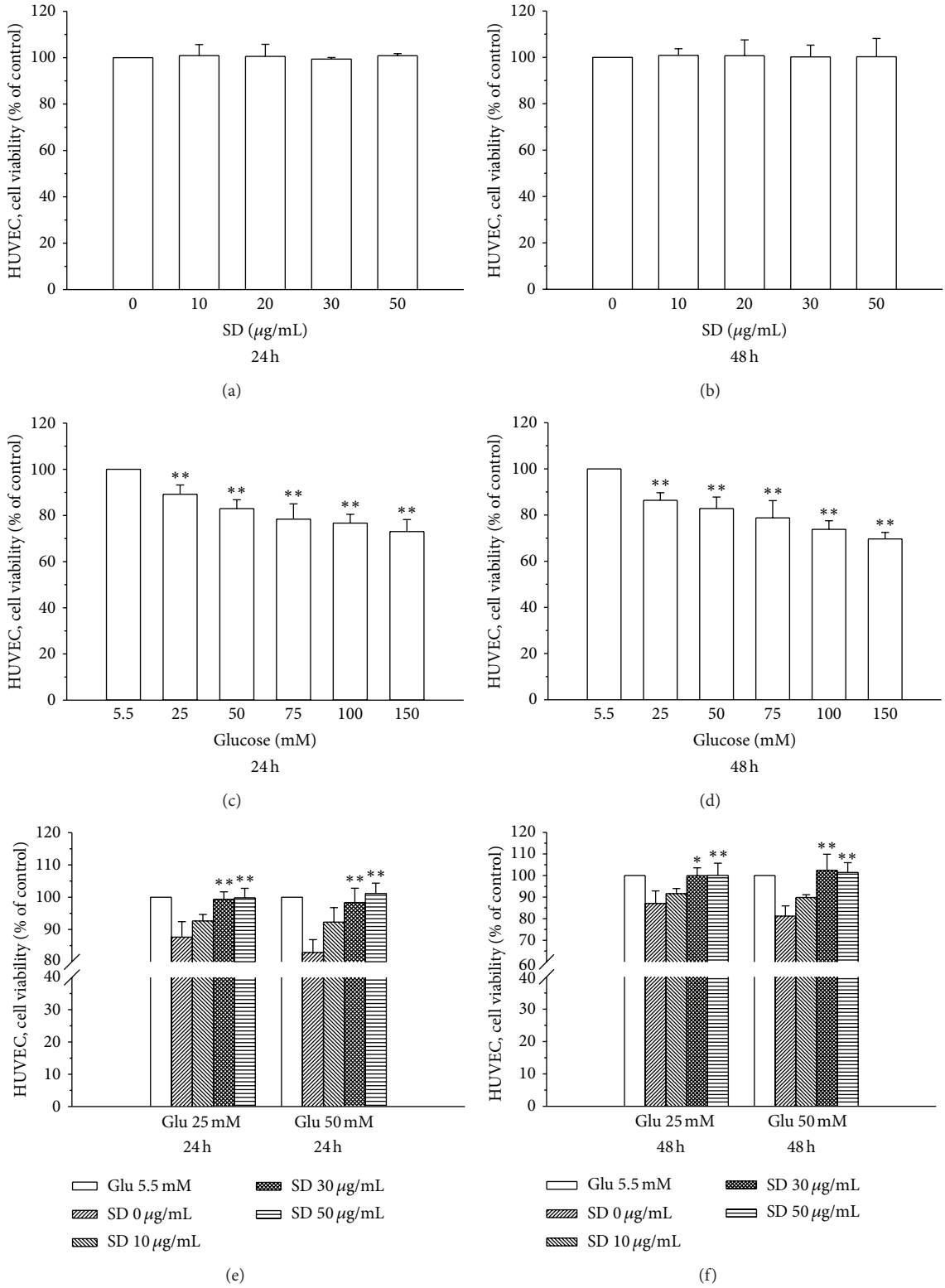

Figure 1: Effects of SD on the cell viability of human umbilical vein endothelial cells (HUVEC): ((a), (b)) the viability of HUVECs during treatment with various concentrations (10–50 μg/mL) of SD for 24 and 48 h; ((c), (d)) the viability of HUVECs during treatment with various concentrations (25–150 mM) of glucose for 24 and 48 h; ((e), (f)) the viability of HUVECs upon treatment with various concentrations (0–50 μg/mL) of SD in glucose-induced (25 and 50 mM) HUVECs for 24 and 48 h. Data are shown as the mean ± SEM of three independent experiments. $^{*}P < 0.05$; $^{**}P < 0.01$, compared with the glucose treated group.

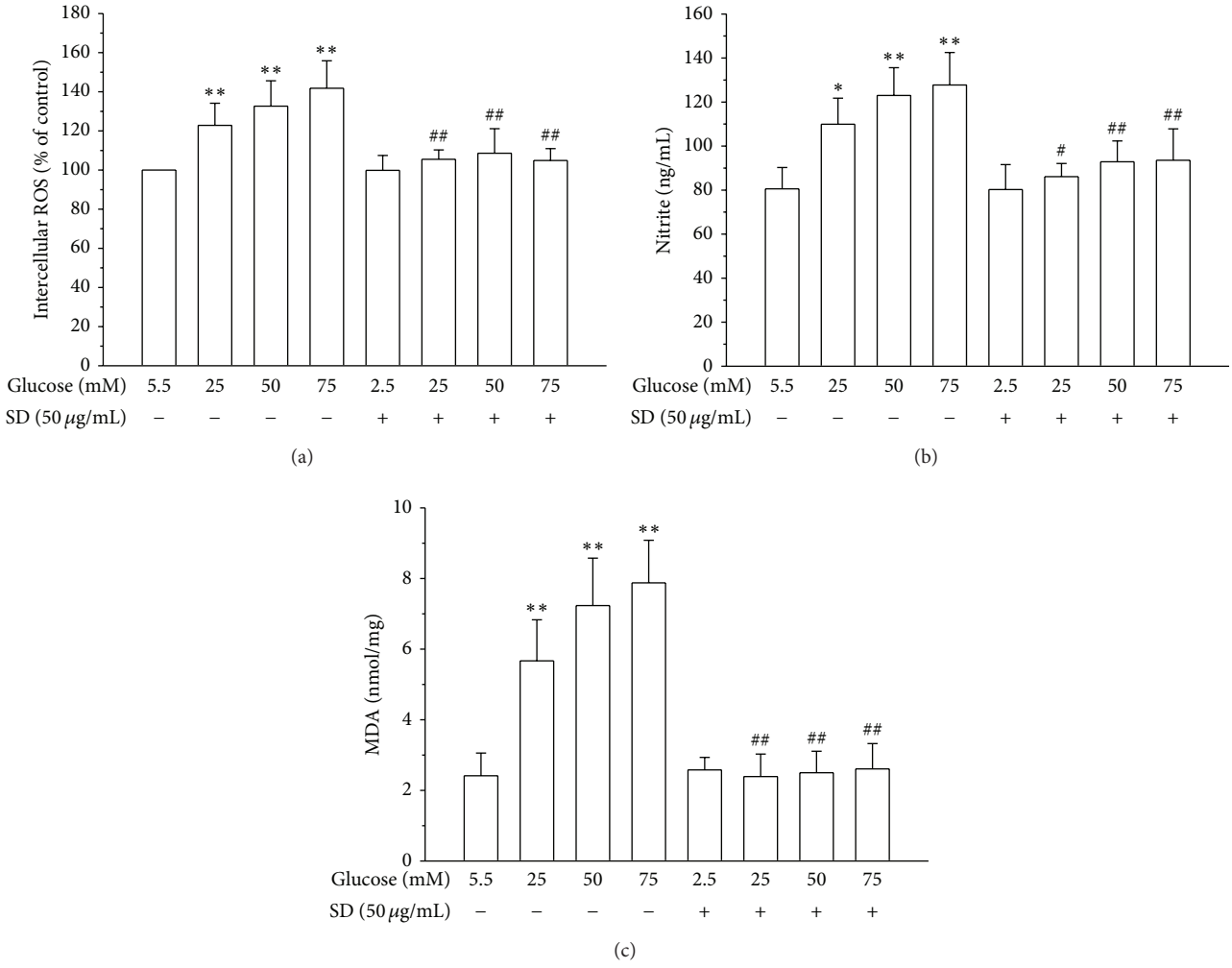

Figure 2: Effects of SD on HG-induced formation of ROS, NO, and LPO in HUVECs: (a) ROS production was determined as described in Materials and Methods; (b) the nitrite concentration in the culture medium was determined by Griess reagent; and (c) lipid peroxidation was assayed by measuring the amount of TBARS formation (malondialdehyde, MDA); Data are shown as the mean ± SEM of three independent experiments. $^{*}P < 0.05$; $^{**}P < 0.01$, compared with the normal group; $^{\#}P < 0.05$; $^{\#\#}P < 0.01$, compared with the HG-treated group.

3.5. SD Inhibited the Phosphorylation of ERK and NF-κB. To determine whether SD affects the activation of the MAPK pathway, we analyzed the phosphorylation levels of pERK MAPK. First, HUVECs were pretreated with SD (30 and 50 μg/mL) for 30 min and then stimulated with 50 mM glucose for 1 h. The HG-induced increased phosphorylation of pERK was inhibited by SD in a concentration-dependent manner (Figure 3(b)) and restored it to the level in cells exposed to 5.5 mM glucose. Moreover, we measured NF-κB activation in HG-induced HUVECs, as it is suggested that increased ROS production in HG-induced HUVEC may partially cause the activation of NF-κB. As we expected, the expression of NF-κB was increased markedly in HUVEC cells treated with high glucose (50 mM). In addition, pretreatment with SD (30 and 50 μg/mL) markedly inhibited the HG-induced expression of NF-κB concentration dependently (Figure 3(c)).

3.6. Effects of SD on HG-Induced Endothelial Cell Adhesion Molecules. To examine whether glucose induces expression of VCAM-1 and E-selectin in HUVECs, we cultured HUVECs at normal glucose (5.5 mM) and high glucose (50 mM) concentrations for 24 h. Immunoblot analysis showed that stimulation of HUVECs with high concentrations of glucose increased the production of VCAM-1 and E-selectin (Figure 4(a)). To further determine whether SD can inhibit the expression of endothelial adhesion molecules, HUVECs were pretreated with SD at concentrations of 30 and 50 μg/mL and stimulated with 50 mM glucose for 24 h. As shown in Figure 4(a), pretreatment of SD in HUVEC significantly inhibited the HG-induced expression of ICAM-1 and E-selectin in a concentration manner.

3.7. Effects of SD on HG-Induced PARP-1 Overactivation. As previously described, the full PARP-1 protein is 116 kDa, and

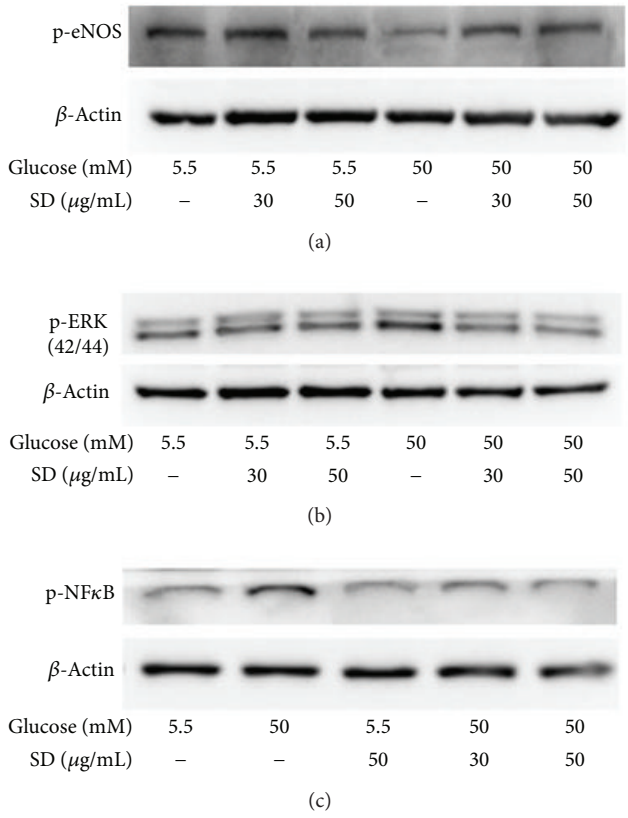

Figure 3: Effects of SD on HG-induced phosphorylation of eNOS, ERK, and NF-κB in HUVECs: HUVECs (2×10^5 cells/well) were pretreated with SD (30 and 50 μg/mL) for 2 h and then treated with glucose (50 mM) for 30 min to detect the phosphorylation of (a) eNOS, (b) ERK1/2, and (c) NF-κB. The β-actin was used as an internal control.

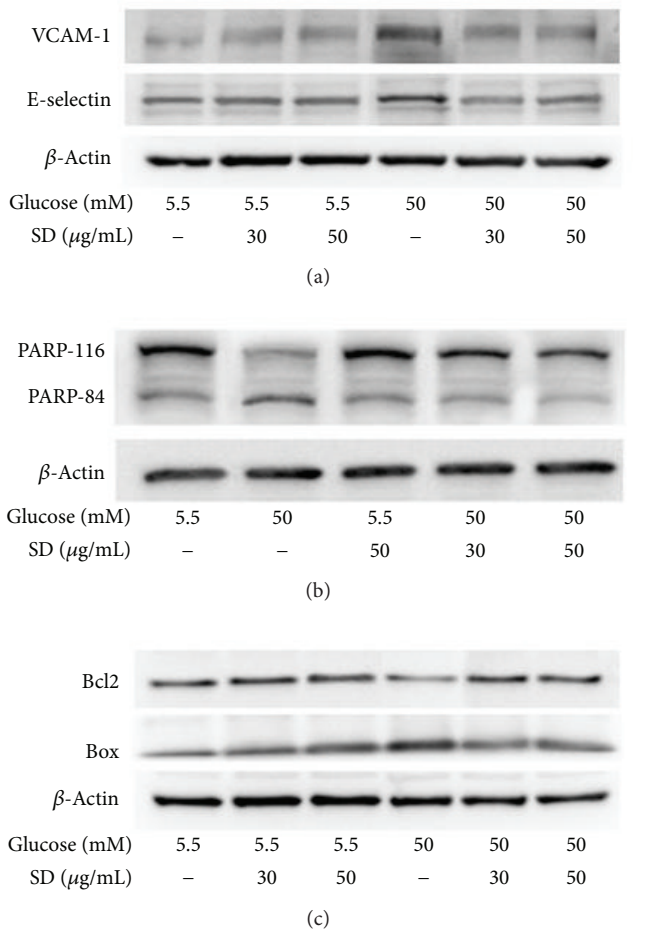

Figure 4: Effects of SD on HG-induced expression of VCAM-1, E-selectin, PARP-1, and Bax/Bcl2 in HUVEC: HUVECs (2×10^5 cells/well) were pretreated with SD (30 and 50 μg/mL) for 2 h and then treated with glucose (50 mM) for 30 min to detect the expression of (a) VCAM-1 and E-selectin, (b) PARP-1, and (c) Bax/Bcl2. The β-actin was used as an internal control.

the 85 kDa cleavage product is an early marker of apoptosis. In this experiment, we detected both the 116 kDa full PARP protein and the 85 kDa breakdown product. The results revealed that exposure of HUVEC to high glucose concentrations (50 mM) for 24 h resulted in a significant decrease in the amount of PARP-116 kDa protein and increased their breakdown product of 85 kDa protein. Interestingly, treatment of SD alone significantly enhanced the amount of PARP-116 full protein in HUVEC. Moreover, the amount of 85 kDa PARP breakdown product induced by high glucose (50 mM) was markedly reduced in SD treated cells in a concentration dependent manner (30 and 50 μg/mL) (Figure 4(b)).

3.8. Effects of SD on HG-Induced Bcl-2/Bax Expression. As shown in Figure 2(a), the inhibition of HG-induced ROS by SD led us to evaluate any possible effects of SD on other mediators of oxidative stress-induced apoptosis. The results revealed that the ratio between the anti- and proapoptotic mediators Bcl2 and Bax was not much affected by SD treatment alone, especially that Bcl-2 did not alter between normal and SD treated cells (Figure 4(c)). Moreover, HG-induced Bax was moderately reversed by SD, which indicated that Bax might play a role in this effect.

4. Discussion

In diabetes, hyperglycemia causes vascular complications that are produced mainly by the overproduction of ROS [22]. Dysfunction and activation of the endothelium are regarded as important factors in the pathogenesis of vascular disease in diabetes mellitus [23]. In this work, we evaluated the protective effect of *Sanguis draconis* (SD), a kind of red resin, against the dysfunction and activation of endothelial cells induced by high concentrations of glucose. The major finding of this study is that SD was capable of attenuating the increase of ROS, NO, and MDA and inhibits overactivation of PARPs, VCAM-1, NF-κB, and Bcl2 in cells exposed to high glucose concentration, and our data contribute in part to elucidate the molecular mechanisms involved in this effect.

Oxidative stress, a hallmark of high glucose-induced endothelial dysfunction, was significantly attenuated by SD treatment in the current study. There is growing evidence that oxidative stress is involved in the pathogenesis of diabetic complications [24] and an acute increase of glycemia is reported to be accompanied by oxidative stress generation [25]. Lipid peroxidation (LPO), a process induced by free radicals, leads to oxidative deterioration of polyunsaturated lipids. Malondialdehyde (MDA), a secondary product of lipid peroxidation, is used as an indicator of tissue or cell damage. In previous studies, it was found that MDA level was increased in HUVECs when cells were incubated with glycated protein and iron [26]. An increased production of ROS has been reported in inflammatory responses, and it acts as a potential mediator of diabetes mellitus-associated vascular diseases. ROS is also considered to be of the important mediators of several biologic responses, including cell proliferation and extracellular matrix deposition. A recent study showed that hyperglycemia stimulates the generation of free radicals and oxidative stress in various cell types [27]. In this study, an elevation in HG-mediated production of cellular MDA and ROS indicate that oxidative stress induced by high glucose in HUVEC is important in determining the character of diabetic complication as well as vascular inflammation. Interestingly, we found that SD treatment potentially inhibited the high glucose-induced MDA and ROS formation, suggesting a role of protecting oxidative insults in HG-induced HUVEC.

Bioavailability of endothelial NO observed in individuals with hyperglycemia is considered to be a critical and initiating factor in the pathogenesis of diabetic vascular complications [28]. NO is synthesized in endothelial cells from the substrate L-arginine via endothelial NO synthase (eNOS) [26], and this enzyme plays an important role for the maintenance of cardiovascular function by producing NO synthesis. Nevertheless, this enzyme can be detached, leading to the generation of superoxide instead of NO under certain pathological circumstances and oxidative stress conditions [29]. Our previous study showed that SD inhibits NO production induced by IL-1β/IFN-γ in endothelial cells [17]. The results of this study revealed that high glucose causes a significant degree of oxidative stress, which leads to increases in the formation of NO; convincingly pretreatment of SD could reverse the effect of high glucose by suppressing NO production. These results indicate that SD may have a protective effect on HUVEC by preventing or decreasing the injury of endothelial cells by interfering with NO synthase and NO.

In HUVEC, high glucose-induced cellular damage could lead to cell apoptosis probably viaERK activation. To make this hypothesis solid, we next aimed to gain insight into the cell signaling pathways mediating the action of SD on HG-induced human endothelial cells. We found that HG potentiated the activation of both ERK1/2 and NF-κB, indicating that overactivation of endothelial signaling molecules can be triggered by HG stimulations. ERK is the signal cascade involved in the protection of oxidative damage and its activation is generally thought to mediate cell survival [30]. In agreement with our study, a previous study has shown that high D-glucose activates the ERK1/2, NF-κB, and *i*NOS when this signaling pathway is formerly triggered by an exogenous inflammatory stimulus in cultured HUVEC [31]. Chronic activation of NF-κB is associated with various pathological conditions, including insulin resistance. Human subjects with type 2 diabetes exhibit increased activity of NF-κB in muscle that directly correlates with impaired insulin mediated glucose disposal. Enduring hyperglycemia and/or extreme perturbations in glycemia are common generators of oxidative stress, which has been shown to induce insulin resistance through activity of NF-κB. Interestingly, administration of the common salicylate aspirin (7.0 g/day) in patients with type 2 diabetes enhances glucose homeostasis and peripheral insulin sensitivity, at least in part through the inhibition of NF-κB nuclear activity [32]. Targeted manipulation or ablation of NF-κB, therefore, remains at the forefront of innovative treatments for diabetes and inflammatory pathologies. Our study also shows that high glucose elevated the expression of NF-κB in HUVEC and these effects were blocked by SD treatment. Changes in expression of activated ERK and NF-κB closely reflect the cell damage; such results suggest that high glucose-induced HUVEC cell damage is protected, at least partly, by inhibiting ERK and NF-κB activation.

In agreement with others [33], we have further found that ERK1/2 and NF-κB activation was responsible for endothelial VCAM-1 and E-selectin induction. Other signaling molecule, like PARP-1, has been reported as promoters of ICAM-1 expression in different vascular cell types [34] and might therefore be involved in the induction of ICAM-1 in HG-induced HUVEC. Adhesion induced by glucose was almost completely abrogated by SD when added before the addition of glucose, indicating that SD can have a preventive and protective effect against the endothelial activation induced by hyperglycemia. SD treatment was also capable of decreasing the glucose-induced expression of VCAM-1 and E-selectin. Similar results have been described in a previous study in endothelial cells, where they have reported that dehydroepiandrosterone (DHEA), an adrenal steroid abrogated expression of adhesion molecules in HUVEC, activated with either TNF-α or oxidized low density proteins [35]. Recently, various phytochemicals have been shown to inhibit the expression of adhesion molecules in endothelial cells. For instance, epigallocatechin-3-O-gallate (EGCG) inhibits angiotensin II-induced adhesion molecule expression by inhibiting p38 MAPK and ERK1/2 phosphorylation [36]. Anthocyanins inhibited TNF-α-induced ICAM-1 and VCAM-1 expressions via the NF-κB-dependent pathway [37]. Phloretin inhibited the TNF-α-stimulated expression of adhesion molecules without activating NF-κB [38]. Grape seed proanthocyanidin extract inhibited VCAM-1 expression in HUVECs via the NF-κB-independent pathway [39]. In this study, the observed effect of SD on suppressing HG-induced expression of VCAM-1 and E-selectin may perhaps via inhibition of the ERK1/2 phosphorylation and NF-κB-dependent pathway. Thus, development of therapeutic drugs for diabetic complications targeting CAMs expression may prove useful in the prevention of vascular inflammation.

Moreover, recent studies have demonstrated that activation of PARP is associated with the pathogenesis of diabetes and diabetic complications, including cardiovascular dysfunction. PARP has been shown to act as a coactivator in NF-κB-mediated transcription [40]. Some studies have indicated that PARP inhibitor prevents the diabetes-induced elevation in circulating nitrite levels in streptozotocin-induced diabetes. A study has reported that PARP deficiency suppresses NF-κB activation in cultured endothelial cells under high glucose stimulation [6], another study has also shown that NF-κB is regulated by PARP in diabetic retinopathy [41]. In this study, it was found that high glucose induced breakdown of the full PARP protein-116 kDa in HUVECs. It has been demonstrated that PARP-1 inhibition attenuates the development of albuminuria and podocyte apoptosis and depletion in diabetic mice [42]. Our findings revealed that SD significantly abrogated HG-stimulated breakdown of the full protein PARP-116 in HUVEC. Furthermore, the ROS reducing effect of SD prompted us to verify whether this drug could reduce apoptosis rate by affecting other regulators of the oxidative stress-induced apoptosis, such as the anti- and proapoptotic Bcl2 family members Bcl2/Bax (Figure 4(c)). We noticed a significant variation in Bcl2/Bax ratio in HG compared to normal glucose-treated cells. However, SD treatment only affected Bax, as it significantly reduced their expression in HG-induced HUVEC cells. This result indicates that SD reduces HG-induced endothelial apoptotic rate via Bax inhibition, favoring the maintenance of the integrity of the endothelial cells and thus possibly contributing to reduce vascular inflammation. A previous study has also demonstrated that the ratio between Bcl2/Bax was not affected by fenofibrate, a PPARα agonist, and also did not differ between normal and high glucose conditions [43].

In conclusion, the present work provides experimental evidence that *Sanguis draconis* (SD) could suppress high glucose-induced endothelial dysfunction and oxidative stress via inhibition of ERK/NF-κB/PARP-1 activation in primary cultured HUVEC. Moreover, SD was found to exert an inhibitory effect against the HG-induced production of oxidative stress markers, including ROS, NO, and LPO, and the activation of VCAM-1 and E-selectin in HUVECs. Taken together, the results of this study may suggest that SD might be very useful in the treatment of diabetes mellitus vascular complications.

Abbreviations

HG:	High glucose
SD:	Sanguis draconis
HUVEC:	Human umbilical vein endothelial cells
NO:	Nitrite
LPO:	Lipid peroxidation
MDA:	Malon-di-aldehyde
ROS:	Reactive oxygen species
PARP:	Poly-ADP ribose polymerase
NF-κB:	Nuclear transcription factor-κB
VCAM-1:	Vascular cell adhesion molecule-1.

Conflict of Interests

The authors declare that there is no conflict of interests.

Authors' Contribution

Dr. Yi Chang and Dr. Ting-Chen Chang contributed equally to this work.

Acknowledgments

This work was financially supported by the research Grants from the Incubation Center of National Taiwan University of Technology (NTUT-TMU-98-09) and National Science Council of Taiwan (NSC96-2320-B-038-021-MY3). This study was also supported by Shin Kong Wu Ho-Su Memorial Hospital (SKH-8302-101-DR-25) and Wan Fang Hospital, Taipei Medical University (101TMU-WFH-01-3).

References

[1] M. F. Lopes-Virella and G. Virella, "Immune mechanisms of atherosclerosis in diabetes mellitus," *Diabetes*, vol. 41, no. 2, pp. 86–91, 1992.

[2] B. L. Thurberg and T. Collins, "The nuclear factor-κB/inhibitor of kappa B autoregulatory system and atherosclerosis," *Current Opinion in Lipidology*, vol. 9, no. 5, pp. 387–396, 1998.

[3] D. Ham and S. C. Skoryna, "Cellular defense against oxidized low density lipoproteins and fibrillar amyloid beta in murine cells of monocyte origin with possible susceptibility to the oxidative stress induction," *Experimental Gerontology*, vol. 39, no. 2, pp. 225–231, 2004.

[4] S. Srinivasan, M. E. Hatley, D. T. Bolick et al., "Hyperglycaemia-induced superoxide production decreases eNOS expression via AP-1 activation in aortic endothelial cells," *Diabetologia*, vol. 47, no. 10, pp. 1727–1734, 2004.

[5] N. R. Madamanchi, A. Vendrov, and M. S. Runge, "Oxidative stress and vascular disease," *Arteriosclerosis, Thrombosis, and Vascular Biology*, vol. 25, no. 1, pp. 29–38, 2005.

[6] F. Garcia Soriano, L. Virág, P. Jagtap et al., "Diabetic endothelial dysfunction: the role of poly(ADP-ribose) polymerase activation," *Nature Medicine*, vol. 7, no. 1, pp. 108–113, 2001.

[7] B. Zingarelli, A. L. Salzman, and C. Szabó, "Genetic disruption of poly (ADP-ribose) synthetase inhibits the expression of P-selectin and intercellular adhesion molecule-1 in myocardial ischemia/reperfusion injury," *Circulation Research*, vol. 83, no. 1, pp. 85–94, 1998.

[8] A. Ceriello, L. Quagliaro, M. D'Amico et al., "Acute hyperglycemia induces nitrotyrosine formation and apoptosis in perfused heart from rat," *Diabetes*, vol. 51, no. 4, pp. 1076–1082, 2002.

[9] C. Szabó, A. Biser, R. Benko, E. Böttinger, and K. Suszták, "Poly(ADP-ribose) polymerase inhibitors ameliorate nephropathy of type 2 diabetic Leprdb/db mice," *Diabetes*, vol. 55, no. 11, pp. 3004–3012, 2006.

[10] H. G. M. Edwards, L. F. C. de Oliveira, and H. D. V. Prendergast, "Raman spectroscopic analysis of dragon's blood resins—basis for distinguishing between Dracaena (Convallariaceae), Daemonorops (Palmae) and Croton (Euphorbiaceae)," *Analyst*, vol. 129, no. 2, pp. 134–138, 2004.

[11] H. H. Chen, C. C. Sun, M. P. Tseng, and C. J. Hsu, "A patch test study of 27 crude drugs commonly used in Chinese topical medicaments," *Contact Dermatitis*, vol. 49, no. 1, pp. 8–14, 2003.

[12] Z. Hou, Z. Zhang, and H. Wu, "Effect of Sanguis draxonis (a Chinese traditional herb) on the formation of insulin resistance in rats," *Diabetes Research and Clinical Practice*, vol. 68, no. 1, pp. 3–11, 2005.

[13] R. X. Zhang, J. R. Wang, and C. F. Wu, "Effects of Sanguis draxonis on the levels of blood glucose, insulin and lipids in rats," *Traditional Chinese Drug Research and Clinical Pharmacology*, vol. 13, pp. 23–26, 2002.

[14] H. J. Gu, J. C. Lv, K. L. Yong, X. Chen, P. P. Liu, and X. B. Zhang, "Antidiabetic effect of an active fraction extracted from dragon's blood (Dracaena cochinchinensis)," *Journal of Enzyme Inhibition and Medicinal Chemistry*, vol. 24, no. 1, pp. 136–139, 2009.

[15] J. J. Ma, Y. Song, M. Jia, and C. L. Li, "Effect of total flavone in Sanguis draconis on platelet aggregation, thrombus formation and myocardial ischemia," *Chinese Traditional Herbal Drugs*, vol. 33, pp. 1008–1010, 2002.

[16] C. M. Hu, J. S. Li, K. P. Cheah et al., "Effect of Sanguis draconis (a dragon's blood resin) on streptozotocin- and cytokine-induced β-cell damage, in vitro and in vivo," *Diabetes Research and Clinical Practice*, vol. 94, no. 3, pp. 417–425, 2011.

[17] C. S. Choy, C. M. Hu, W. T. Chiu et al., "Suppression of lipopolysaccharide-induced of inducible nitric oxide synthase and cyclooxygenase-2 by Sanguis Draconis, a dragon's blood resin, in RAW 264.7 cells," *Journal of Ethnopharmacology*, vol. 115, no. 3, pp. 455–462, 2007.

[18] P. Rosenkranz-Weiss, W. C. Sessa, S. Milstien, S. Kaufman, C. A. Watson, and J. S. Pober, "Regulation of nitric oxide synthesis by proinflammatory cytokines in human umbilical vein endothelial cells. Elevations in tetrahydrobiopterin levels enhance endothelial nitric oxide synthase specific activity," *Journal of Clinical Investigation*, vol. 93, no. 5, pp. 2236–2243, 1994.

[19] N. Janel, A. M. Dosne, B. Obert, D. Meyer, and D. Kerbiriou-Nabias, "Functional characterization of bovine von Willebrand factor gene promoter in bovine endothelial cells demonstrates species-specific properties," *Gene*, vol. 198, no. 1-2, pp. 127–134, 1997.

[20] J. F. Ewing and D. R. Janero, "Specific S-nitrosothiol (thionitrite) quantification as solution nitrite after vanadium(III) reduction and ozone-chemiluminescent detection," *Free Radical Biology and Medicine*, vol. 25, no. 4-5, pp. 621–628, 1998.

[21] G. Hsiao, K. H. Lin, Y. Chang et al., "Protective mechanisms of inosine in platelet activation and cerebral ischemic damage," *Arteriosclerosis, Thrombosis, and Vascular Biology*, vol. 25, no. 9, pp. 1998–2004, 2005.

[22] S. Simsek, I. A. M. van den Oever, H. G. Raterman, and M. T. Nurmohamed, "Endothelial dysfunction, inflammation, and apoptosis in diabetes mellitus," *Mediators of Inflammation*, vol. 2010, Article ID 792393, 15 pages, 2010.

[23] C. G. Schalkwijk and C. D. A. Stehouwer, "Vascular complications in diabetes mellitus: the role of endothelial dysfunction," *Clinical Science*, vol. 109, no. 2, pp. 143–159, 2005.

[24] M. Morohoshi, K. Fujisawa, I. Uchimura, and F. Numano, "Glucose-dependent interleukin 6 and tumor necrosis factor production by human peripheral blood monocytes in vitro," *Diabetes*, vol. 45, no. 3, pp. 954–959, 1996.

[25] A. Ceriello, "Acute hyperglycaemia and oxidative stress generation," *Diabetic Medicine*, vol. 14, no. 4, pp. S45–S49, 1997.

[26] T. Minamino, H. Miyauchi, T. Yoshida, Y. Ishida, H. Yoshida, and I. Komuro, "Endothelial cell senescence in human atherosclerosis: role of telomere in endothelial dysfunction," *Circulation*, vol. 105, no. 13, pp. 1541–1544, 2002.

[27] M. L. Sheu, F. M. Ho, R. S. Yang et al., "High glucose induces human endothelial cell apoptosis through a phosphoinositide 3-kinase-regulated cyclooxygenase-2 pathway," *Arteriosclerosis, Thrombosis, and Vascular Biology*, vol. 25, no. 3, pp. 539–545, 2005.

[28] A. Prasad, J. Zhu, J. P. J. Halcox, M. A. Waclawiw, S. E. Epstein, and A. A. Quyyumi, "Predisposition to atherosclerosis by infections: role of endothelial dysfunction," *Circulation*, vol. 106, no. 2, pp. 184–190, 2002.

[29] U. Förstermann, "Nitric oxide and oxidative stress in vascular disease," *Pflugers Archiv European Journal of Physiology*, vol. 459, no. 6, pp. 923–939, 2010.

[30] X. Guillonneau, F. Régnier-Ricard, C. Dupuis, Y. Courtois, and F. Mascarelli, "Paracrine effects of phosphorylated and excreted FGF1 by retinal pigmented epithelial cells," *Growth Factors*, vol. 15, no. 2, pp. 95–112, 1998.

[31] N. Lafuente, N. Matesanz, V. Azcutia et al., "The deleterious effect of high concentrations of D-glucose requires pro-inflammatory preconditioning," *Journal of Hypertension*, vol. 26, no. 3, pp. 478–485, 2008.

[32] R. S. Hundal, K. F. Petersen, A. B. Mayerson et al., "Mechanism by which high-dose aspirin improves glucose metabolism in type 2 diabetes," *Journal of Clinical Investigation*, vol. 109, no. 10, pp. 1321–1326, 2002.

[33] V. Modur, G. A. Zimmerman, S. M. Prescott, and T. M. McIntyre, "Endothelial cell inflammatory responses to tumor necrosis factor α: ceramide-dependent and -independent mitogen-activated protein kinase cascades," *Journal of Biological Chemistry*, vol. 271, no. 22, pp. 13094–13102, 1996.

[34] M. Zerfaoui, Y. Suzuki, A. S. Naura, C. P. Hans, C. Nichols, and A. H. Boulares, "Nuclear translocation of p65 NF-κB is sufficient for VCAM-1, but not ICAM-1, expression in TNF-stimulated smooth muscle cells: differential requirement for PARP-1 expression and interaction," *Cellular Signalling*, vol. 20, no. 1, pp. 186–194, 2008.

[35] G. Gutiérrez, C. Mendoza, E. Zapata et al., "Dehydroepiandrosterone inhibits the TNF-alpha-induced inflammatory response in human umbilical vein endothelial cells," *Atherosclerosis*, vol. 190, no. 1, pp. 90–99, 2007.

[36] E. Huerta-García, J. L. Ventura-Gallegos, M. E. C. Victoriano, A. Montiél-Dávalos, G. Tinoco-Jaramillo, and R. López-Marure, "Dehydroepiandrosterone inhibits the activation and dysfunction of endothelial cells induced by high glucose concentration," *Steroids*, vol. 77, no. 3, pp. 233–240, 2012.

[37] H. J. Kim, I. Tsoy, J. M. Park, J. I. Chung, S. C. Shin, and K. C. Chang, "Anthocyanins from soybean seed coat inhibit the expression of TNF-α-induced genes associated with ischemia/reperfusion in endothelial cell by NF-κB-dependent pathway and reduce rat myocardial damages incurred by ischemia and reperfusion in vivo," *FEBS Letters*, vol. 580, no. 5, pp. 1391–1397, 2006.

[38] V. Stangl, M. Lorenz, A. Ludwig et al., "The flavonoid phloretin suppresses stimulated expression of endothelial adhesion molecules and reduces activation of human platelets," *Journal of Nutrition*, vol. 135, no. 2, pp. 172–178, 2005.

[39] C. K. Sen and D. Bagchi, "Regulation of inducible adhesion molecule expression in human endothelial cells by grape seed

proanthocyanidin extract," *Molecular and Cellular Biochemistry*, vol. 216, no. 1-2, pp. 1–7, 2001.

[40] P. Pacher and C. Szabó, "Role of poly(ADP-ribose) polymerase-1 activation in the pathogenesis of diabetic complications: Endothelial dysfunction, as a common underlying theme," *Antioxidants and Redox Signaling*, vol. 7, no. 11-12, pp. 1568–1580, 2005.

[41] L. Zheng, C. Szabó, and T. S. Kern, "Poly(ADP-ribose) polymerase is involved in the development of diabetic retinopathy via regulation of nuclear factor-κB," *Diabetes*, vol. 53, no. 11, pp. 2960–2967, 2004.

[42] E. B. Peixoto, A. Papadimitriou, J. M. Lopes de Faria, and J. B. Lopes de Faria, "Tempol reduces podocyte apoptosis via PARP signaling pathway in experimental diabetes mellitus," *Nephron Experimental Nephrology*, vol. 120, no. 2, pp. 81–90, 2012.

[43] M. Zanetti, A. Stocca, B. Dapas et al., "Inhibitory effects of fenofibrate on apoptosis and cell proliferation in human endothelial cells in high glucose," *Journal of Molecular Medicine*, vol. 86, no. 2, pp. 185–195, 2008.